Determining new functions of Adenovirus VA-RNAI and its use in cancer therapy

Binny, Christopher Jonathan

Determining new functions of Adenovirus VA-RNAI and its use in cancer therapy

Christopher Jonathan Binny

A Thesis Submitted for the Degree of Doctor of Philosophy

June 2009

Centre for Molecular Oncology and Imaging
Institute of Cancer
Barts and The London School of Medicine and Dentistry
Queen Mary University of London

Declaration

I hereby declare that the material presented in this thesis is the result of original work done by the author, Christopher Binny, at the Centre for Molecular Oncology and Imaging, Barts and The London School of Medicine and Dentistry, Queen Mary University of London. All external sources have been properly acknowledged.

Acknowledgments

I am greatly indebted to my supervisors Dr. Yaohe Wang and Prof. Nick Lemoine, without whose excellent advice, wise guidance and continued support this work would not have been possible. I would also like to extend my sincere thanks to Dr. Claude Chelala for her work analysing the expression microarray data presented in this thesis.

Many other friends and colleagues have contributed less directly to this work, from helping me to refine laboratory and analysis techniques to the less formal but equally essential joint efforts of keeping each other sane and cheerful during those long, late-night sessions in the lab. For these and all gradations in between, I must particularly thank Ka Yi Chan, Virginie Adam, Enrique Miranda Rota, Katrina Sweeney, Dr Chiat Cheong, Dr Stephan Leitner, Dr Daniel Oberg and Dr Chiara Berlato, along with all other members of the Centre for Molecular Oncology and Imaging.

Finally, I owe a great debt to my family for their unending support and patience throughout my life, and especially during the completion of this thesis.

For Rob and Jill

Glossary of abbreviations

2’5’-oas	2’5’-oligoadenylate synthetase
5-FU	5-fluorouracil
AO	Acridine Orange
AVOs	Acidic Vesicular Organelles
CMA	Chaperone Mediated Autophagy
CMV	Cytomegalovirus
CTL	Cytotoxic T lymphocytes
EBV	Epstein Barr Virus
EC_{50}	Effective concentration inducing 50% cell death
ER	Endoplasmic Reticulum
GFP	Green Fluorescent Protein
HBSS	Hank’s Balanced Salt Solution
HSV-1	Herpes Simplex Virus 1
IFNα	Interferon alpha
IFNβ	Interferon beta
IFNγ	Interferon gamma
MDC	Monodansylcadaverine
MDH	Monodansylamylamine
MHC	Major Histocompatibility Complex
MIIC	MHC Class II compartment
NFκB	Nuclear Factor κB
PARP	Poly(ADP-ribose) polymerase
PBS	Phosphate Buffered Saline
PCR	Polymerase Chain Reaction
pfu	Plaque-Forming Unit
PERK	PKR-like endoplasmic reticulum-localised eIF2α kinase
pGEM	pGEM
PI 3-K	Phosphatidylinositol 3-kinase

PI(3)P	Phosphatidylinositol 3-phosphate
PKR	dsRNA-dependant protein kinase
qPCR	Quantitative (or “Real Time”) PCR
TCID50	Tissue Culture Infectious Dose 50%; dose of virus required to infect 50% of cells
VAI	VA-RNAI; Virus-associated RNA I
VA-RNAI	VAI; Virus-associated RNA I

Abstract

Virus-Associated RNA I (VA-RNAI; VAI) of adenovirus is a non-translated RNA molecule known to interact with several dsRNA-binding molecules in host cells. Adenovirus lacking VA-RNAI shows reduced replication and toxicity in normal tissues but replicates with high efficiency in some cancer cell lines.

In this work, efficient replication of VA-RNAI-deleted adenovirus *dl*331 was confirmed to be independent of cancer cells' *k*-ras mutation status, leaving the basis of its selectivity unknown.

VA-RNAI expression was necessary to prevent dsRNA-dependent phosphorylation of eIF2α in Suit-2 and HCT116 cells, with a smaller effect in PANC-1 and none in MiaPaCa2.

VA-RNAI was shown to suppress virus-induced autophagy in two cell lines, whether expressed from the virus or a plasmid. Unexpectedly, the viral protein E1A was observed to colocalise with autophagic vesicles. VA-RNAI was also shown to prevent starvation-induced autophagy in susceptible cell lines.

RNA was collected from normal NHBE cells infected with VA-RNAI-deleted *dl*331 or VA-RNAI-intact control *dl*309 viruses. Microarray analysis of these samples showed a significant change in gene expression as VA-RNAI accumulated in the cells. Most notably, several genes involved in cell cycle progression were upregulated during infection with *dl*331 when compared to *dl*309. RT-qPCR showed a similar pattern of gene regulation in Suit-2 cells responding to infection.

Cell cycle analysis of infected Suit-2 cells showed a transient accumulation of cells in S-phase in response to *dl*309 but not *dl*331 at the approximate time that VA-RNAI reached its highest level.

This work has demonstrated that VA-RNAI's ability to block eIF2α phosphorylation inhibits the induction of autophagy after infection or starvation. Given the newly understood importance of autophagy in cancer pathogenesis and the responses of malignant cells to radiation and chemotherapeutic drugs, this new function is potentially important for the

design of future oncolytic adenoviruses. However, this activity is not sufficient to explain support for replication of VA-RNAI-deleted viruses in cancer cell lines. Data from the microarray and cell cycle analyses suggest that VA-RNAI may play a further role in modulating the host cell's replication cycle, although the mechanism for this is currently unclear.

Table of contents

1 Introduction

1.1 Adenovirus host immune response and cancer therapy

1.1.1 Classification and host range of Adenovirus

The family *Adenoviridae* is divided into two genera: Aviadenoviruses, which are limited to infecting birds; and Mastadenoviruses, whose hosts include human, simian, murine, bovine, equine, porcine, and canine species. Despite conserved epitopes between the coat proteins of closely related adenoviruses, there is no known antigen common to all types.

Human adenoviruses are a diverse group, with 51 serotypes identified to date, divided into subgroups A to G (see Table 1). These vary in tissue tropism and severity of symptoms, with these ranging from subclinical to diarrhoea or keratitis.

During this introduction I will focus on human adenovirus types 2 and 5, the best-studied serotypes. Ads2 and 5 are both members of subgroup C, have very similar genome structures and share tropism towards the lower respiratory tract. Together they are responsible for 5-10% of respiratory tract illness observed in children.[2] Infections are self-contained, with mortality usually associated only with immunocompromised patients.

Table 1: Human Adenovirus Subgroups and Serotypes[3]

Subgroup	Tissue Tropism	Serotypes
A	GI tract	12, 18, 31
B	Urinary Tract, Lung	3, 7, 11, 14, 16, 21, 34, 35, 50
C	Upper / Lower Respiratory Tract	1, 2, 5, 6
D	Eye, GI Tract	8-10, 13, 15, 17, 19, 20, 22-30, 32, 33, 36-39, 42-49, 51
E	Respiratory Tract	4
F-G	GI Tract	40, 41

1.1.2 Physical composition of the viral particle

Adenoviruses are dsDNA-based viruses encased in non-enveloped icosahedral capsids, approximately 90nm in diameter with a mass of $150x10^6$ daltons.[4] Biochemical analysis of purified virus particles shows a composition by mass of 13% DNA and 87% protein. Analysis of purified DNA shows a composition of 22% adenine, 21% thymidine, 27% guanine and 29% cytosine. This contrasts with the DNA of their mammalian and avian hosts, in which adenine and thymine predominate.[5]

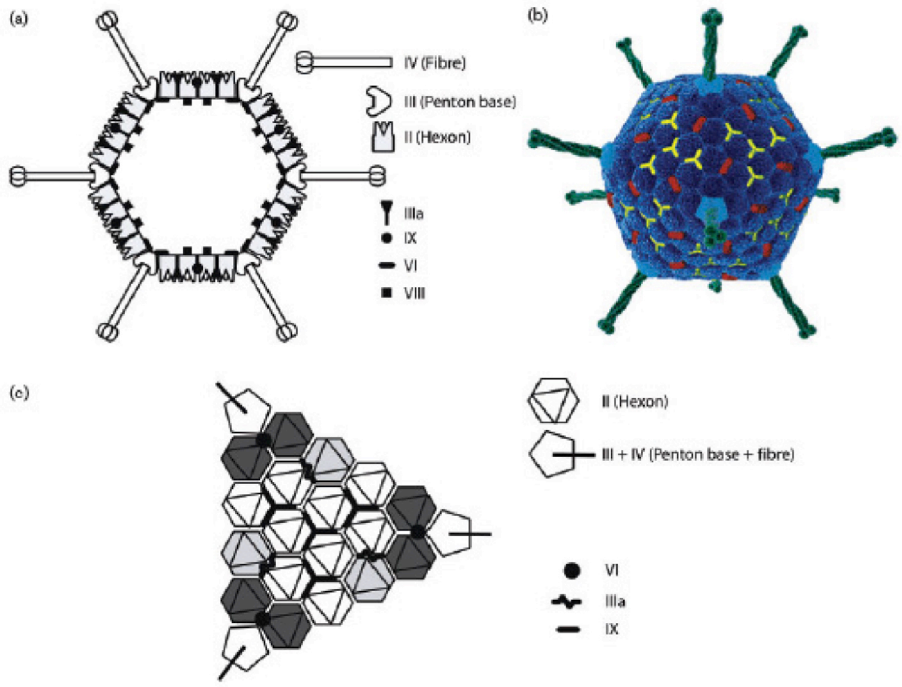

Figure 1 - Representation of Adenovirus capsid structure: (a) shows a representation of the general capsid structure; (b) shows a 3D image of the icosahedron with hexon in dark blue, penton base in light blue, hexon in green, protein IX in red and protein IIIa in yellow (c) shows the detailed structure of a face of the icosohedron (From Vellinga et al 2005[4])

1.1.2.1 Capsid Structure

The adenovirus capsid is primarily constructed from 252 protein subunits referred to as capsomeres. 240 of these are trimers of hexon protein and 12 are pentamers of penton base protein (Figure 1). Hexon trimers interlock to form the faces of the icosahedral capsid. The capsid's vertices are penton base structures, from which long trimeric "fibre" proteins stand upright from the capsid surface. This fibre structure is the main attachment domain of adenovirus; changes in its length and the structure of its C-terminal globular knob domain determine the virus's tropism and antigenicity.[6]

Beneath the penton and fibre structure lie hexamers of protein VI, which penetrates the capsid and interacts with protein V in the core.[4] Similarities between pVI and pVII suggest that pVI may also be able to directly bind to the viral chromosome. pVI protein may also be involved in adenovirus's escape from the endosome during infection by disrupting the compartment's membrane in a pH-independent manner.[7]

The icosahedron's edges are lined with protein IIIa. This protein is believed to penetrate the capsid to interact with the histone-like protein VII. It also plays a role in the stable assembly of the icosahedron's faces.[4]

The smallest of the minor capsid proteins is pIX. Homotrimers of pIX aggregate to form structures known as Groups-Of-Nine (GONs), which stabilise the centres of the icosahedron's faces. Mutant adenoviruses lacking pIX can be propagated in culture with approximately the same efficiency as wild-type virus, but the resulting particles are less thermostable.[8]

1.1.2.2 Core structure

The virus's core is composed of 34-48kb of linear, non-segmented, double-stranded DNA strongly associated with several viral polypeptides.

Precursor terminal protein (pTP) is covalently bound to inverted terminal repeats at each end of the viral genome. Bound in this position, pTP is used during the infection to prime the viral transcription complex.

Protein VII is the most abundant protein component of the viral core,

with between 1170 and 1350 copies present in each particle. Its role is analogous to histone in eukaryotic nuclei, binding the viral DNA into a compact nucleosome-like structure.

Protein V and peptide μ (also called pX) assist in stabilising this structure.[9] Protein V is also believed to link the viral chromosome to the capsid shell.[2]

1.1.2.3 Genome

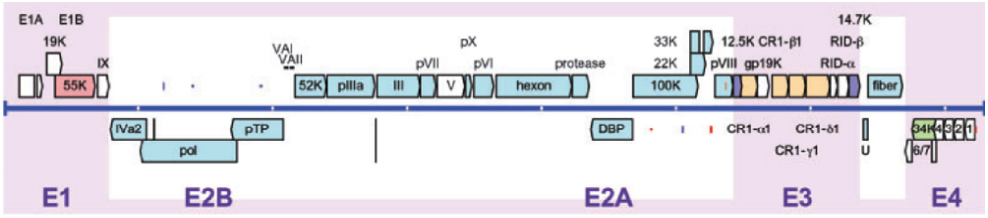

Figure 2 - (From Davison, Benko and Harrach, 2003[10]): Mastadenovirus genome

Adenoviruses are a large and diverse group, with genomes ranging between 34-48kb in length. Adenoviruses types 2 and 5 have genomes of approximately 35.9kb. The genome is flanked by 103bp inverted terminal repeats, which act as recognition sites for the transcription and replication primer protein pTP.

The structure of a typical Mastadenovirus genome is shown in Figure 2. The genome contains two origins of replication, located at the inverted terminal repeat at the 5' end of each strand. Transcription units are loosely divided into "early" or "late" genes, with genes encoded closest to the 5' end of their strand generally being expressed earlier in the infection.

Many adenoviral mRNAs undergo splicing to produce several polypeptides with distinct, although often related functions. For example, two proteins are produced by splice forms of the immediate / early gene E1A. Together, these induce the host cell to enter S phase and promote expression of additional viral genes.

1.1.3 Adenovirus Life Cycle

1.1.3.1 Attachment and internalisation

The virus first attaches to its target cells via binding domains of the globular knob proteins carried at the tips of fibre capsomeres. Different subtypes of adenovirus target different host cell surface proteins.[11] One notable example is CD46, a complement regulatory protein. This molecule is a target for many adenoviral subtypes, presumably due to its expression on a wide range of tissue types.[12]

For adenovirus types 2 and 5 the primary attachment receptor on host cells is the Coxsackie and Adenovirus Receptor (CAR). CAR has two immunoglobulin-like extracellular domains and is involved in mediating homotypic cell adhesion.[13] It is found in specialised intercellular junctions including the tight junction of polarised epithelial cells.[14] These sites seem inaccessible to virus, so infections via CAR may require disruption of the junctions or physical damage to the epithelium.

The distribution of CAR expression in humans is not well known. However, CAR mRNA has been found in a wide range of organs including the lungs, liver, pancreas and intestine.[11]

Blocking CAR using monoclonal antibodies significantly reduces viral attachment and entry but does not completely prevent successful infection. The initial attachment step of Ads 2 and 5 also involves binding to Heparin Sulphate Glycosaminoglycans (HS GAGs).

HS GAGs are a heterogeneous family of long, heavily sulphated carbohydrates which are abundant within the extracellular matrix and the cellular glycocalyx.[11] Proteins usually bind to HS GAGs via basic domains; the KKTK motif contained in the fibre shaft of Ads 2 and 5 is a putative HS GAG-binding motif. Inactivating HS GAGs by treating cells with heparin lyases significantly reduces adenoviral attachment and entry. Simultaneously blocking CAR and inactivating HS GAGs entirely prevents viral replication.[15]

In addition to binding CAR, most adenoviruses bind a secondary

"entry" receptor. For adenovirus types 2 and 5, RGD motifs in the penton base structure interact with integrins on the cell surface such as αvβ3, αvβ5, α3β1 or α5β1. This behaviour is highly conserved among adenoviruses, as the RGD motifs have been found in all but two (Ads 40 and 41, in serotype F) of the adenoviruses sequenced to date.[11] Viral binding to αvβ3 leads to conformational change in the integrins, possibly triggering an intracellular signal. Uptake of Ad5 is associated with activation of integrin-dependent PI(3) Kinase. Substrates of PI(3) kinase have been linked with cell cycle progression and regulation of vesicle trafficking.[16]

Interestingly, mutating the RGD motif in Ad2 slows but does not prevent viral uptake,[17] suggesting that this RGD-integrin interaction is not essential for viral entry to the host cell.

Electron microscopic analysis of infected cells detected Ads type 2 and 5 in clathrin-coated pits and vesicles. Later work has confirmed that viral entry to epithelial cells is a clathrin-dependent process, specifically macropinocytosis.[18]

Macropinocytosis is mediated by a wide range of membrane-bound receptors including lectins and several of the integrins bound by Ads 2 and 5. Processive macropinocytosis is involved in the uptake of large bodies such as bacteria and apoptotic cells. These are then enveloped into large endocytic vesicles for degradation by acidic conditions and a range of degradative enzymes.

Once the virus has been endocytosed, it must escape from the endosome to the cytosol and translocate to the nucleus. The process of endosomal escape is poorly understood, but involves rapid disassembly of the viral particle. Within 10 minutes of endocytosis and before acidification of the endosome, half of the fibre proteins are released from the capsid; after 30 minutes over 90% of particles have shed their fibres.[19] Following this, penton base structures are dissociated, followed by release of the capsid-stabilising proteins IIIa and VIII.[20]

Soon afterwards, acidification of the endosome allows activation of the viral cytosine protease p23. This protease cleaves pVI, freeing the packaged

genome from its association with hexons and other outer coat proteins. When the endosome reaches pH 6.0 the viral genome and its remaining associated proteins are able to escape to the cytosol. This process requires a pH-dependent conformational change in penton, exposing the protein's hydrophobic regions.[21] Additionally, at low pH the virus binds selectively to αvβ5 integrins. The cytoplasmic domain of β5 contains a TVD motif which mediates membrane penetration, although no cellular proteins are known to bind to it.[22]

After endosomal escape the partially degraded capsid is translocated to the nucleus. This trafficking is achieved by at least two separate pathways. Firstly, viral binding to extracellular integrins activates the second messenger cAMP, which activates the protein kinase PKA. Together, these molecules are responsible for phosphorylating cellular motor proteins, upregulating transport toward the cell nucleus.[23] The second pathway requires activation of p38/MAPK to suppress motility toward the cell periphery. These two pathways combined create a net movement toward the cell nucleus.[24]

When the capsid reaches the perinuclear envelope it docks with a nuclear pore complex (NPC) and sheds most of its remaining protein components. This process is dependent on active p23, which completes degradation of the already weakened pVII. After this disassembly step the viral DNA, associated with the terminal protein pTP and stabilising proteins V, VII and μ is translocated into the nucleus. This translocation may be aided by the classical nuclear localisation signal carried at the end of pTP.

1.1.3.2 Early Viral Gene Expression

The first adenoviral gene to be expressed is the "early" gene E1A, under the control of a constitutively active promoter sequence. Two polypeptides are produced from this gene as a result of differential splicing. The larger polypeptide (E1A 13s) contains conserved regions CR1, 2, 3 & 4; the smaller polypeptide (E1A 12s) contains only CR1, 2 & 4.

The CR 2 domain of both E1A types is able to bind the retinoblastoma

(Rb) family of proteins including pRB, p107 and p130.[25] Rb proteins bind cellular transcription factor E2F, blocking its activity and thus arresting the cell cycle in G_1 phase. However, E1A is able to displace and sequester Rb proteins, freeing E2F to initiate transcription of its target genes.[26] The genes upregulated by this action include CDK2 along with cyclins A and E[27] and are sufficient to drive the cell into S-phase.

The CR1 domain also acts to push cells into S-phase, through interactions with cAMP response element-binding protein (CBP) and P300. These highly related proteins share an ability to acetylate histones, changing their conformation. This conformational change may allow additional proteins to associate with promoter or enhancer regions of CBP/p300's target genes. They may also share the ability to acetylate and regulate a variety of transcription factors including p53, NF-κB and c-Myc.[28]

The CR3 domain of E1A 13s acts as a transcription factor to initiate expression of the remaining adenoviral early genes (E2, E3, E4). Unusually, the CR3 is not a sequence-specific DNA binding protein. Instead, it associates with the DNA-binding domains of cellular transcription factors bound to early adenoviral promoters.[27]

The CR4 domain binds to a cellular transcription regulatory protein called E1A c-terminal-binding protein (CtBP). This inactivates CtBP's inhibitory functions and allows upregulation of transcription. CR4 also contains a nuclear localisation signal, allowing newly synthesised E1A to move to the nucleus and help to drive the cell through S-phase.

One consequence of E1A's activity is the induction and stabilisation of p53. This would lead to cell cycle arrest and apoptosis if not blocked by E1B-55K, a product of the next viral gene to be expressed. E1B-55K is a component of the viral ubiquitin ligase complex. It recognises p53 and marks it for destruction by the proteosome. E1B also plays a role in upregulating the export of viral mRNA from the nucleus, for translation in the cytoplasm.[29]

Similarly, E1A's activity leads to the degradation of BCL-2 family member MCL-1, which would lead to release of cytochrome C and trigger

an apoptosis pathway. E1B-19K mimics MCL-1 by sequestering pro-apoptotic BAK and BAX, saving the cell from apoptosis.[27]

The next section of the viral genome to be transcribed is the E2 region, which encodes the terminal binding protein pTP, a DNA polymerase with proofreading ability and DNA binding protein. Once these products have accumulated to a sufficient concentration, replication of the viral genome is able to begin. Briefly, the pTP binds to the inverted terminal repeats at each end of the viral genome. Here it acts as a primer for DNA replication. This process depends on the viral ssDNA binding protein and DNA polymerase, responsible for strand separation and duplication, respectively. The cellular protein nuclear factor II is also required.

Transcripts from the E3 gene encode non-secreted proteins whose primary functions are the suppression of host immune responses against the virus. These functions will be discussed in the section "Interactions with the immune system."

E4 gene products interact with a wide range of cellular pathways to improve the efficiency of viral replication. Targets include components of apoptosis, cell cycle control, DNA repair and posttranslational modification of proteins. These functions are divided between at least six distinct polypeptides, transcribed from different origins within the E4 region but sharing the same termination signal.[30]

E4 ORF1 slowly accumulates in the cytoplasm during the infection, reaching high levels at late stages. Its sequence and predicted protein structure are similar to dUTP phosphatase enzymes, involved in nucleotide metabolism. While it lacks dUTP phosphatase's enzymatic activity, it is known to bind to similar targets such as DLG, MUPP1 and MAGI-1. The role these interactions play during the course of infection is unknown, but this ORF is critical in Ad9-induced tumourogenesis.[31]

The E4 ORF2 is conserved among human adenoviral serotypes,[32] but its function is currently unknown.

E4 ORF3 augments viral DNA replication, late protein synthesis and shutoff of host protein synthesis. It also prevents concatenation of viral

DNA strands. These activities are dependent on the protein's ability to stabilise late viral mRNAs and bind to cellular proteins. One of E4 ORF3's target proteins is DNA-dependent protein kinase (DNA-PK), an essential element of the double-strand break repair system. DNA-PK is inhibited by this interaction, blocking the process of V(D)J joining, which could otherwise lead to concatenation of viral genome sequences. E4 ORF3 also appears to bind E1B 55k, the viral ubiquitin ligase. This interaction results in the polyubiquitination of certain virally induced structures within the nucleus during specific phases of the infection.

E4 ORF4 represses the activity of the cellular protein phosphatase 2A (PP2A). Inhibition of this serene-threonine phosphatase influences several cellular pathways, including: the downregulation of virus-induced signalling; and regulation of viral and cellular gene expression at both transcription and translation levels.[30] This interaction is also required for induction of p53-independent cell death.[33] E4 ORF4 translocates to cytoplasmic sites and associates with an actin-myosin complex. Once there, it triggers a myosin II motor to begin *de novo* actin polymerisation, recruiting endosomes to the sites. This eventually leads to nuclear shrinkage, polarised membrane blebbing and cell death.[34]

E4 ORF6 is involved in several aspects of the replication cycle. Pathways ORF6 is involved with include late viral mRNA splicing and transport, viral DNA synthesis and host cell shut-off.[30] These functions are dependent on interaction with several viral and cellular proteins. For example, a complex with E1B-55k binds viral mRNA for selective export from the nucleus and may be involved in its splicing. This complex also interacts with p53, leading to its rapid degradation.[35] ORF6 also interacts with E4 ORF3 to inhibit DNA-PK (see above).

The overall effect of early gene expression is to create an ideal environment for the manufacture and eventual release of new viral particles. The host cell is now in S-phase, intracellular responses against the virus have been circumvented (discussed below), host cell shutdown has begun and the viral DNA polymerase has accumulated in the nucleus.

1.1.3.3 Late Gene Expression and Viral Assembly

Expression of intermediate and late genes of adenovirus begins after replication of the viral genome. The late genes are grouped in a single transcription unit of approximately 29kb in length, the major late transcription unit (MLTU). This transcription unit is controlled by a single promoter sequence. Activation of this promoter is strongly upregulated by E1A and also requires a *cis*-acting change in the viral chromosome (perhaps related to the histone acetylation activity of CREB/p300) and an additional viral transcription factor.

Transcription from the MLTU produces a wide range of mRNAs through use of several poly(A) signals and splice sites. The resulting transcripts are grouped into five families labelled L1 – L5, based on termination at common poly(A) sites. The protein products of these genes are mostly structural components of the new viral capsids. One key non-structural protein produced at the late stage of infection is the adenoviral death protein (ADP), which plays a key role in causing cell death, enabling the virus progeny to escape.

The earliest step in capsid assembly is the formation of hexon capsomeres. This takes place in the cytoplasm assisted by an unknown chaperone protein. Completed capsomeres associate with viral protein VI, a structural protein located underneath hexon capsomeres in mature particles. Protein VI transports the hexon capsomeres to the nucleus via an importin α/β-dependent mechanism.[36] As capsid proteins and copies of the genome accumulate in the nucleus, immature particles are assembled. It is not clear whether this process involves insertion of pTP-bound DNA into an empty capsid[37] or the assembly of capsids around a nucleoprotein core.[38] After formation of this complete particle, a maturation process occurs. This involves cleavage of several viral proteins (including pVI) by viral cytosine protease p23.[19]

1.1.3.4 Escape from the Cell

Relatively little is known about how the mature virus particles escape from the cell, although it is known to involve the cell's death. The adenovirus death protein (ADP) is required for efficient cell lysis and adenoviral escape.[39,40] Unusually, ADP is encoded by the E3 region but controlled by the major late promoter. Consequentially, ADP only reaches high levels within the cell (usually associated with the endoplasmic reticulum or other intracellular membrane-bound bodies) at late times after infection.[39] Other methods of cell killing may also be involved. One possibility is the cytotoxic activity of E4 ORF4, described above.

After cell death, adenovirus must escape the immediate surroundings to disperse and infect surrounding tissues. To aid this escape, adenovirus fibre disrupts CAR-mediated intercellular adhesion. This disruption of cell-cell contact weakens or distorts the epithelium, allowing the virus to filter between the cells and emerge at the apical side.[41]

1.1.4 The immune response of host cells to adenovirus

Free virus particles are susceptible to detection by the cellular arm of the innate immune response, and subsequent presentation of antigens to the adaptive immune system. Immature antigen-presenting cells such as macrophages and dendritic cells can be found throughout various tissues and especially at the mucosal epithelia. These immature APCs tend to have a high level of phagocytic activity, constantly sampling their environment.[42]

Generally, when a pathogen is engulfed in this manner, it is degraded along with the rest of the phagophore content and passed to an endosomal compartment. Within these compartments are the innate pattern recognition receptors (PRRs), germline-encoded receptors that recognise antigens such as the lipo-polysaccharides and unmethylated CpG DNA motifs typical of bacteria and viruses. Also among the main viral patterns recognised by PRRs is dsRNA, a common by-product of viral replication.

During an adenovirus infection, recognition of the virus is primarily dependent on TLR9 and TLR2.[43] Recognition of an antigen leads to a signalling cascade, possibly through MyD88,[44] that leads to secretion of inflammatory cytokines (e.g. IL-6, TNFα) and interferons to upregulate the innate immune response, and to the maturation of the dendritic cell.[43,45]

The mature dendritic cells migrate to local draining lymph nodes, where they present the antigens on MHC molecules along with a co-stimulatory molecule, such as B7 (CD28 ligand) or CD40, whose expression is upregulated during the maturation process.[42]

The next step is dependent on the route of presentation of the antigen. An adenovirus is typically able to escape the phagosome to infect a dendritic cell, so its antigens will likely be presented via the MHCI pathway. This results in presentation of the antigens to $CD8^+$ T lymphocytes. Presentation of the antigen to a $CD8^+$ T lymphocyte with a complementary T cell receptor (TCR) results in the activation and proliferation of that T cell. Activated $CD8^+$ T lymphocytes are then able to migrate from the lymph node to the site of infection, by binding to epithelial

cells expressing adherence proteins upregulated by infection or by cytokines secreted by infected cells and/or activated dendritic cells.

Upon encountering an infected cell, the $CD8^+$ T lymphocyte is then able to recognise it through an interaction between the T cell receptor (TCR) and the MHCI-bound antigen on the cell surface, along with co-stimulatory molecules. For the majority of cells, the lymphocyte will trigger a signalling cascade in the infected cell leading to a programmed cell death, halting that infection. Alternatively, it may signal professional antigen-presenting cells to destroy the contents of its autophagosomes and further contribute to the antiviral response through the secretion of pro-inflammatory cytokines and/or the continued phagocytosis and subsequent destruction of free virus particles.[46]

The innate response against viral infection primarily depends on the induction of type 1 interferons (IFNα and IFNβ) and the recruitment of cytotoxic NK cells. Broadly, the IFNs act as autocrine and paracrine signals, upregulating antiviral genes to create a hostile environment within cells. NK cells monitor levels of MHC1 complexes displayed on cell surfaces. An unusually low level of MHC1 expression is a common indicator of viral infection; when NK cells encounter this, the infected cell is killed.[46,47]

Although important for the wider spread of the virus throughout its host, the adaptive immune response will not be the main focus of this introduction. VA-RNAI's most well established function is involved in the control of the intracellular response to viral infection.

1.1.5 The intracellular Response

Several pathways trigger the intracellular response to Adenoviral infection. The best known of these involves dsRNA-dependent Protein Kinase (PKR). More recently a second pathway dependent on the RNA helicase RIG-i was found. In both cases the detection of dsRNA leads to a shutdown of protein synthesis and induction of the interferon response.[48] Other dsRNA-sensing molecules (e.g. 2'5'-oligoadenylate synthetase) also play a role in this process. In addition to dsRNA, detection of unmethylated CpG motifs typical of viral and microbial dsDNA may be detected by Toll-Like Receptor 9 (TLR9).[47] A brief summary of these interactions is illustrated in Figure 3.

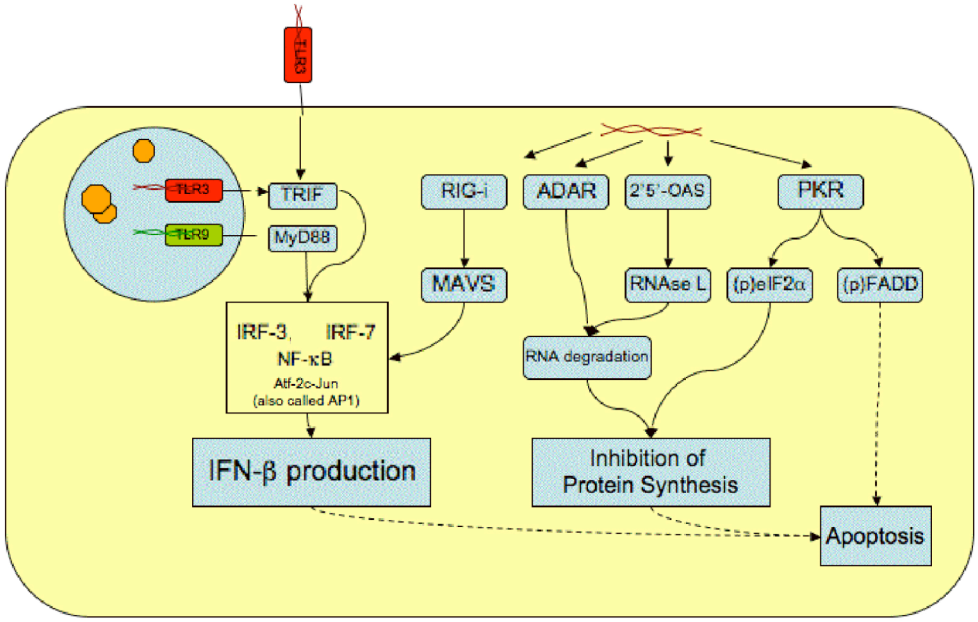

Figure 3 - Outline of dsRNA (red) and dsDNA (green) -sensing pathways in the intracellular immune response

1.1.5.1 dsRNA-dependent Protein Kinase (PKR)

PKR (also called p68 kinase or DAI) is a ubiquitously expressed serine-threonine kinase. Its expression is upregulated by interferon although it must be activated by binding to dsRNA, leading to conformational change and autophosphorylation.[49]

Its targets include the B56α subunit of Protein Phosphatase 2A (PP2A)

and the α subunit of eukaryotic initiation factor 2 (eIF2α), inhibiting translation. PKR can also regulate transcription via stress-activated protein kinase family (e.g. JNK) and IKK, whose phosphorylation leads to activation of NF-kB. Finally, activated PKR may promote apoptosis by phosphorylation of Fas-Associated Death Domain (FADD), leading to activation of the apoptotic caspase pathways (reviewed by Williams, 2001[50]).

PKR is expressed at high levels in response to interferon and activated by binding dsRNA. It then phosphorylates the α subunit of eukaryotic initiation factor 2 (eIF2α, Figure 4). eIF2 is a necessary component of the protein synthesis machinery, responsible for loading the chain-initiating methionine into the assembling ribosome complex. In its free state, eIF2β forms a complex with a $tRNA_i^{Met}$ and a molecule of GTP; this complex is stabilised by further association with two small ribosomal subunits and further initiation subunits. After encountering an mRNA strand, hydrolysis of the GTP to GDP provides the energy necessary to add the 60s ribosomal subunit to the complex, thus completing the assembly of a complete ribosome. PKR's target, eIF2α, is responsible for supplying eIF2β with its next GTP, to enable this process to repeat. Given sufficient availability of mRNAs and loaded tRNAs, this supply of GTP by eIF2α can become a rate-limiting step for protein synthesis.[51]

After phosphorylation by activated PKR, eIF2α irreversibly binds to eIF2β and is then unable to fulfil its normal role in the initiation of translation. Thus activation of PKR leads to a rate-limiting shortage of prepared translation initiation complexes. This non-specifically inhibits the translation of mRNA to protein, preventing viral replication within the cell.

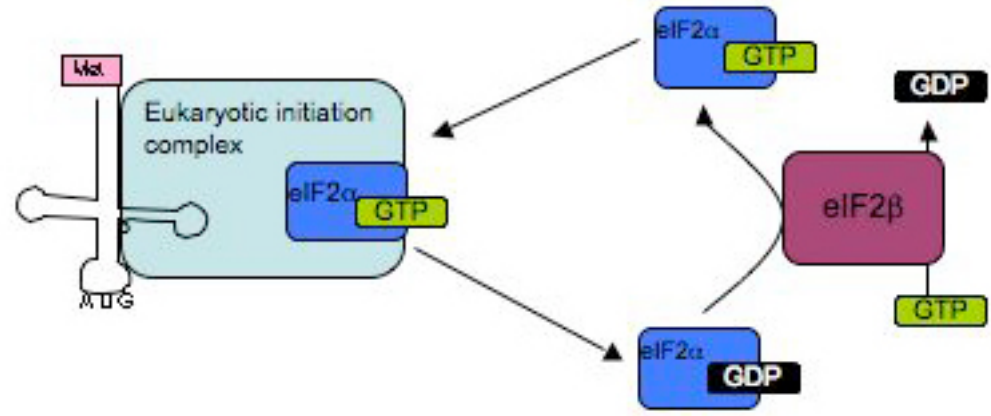

Figure 4 - eIF2α is involved in charging the translation initiation complex with a primed tRNA. Phosphorylation by PKR causes eIF2α to bind eIF2β, inhibiting this process

1.1.5.2 2'5'-Oligoadenylate Synthetase and RNAse L

2'5'-oas (also called OAS1) is a dsRNA-dependent enzyme, which uses adenosine from ATP to manufacture short chains of 2'5'-linked adenosine molecules called 2-5A. The linkages are phosphodiester bonds between the 2' and 5' groups, and the chain takes the general form [ppp5'(A2'p5')2A]. This activity is only permitted when the enzyme is bound to dsRNA or ssRNA with stable secondary or tertiary structures.[52] The resulting molecules of oligoadenylate serve to activate the endoribonuclease RNAse L, the main effector of this system.

RNAse L is an 84kDa protein widely expressed in mammalian tissues. Analysis of its sequence reveals a 2-5A binding pocket, a domain with possible kinase activity and an endonuclease domain. Binding with 2-5A causes the enzyme to dimerise, then begin to degrade any RNA molecules it encounters. This activity is not selective for viral RNA and therefore inhibits all gene expression in the cell. Additionally, at high levels of activation extensive rRNA cleavage occurs, possibly contributing to the enzyme's pro-apoptotic activity.[53,54]

At least one isozyme of 2'5-oas has a pro-apoptotic function independent of RNAse L. The 9-2 isozyme contains a Bcl2-homology

domain. Through this the dsRNA-activated enzyme is able to bind and inhibit members of the anti-apoptotic Bcl2 protein family.[55]

1.1.5.3 Adenosine Deaminase (ADAR)

ADAR (also called dsRAD or DRADA) is an IFN-inducible RNA editing enzyme which catalyses the C-6 deamination of adenosine to inosine in cellular pre-mRNAs and some viral RNAs.[56] Its known cellular targets include the glutamate-gated ion channel GluR receptor, where the mutations introduced influence the completed ion channel's permeability;[57] and the serotonin 5-HT_{2c} receptor, in which tissue-specific editing of pre-mRNAs regulates the receptor's signal transduction efficiency.[58] This editing activity can also lead to the specific cleavage of the edited RNA molecules at alternating UI IU base pairs.[59]

ADAR binds its substrates via three dsRNA binding motifs very similar to those found in PKR.[56]

Hepatitis C replicons (single-stranded positive sense RNA) are subject to extensive editing by ADAR during their course of infection. This editing has been suggested as a key factor in their clearance from the cell, through accumulation of lethal mutations and possibly degradation by inosine-specific RNAses.[59]

1.1.5.4 RIG-i

RIG-i's full name is retinoic acid-inducible protein i, and is also called Dddx58. This non-secreted cytosolic protein is a DExH-box RNA helicase, able to unwind dsRNA with its intrinsic ATPase activity.[60,61] Unusually for this type of helicase, it contains tandem caspase recruitment domains (CARDs). When the helicase domain of RIG-i binds dsDNA, its CARDs initiate a signalling cascade. The details of this cascade are not currently known, but result in upregulation of NF-κB, IRF3 and therefore eventually IFN-β.[62]

Although no interaction between RIG-i and VA-RNAI has been identified, RIG-i is known to bind the EBV transcript EBER. EBERs are non-translated RNA molecules produced by Epstein-Barr virus. Like VA-

RNAI, they are predicted to fold into complex stem-loop structures and inhibit PKR activity.[63] Whether binding PKR is the method by which EBERs confer interferon resistance remains controversial.[64] Due to these structural similarities, EBERs' ability to bind and activate RIG-i[65] suggests that VA-RNAI may do the same.

1.1.5.5 Toll-like receptors

The TLR family in mammals includes 11 members, each of which recognises a distinct pattern associated with microbial pathogens (PAMPs). These include a diverse range of molecules, such as bacterial membrane component lipopolysaccharide (LPS), peptidoglycan, flagellin and specific ssRNA sequences unique to various viruses. They are typically membrane-associated molecules, with extracellular (or intra-luminal) receptors and cytoplasmic signalling domains. The TLRs share a common signalling pathway, leading via MyD88 (or TRIF for TLR3) to initiate the IκB kinase complex. Phosphorylation of IκB releases the transcription factor NF-κB, a key promoter of IFNβ and other inflammatory genes.[46]

The TLRs likely to be involved in detection of Adenovirus are TLR3 and TLR9, which detect dsRNA and unmethylated CpG linkages typical of viral dsDNA, respectively. TLRs 7 and 9 detect G/U rich ssRNA typical of viruses, so may also be involved. However, all of these are located in endosomal compartments.[66] It is unclear whether the adenoviral uncoating sequence could expose its DNA to TLR9 before endosomal escape. Similarly, uptake of adenoviral ssRNA or dsRNA into endosomes has not been demonstrated. Therefore the importance of TLRs in the response to adenovirus remains undetermined.

1.1.5.6 The Interferon Response

The interferon response is the first defence against viral infection. Rapidly induced by a range of intracellular receptors, its purpose is to prevent viral replication within and spread from the cell. This can result in clearance of virus from the cell, but prolonged stimulation by interferon leads to the upregulation of pro-apoptotic genes and therefore potentially to

cell death.

Interferons are a family of small, secreted proteins. Within this family are several Type I species, IFNs α, β, ω and κ. There is a single type II species, IFN γ. The first interferon type to be expressed by a virus-infected fibroblast or epithelial cell is IFNβ, although several versions of IFNα follow. Although a few genes are responsive only to one species of interferon, the functions of type I interferons broadly overlap. IFNγ is normally only expressed by Th-1 lymphocytes and NK cells.[67]

All interferons act as auto- and paracrine signals. IFNs bind to extracellular receptors, activating JAK-STAT (Janus Activated Kinase – Signal Transducers and Activators of Transcription) pathways. The JAKs are tyrosine kinases, which recruit and phosphorylate STAT molecules with the help of SH2 domain-containing adapter molecules. These phosphorylated STAT molecules form homo- or heterodimers and translocate to the nucleus. In the nucleus, the STAT dimers bind to specific promoter sequences to activate transcription of interferon-stimulated genes (ISGs).[68] Activation of STAT molecules is usually transient due to the action of an unknown tyrosine phosphatase.[69]

Whether the interferon signal is endogenous or from an external source, the cell responds by upregulating over 300 genes.[68] This complex network is not fully understood and contains apparent contradictions. For example, both pro- and anti-apoptotic genes are expressed in response to IFNβ.[67] Crucially, IFNβ stimulates the expression of its own promoters, including NFκB, P300 and IRFs 3&7. Production of IFNα is also promoted by these ISGs, along with IFNγ in dendritic cells.[69]

The genes upregulated by IFNβ include 2'5'-oas, ADAR and PKR, described above. This contributes to the creation of an antiviral state within the cell, inhibiting a virus's replication.[70] Also upregulated is MHC class I and the enzymes that process peptides for MHC display. This increased presentation of intracellular peptides on the cell surface increases the possibility of discovery by an activated cytotoxic $CD8^+$ T lymphocyte. Type I IFN also stimulates the development of T_H1 cells, via upregulation of

IL-12 receptors in T lymphocytes.[46] This drives the activation and recruitment of $CD8^+$ T lymphocytes in the adaptive arm of the immune response.

The Mx proteins, also upregulated by IFNs, are a pair of cytoplasmic proteins, MxA and MxB (many other types exist in other species).[71] They belong to the dynamin superfamily of GTPases involved in a range of processes including endocytosis and vesicle transport.[68] MxA (encoded by the Mx1 gene) is rapidly expressed in response to IFN stimulation and is associated with a powerful antiviral response. Its mechanism of action has been extensively studied but is incompletely understood. MxA's reported activity is limited to RNA viruses and Hepatitis B, an ssDNA virus, which uses an RNA intermediate in its genome replication process. As such, this antiviral gene may not be relevant to the anti-adenoviral response.[71]

Several other antiviral pathways which are unlikely to affect Adenovirus – such as the ISG20, an RNAse specific to ssRNA virus genomes[72] – have been described, but are outside the scope of this introduction.

Members of the P200 protein family are also strongly induced by type I interferons. Of special note is P202, a nucleolar protein that binds and inhibits many cell factors including NFκB, E2F, c-Myc and Rb. This may be a major contributor to IFN's powerful antiproliferative effect.[68]

IFNβ has a delayed pro-apoptotic effect. Although precise details of the pathway have not been elucidated, it is generally associated with the FADD/caspase-8 apoptotic pathway. Induction of this pathway leads to the cytochrome C release, caspase activation cascade and DNA fragmentation typical of apoptosis. This is a late effect of interferon stimulation – *in vitro* studies show this activity beginning after 48 hours of exposure to high levels of IFNβ. This is likely to be the result of the prolonged upregulation of pro-apoptotic ISGs such as caspases 4 & 8, TRAIL, Fas, PKR and 2'5'-oas.[73]

1.1.5.7 Antiviral autophagy

Macroautophagy, here referred to simply as "autophagy", is a process by which cytosolic contents are engulfed in a double-membraned compartment and degraded as the compartment (an autophagosome) lowers its pH and receives input from the lysosomal or endosomal pathways. This uptake of cytosolic components can target objects ranging from peptide fragments to entire exhausted mitochondria. Most – possibly all – mammalian cells maintain a basal level of autophagy as a homeostatic mechanism, but it can be upregulated in response to various stress stimuli.

Autophagy is known to play a role in several viral infections. For example, induction of autophagy by upregulation of Beclin 1 in mice protects them from lethal Sindbis encephalitis virus.

Herpes Simplex Virus 1 (HSV-1) prevents the induction of autophagy by expressing the neurovirulence protein ICP34.5. ICP34.5 binds to the pro-autophagic structural protein Beclin 1 to disrupt its activity. Importantly for this project, this autophagic degradation of HSV-1 requires the activity of phosphorylated PKR to phosphorylate its target eIF2α. In addition to its ability to bind Beclin 1, ICP34.5 has a phosphatase activity, which retargets the cellular phophatase PP1α to dephosphorylate eIF2α.

If ICP34.5 is deleted, high levels of autophagy are induced in infected cells and the viruses targeted for degradation. At a systemic level, this deletion mutant virus is no longer neurovirulent in mice, highlighting the importance of autophagy's protective role.[74]

The link between eIF2α and autophagy is not limited to HSV-1 infection. In both yeast and mammals, the phosphorylation of eIF2α by its kinase (GCN2 and PKR, respectively) is required for starvation- and virus-induced autophagy.[75] This finding has implications for many intracellular pathogens; as described previously, PKR – eIF2α is among the key detectors of virus activity within the cell. The viral genes encoded by various viruses to prevent the phosphorylation of eIF2α (e.g. Influenza virus NS1, Epstein-Barr virus EBER1 and SM, HIV's TAT, etc.) may therefore

be equally important in protecting those viruses from autophagic degradation.[76]

Inevitably, some intracellular pathogens have evolved to avoid, or even exploit, the autophagic response. Several RNA viruses – e.g. poliovirus, equine arterivirus and mouse hepatitis virus – form replication complexes on double-membraned vesicles that resemble autophagosomes. Indeed, poliovirus replication requires successful induction of autophagy to replicate; it has also been proposed that poliovirus subverts the autophagic pathway to enable its release from the cell.[74,76] Similarly, rotavirus appears to induce autophagy deliberately, expressing NSP4 to promote autophagosome production and thus create replication sites for itself.[77]

Degradation of viruses by autophagy appears to be a key mechanism for a cell to fight an infection, but it has wider implications than this. Cells of the innate immune system carry pathogen recognition receptors (PRRs) also called Toll-like receptors (TLRs). Infected plasmacytoid dendritic cells are able to digest viruses by autophagy as described, then present the products of this degradation to TLRs in their endosomal and lysosomal spaces. Recognition of pathogens (e.g. by a conserved peptide or DNA sequence) by the TLRs leads the cell to begin activating an antiviral response, including interferon production and possibly presentation of the antigen to cells of the adaptive immune system.[78]

1.1.5.8 Autophagy in adaptive immunity

Macroautophagy has also been shown to play a role in adaptive immunity. After synthesis in the ER, MHC Class II molecules are stored within endosome-like compartments referred to as MHC Class II Compartment (MIIC or CIIV). In these compartments they are separated from the chaperone invariant chain I_i and its subunit CLIP, and then loaded with processed antigens. These antigens are delivered to the compartment by fusion with endosomes, which typically contain molecules internalised from the extracellular spaces, such as viral particles attached to the cell surface.

Autophagosomes also constitutively deliver fragments of their degraded contents to the MIIC, conveying protein fragments from intracellular sources. This activity occurs in both antigen-presenting cells and normal epithelial cells.[79,80] A strong activation of the "helper" $CD4^+$ T lymphocytes is crucial for a robust adaptive immune response.[81] This presentation of intracellular protein fragments to the adaptive immune system may be crucial for the development of cytotoxic responses against cells that have become infected or cancerous.[81]

One example of this is the display of Epstein Barr Virus's (EBV) nuclear antigen 1 (EBNA1), which is displayed by MHCII complexes in infected cells and tumours.[82] Unsurprisingly, many intracellular pathogens have evolved mechanisms to evade or subvert the autophagic pathways. While this suppression may also serve other purposes for the pathogens, it seems very plausible that protecting their antigens from display to the adaptive immune system is a key part of their survival strategy.[83] Indeed, induction of macroautophagy in cells expressing influenza virus matrix protein 1 (MP1) increases recognition of those cells by $CD4^+$ T-cells. Similarly, specifically targeting MP1 to the autophagosome by fusion to LC3 leads to an increase in MHCII peptide display and a resulting increase in IFNγ production by the $CD4^+$ T cells.[84] Cytolytic $CD4^+$ T cells have previously been observed associating with endothelial cells expressing MHCII[85] and are known to play an important role in controlling intracellular infections.[86,87] Interestingly, IFNγ upregulates both MHCII presentation at cell surfaces and the uptake and processing of cytosolic proteins by macroautophagy, supporting the idea of macroautophagy as a mechanism for immune surveillance of the cytosol.

This involvement of autophagy in adaptive immunity may be dependent on the polarisation of the response toward the T helper cell 1 (Th1) or Th2 response. As described above, the prototypical Th1 cytokine IFNγ is known to upregulate autophagy, and contributes to the elimination of intracellular pathogens such as Epstein Barr virus[82] and *Mycobacterium tuberculosis*.[88] TNF-α may have a similar effect, having been shown to aid autophagic

elimination of *Toxoplasma gondii* from infected macrophages.[89] In contrast, however, the Th2 cytokines IL-4 and IL-13 inhibit starvation-induced autophagy and autophagic clearance of *Mycobacterium tuberculosis.*[90] IL-13 is a potent activator of Class 1 PI 3-kinase and the AKT signal transduction pathway,[91] the activation of which can act as a potent inhibitor of autophagy induction, presumably by preventing the activation of TOR.[92] IL-4 and IL-13 both signal through the receptor IL-4Rα, resulting in signalling via the insulin receptor substrate (IRS) and STAT6 pathways. This activation of IRS signalling activates the class I PI 3-kinase and Akt pathways, inhibiting maturation of phagosomes.[93]

The prevailing view is that Th1-mediated immune responses lead to inflammation and the activation of cytotoxic $CD8^+$ T lymphocytes ideal for fighting an intracellular pathogen, while Th2-mediated responses tend to lead to the activation of antibody-secreting B lymphocytes for humoural-mediated immunity. The upregulation by Th1 cytokines IFNγ and TNF-α of macroautophagy and the display of its output on MHCII seem logical in this context: together they could lead directly to eradication of an intracellular pathogen, or to priming of the adaptive immune system and subsequent killing of infected cells.

Work presented in this thesis indicates that the antiviral autophagy pathway is very relevant to the study of VA-RNAI and its effects while modulating the intracellular response against the viral infection, among other stimuli. The mechanisms of autophagy and its importance in a range of cellular processes and stress responses will be described in detail in a later section.

1.1.6 Evasion of the immune response by Adenovirus

Adenoviruses have evolved mechanisms to circumvent the intracellular immune response, either by concealing itself or by blocking relevant effector molecules. Most of the known mechanisms are dependent on genes in the E3 region. However, a non-translated virus-associated RNA (VA-RNA) encoded in the L1 region also plays an important role.

The E3 gene encodes a family of non-secreted proteins evolved to suppress various arms of the antiviral response. They are not essential for replication in culture, but deletion of this gene inhibits viral replication in immunocompetent hosts. Interestingly, the E3 gene contains NF-κB binding sites in its promoter sequence.[94] This leads to increased production of E3 proteins in response to cellular stress signals such as the production of interferon.

A key function of the E3 gene is the inhibition of peptide display on the cell surface. Major Histocompatability Complex I (MHC 1) routinely cycles between the endoplasmic reticulum and the cytoplasmic membrane. Its role is to collect peptide fragments from inside the cell for display on the cell surface, for scanning by cytotoxic $CD8^+$ lymphocytes. In this way, foreign peptides such as those from a viral infection are displayed to the immune system. This behaviour is upregulated by activation of the IFN-dependent Jak/STAT pathway. E3-gp19k binds to the heavy chain of class I major histocompatability complex (MHC I) in the endoplasmic reticulum, blocking this pathway. Additionally, E3-gp19k blocks the activity of TAP, the protease responsible for processing proteins into peptides suitable for display by MHC I. This inhibition reduces the pool of peptide fragments available for display by any remaining MHC activity. Cells infected with Adenovirus are thus largely protected from $CD8^+$ lymphocyte-mediated killing.

E3-10.4k and E3-14.5k are also known as receptor internalisation and degradation (RID) proteins. These are responsible for the internalisation and proteosomal degradation of FAS and TRAIL, two key ligand-induced upregulators of apoptosis. Removal of these receptors from the cell surface desensitises the cell to pro-apoptotic signals from $CD8^+$ T lymphocytes and secreted tumour necrosis factors (TNFs). E3-14.7k plays a similar role to these proteins, inhibiting TNF-induced apoptosis.

E3-11.6k is more commonly known as the Adenovirus Death Protein (ADP). It is the only E3 protein known to have a pro-apoptotic function. Unlike the other proteins from the E3 gene, ADP is not under the control of

the E3 promoter. Instead, its expression is controlled by the same switch that activates late gene expression. This control by a late promoter makes ADP accumulate at a late stage of the infection. Expression of ADP does not directly influence the efficiency of viral replication within the cell, but it is required for efficient cell killing and release of virus from the cell. For a more complete overview of the E3 proteins and their interactions with the whole body immune system, see reviews by Burgert & Blusch[95] and Horwitz.[96]

1.1.7 VA-RNAI & II

The gene I will focus on in this project is Virus-Associated RNA I (VA-RNAI or VAI). VA-RNAI is transcribed by RNA polymerase III, which recognises its strongly conserved extra- and intra-genic promoter sequences.[97] The resulting single-stranded RNA molecule is 156 nucleotides long and GC-rich. It is neither polyadenylated nor translated and no additional post-transcriptional modifications have been reported. Instead the RNA folds into a complex secondary structure.[1]

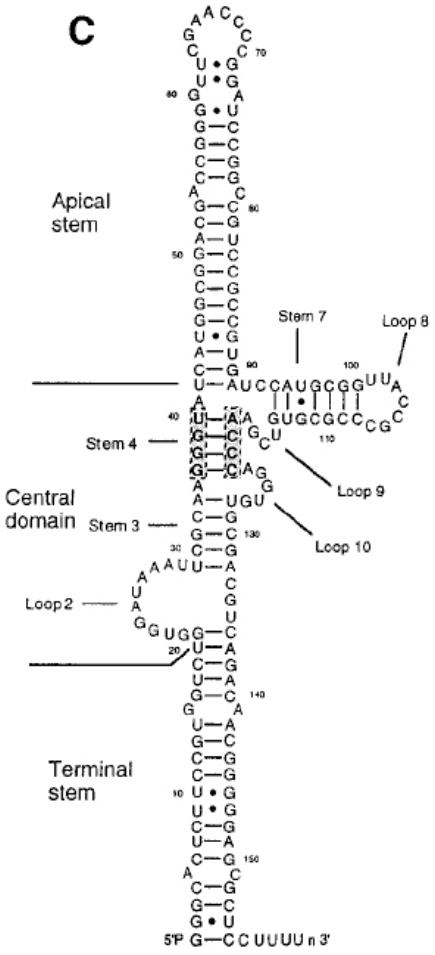

Figure 5 - Secondary Structure of VA-RNAI (from Ma & Matthews, 1996[1]). Structure shown is based on VAI from Ad2.

Expression of VA-RNAI begins relatively late in the replication cycle, as it is transcribed along with its neighbours in the L1 co-termination region. However, after expression begins VA-RNAI quickly accumulates to levels of up to 10^8 copies per cell.[98]

The predicted secondary structure of VA-RNAI is shown in Figure 5, reproduced from Ma & Matthews 1996.[1] Its main features are two imperfectly base-paired dsRNA stems and a more complex central domain containing several loop structures. The long stem regions are believed to be the primary binding sites recognised by host proteins, generally via dsRNA binding motifs. Once bound to its target host proteins, the central domain's loops are necessary for VA-RNAI's ability to inhibit its targets' primary functions. Known targets of this binding and inhibitory activity are discussed below.

1.1.7.1 VAI's known interactions with host proteins

PKR

As described above, PKR's normal role is to detect dsRNA produced from symmetrical transcription of viral genomes.[99] When activated by dsRNA, its activity leads to inhibition of translation and upregulation of pro-interferon and pro-apoptotic genes.

VA-RNAI binds to the dsRNA-Binding Motifs of PKR, inhibiting its autophosphorylation and activation.[100,101,102] Binding occurs via VA-RNAI's imperfectly base-paired long stem domains. Inhibition of PKR's function depends on an intact central loop domain.[103] The presence of VA-RNAI in stressed cells does decrease phosphorylation levels of PKR's target, eIF2α[104,105,106]. Unexpectedly, phosphorylation of eIF2α is not always associated with decreased viral replication.[106] This suggests that additional factors may influence this pathway.

2'5'-oligoadenylate synthetase

VA-RNAI binds to and activates 2-5(A) synthetase (OAS1). Mutational studies showed that VA-RNAI's activation of OAS1 is lessened by the mismatches in its dsRNA stems. However, the resulting activity of 2'5'-oas is sufficient to activate the RNAse L response described above.[107]

Adenosine Deaminase

VA-RNAI also interacts with dsRNA-specific adenosine deaminase (ADAR). VA-RNAI is able to bind to these and inhibits the enzyme's activity without becoming a substrate. Binding occurs by VA-RNAI's stem regions associating with ADAR's dsRNA-binding domains. The inhibitory behaviour is dependent on an intact central stem-loop region. This is reliant on different parts of the loop than inhibition of PKR.[57]

Interestingly, HCV replicon-infected cells transfected with VA-RNAI show greatly reduced rates of deamination and a consequent increase in viral gene expression and replication.[108] Although no work examining adenovirus's interaction with ADAR has been published, it seems plausible

that VA-RNAI could play a similar role in protecting adenoviral RNAs from ADAR.

Interferon Induction

VA-RNAI's interactions with the interferon response are complex. Evidence for its ability to suppress the interferon response has been published, with suggestions on the mechanism of this suppression.[109] Possible mechanisms include inhibition of PKR's ability to upregulate NF-κB.

Conversely, VA-RNAI has also been shown to induce interferon synthesis.[110] The mechanism of this was not determined, but was shown to be independent of IRF3. However, this was shown using VA-RNAI expressed from plasmid DNA rather than whole virus. Therefore it may not be representative of VA-RNAI's function during a normal infection.

RNA Interference

RNA interference (RNAi) is a normal cell response to dsRNA expression. The dsRNA is processed into short (21 to 23nt) fragments by an RNAse III enzyme called Dicer. The resulting "short interfering" RNAs (siRNAs) are incorporated into an RNA-Induced Silencing Complex (RISC). This complex goes on to degrade selectively any RNA molecules containing the same sequence, downregulating or silencing genes at the mRNA level.

Expression of VA-RNAI during adenoviral infection suppresses the RNAi response, reducing the pathway's efficacy at silencing genes. VA-RNAI is processed by Dicer and incorporated into the RISC apparently as normal. The inhibitory function may simply be due to very high levels of VA-RNAI saturating the RNAi pathway. This would block the normal functions by competitive inhibition, either at the level of Dicer's ability to process dsRNA into siRNA or formation of RISCs.

The significance of this effect on the course of adenoviral infection is unknown.[111]

1.1.7.2 Relationship with VA-RNAII

Several serotypes of adenovirus, including types 2 and 5, also carry the related gene VA-RNA II (VAII). This sequence is a similar length to VA-RNAI and shares 67% sequence homology.[109] The proposed structure is also similar (Figure 6), although a higher proportion of the predicted base pairs are mismatched. This increase in mismatched pairs may be responsible for VA-RNAII's relatively poor ability to bind PKR when compared to VA-RNAI. Although strongly conserved between several adenoviral serotypes, deletion of VA-RNAII gives no detectable phenotype.[1]

Expression of VA-RNAII is downregulated by an unknown function of VAI: certain mutations in the central loop domain of VA-RNAI result in a dramatic upregulation of VA-RNAII expression.[112]

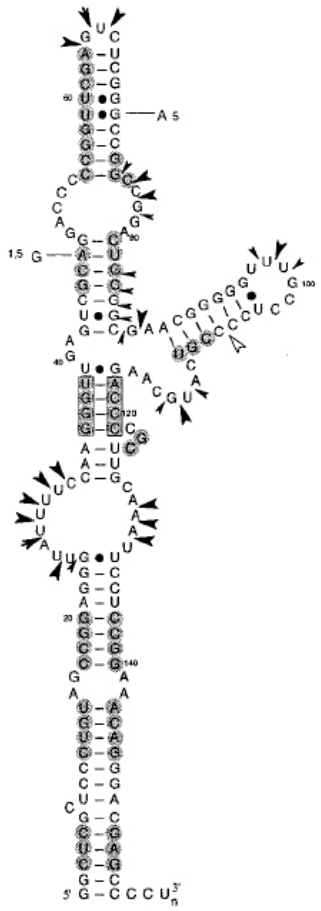

Figure 6 - Secondary Structure of VA-RNAII. Shaded areas indicate mismatched pairs. (Ma & Matthews 1996[1]). Structure shown is based on VA-RNAII from Ad2.

1.1.8 Adenovirus lacking VA-RNAI as a potential oncolytic therapy

1.1.8.1 Replication-selective adenovirus as a new therapeutic for cancer therapy

The replication cycle of normal cells is a tightly controlled process. In order to leave the quiescent G_0 state and progress to the replication cycle, the cell requires input from a range of signals including those from tyrosine kinase receptors, G-protein coupled receptors, TGF-β receptors, integrins and nutrient receptors. These extracellular signals are critical during most of G_1 phase. However, after 80-90% of a cell's time in G_1 has passed, the cell becomes committed to replication; all further checkpoints are solely based on internal conditions.

In cancer, cells have developed the ability to bypass the checkpoints governing the G_0-G_1-S phase transitions. Consequentially, these cells are constitutively able to synthesise protein and replicate DNA. Many cancers acquire additional mutations to inhibit apoptosis and overcome one or more of the internal checkpoints. These mutations make the developing cancer more resistant to pro-apoptotic or anti-proliferative signals, which may be generated by internal or external sources.

As described above, the first role of adenovirus's early proteins is to force the host cell into S-phase, while inhibiting the pro-apoptotic signals this activity generates. Several of the later genes (including VA-RNAI) are intended to prevent cellular inhibition of gene expression, whether at mRNA or protein level. Both of these functions are largely unnecessary in many cancers, as the cellular pathways responsible are already disabled.

More detailed understanding of adenovirus infections and of the molecular biology of cancer have led to the use of mutated adenoviruses as anti-cancer agents. The basis of this strategy is to produce viruses that are only capable of successful replication in cancer cells, either inhibiting their growth or killing them outright. Broadly, two strategies have been use to produce selective viruses: deletion of genes whose functions are crucial for

replication in normal cells but dispensable in cancer cells; and controlling viral gene expression with a tumour-specific promoter.

*dl*1520 (also known as "ONYX 015" and "CI-1042") is an adenovirus type 5 mutant lacking functional E1B-55k. As described earlier, this protein involved in shutdown of host mRNA export and protein synthesis. It also inhibits the activation of p53 and aids nuclear localisation of transcription factor YB1. Tumour cells commonly have inactivated p53 and high levels of YB1, so can be expected to compensate for E1B-55k's absence.[113]

Adenoviruses *dl*922-927 and Δ24 have deletions in the CR2 domain of E1A. This removes their ability to displace Rb, freeing E2F and pushing the cell into S-phase. Since cancer cells commonly have disrupted Rb pathways, this function is often dispensable. In contrast, replication in normal quiescent cells is seriously compromised for these viruses.

Tumour-specific promoters have been used to control expression of early genes, most commonly E1A or E1B. Expression of these viral transcription factors has been placed under the control of genes such as prostate specific antigen (PSA) to limit replication to prostate cells. A similar approach was to link E1A and E1B to the promoter for hTERT, the telomerase gene commonly upregulated in cancers.[114] Osteocalcin, tyrosinase, E2F-1 and Hypoxia-inducible promoters have all been used to target various cancers with varying degrees of success.[115]

Viruses constructed to use one or both of these techniques have shown good selectivity for cancerous tissues, and high safety levels in clinical trials. However, progression to use as a routine therapy has been hindered by low cytotoxicity.[116]

Several attempts have been made to increase the potency of these viruses. Various payload genes have been inserted to achieve this. Directly toxic genes such as fusogenic membrane glycoproteins have been used to kill infected tumour cells and their immediate neighbours.[117] An alternative approach is to upregulate lethal viral genes such as the Adenovirus Death Protein.[115] In a similar approach, *dl*337 is based on Ad5 lacking anti-apoptotic E1B-19k. This deletion resulted in increased cell killing through

virus-induced apoptosis.[118] Another possibility is the expression of enzymes locally to convert relatively harmless prodrugs to highly toxic drugs. The best characterised of these systems is the use of herpes simplex virus's thymidine kinase gene to convert ganciclovir to ganciclovir triphosphate, which inhibits DNA synthesis in the host and neighbouring cells. However, this combination has shown limited success in Adenovirus, possibly because activated ganciclovir inhibits the adenovirus vector's own ability to replicate.[115]

1.1.8.2 VAI-deleted Adenovirus as a potential therapeutic for cancer therapy

Adenoviral mutants lacking functional VA-RNAI are rendered sensitive to inhibition by interferon or other stress signals which lead to upregulation or activation of PKR.[119] Treatment of cells with 2-AP – which blocks PKR autophosphorylation and activation – rescues VAI-deleted virus's vulnerability.

Lack of VAI expression may lead to viral gene expression defects, or low levels of gene expression later in infection.[120] This is due to the production of unusual splice variants of viral proteins.[121] However, this effect was later shown to be only an indirect consequence of VA-RNAI deletion; VA-RNAI is not absolutely necessary for splicing to proceed correctly.[122]

Deletion of VA-RNAI leads to a six- to ten-fold reduction in the replication efficiency of adenovirus grown in certain cell lines.[123] In non-transformed cells, adenovirus lacking VAI and VAII shows a deficiency of over 100-fold when compared to wild-type virus.[112] This makes VAI-deleted Adenovirus an appealing candidate for use as an oncolytic vector.

Two groups have used the VAI-deleted type 5 adenovirus *dl*331 as a therapeutic vector. The first[124] targeted human pancreatic cancer cells xenografted into mice. This study found that *dl*331 was able to replicate selectively in and kill the cancer cells. The second study, published by our group,[104] targeted EBV-associated tumours. In this case replication in tumour cells was rescued by small EBV-associated RNAs, which are

similar to VAI in function. This suggests that VAI-deleted viruses could be effective agents against Epstein-Barr virus-associated cancers.

Efficient replication of VAI-deleted adenovirus correlates strongly – although imperfectly – with the host cell line's ras oncogene mutational status. Generally, replication of VAI-deleted adenovirus proceeds at high efficiency in cells carrying K-ras mutations, while replication in tumour and normal cells with wild-type ras pathways is strongly inhibited.[124] However, this association does not always hold true.[106] The molecular basis of VAI-deleted adenovirus's selectivity for cancer cells is not completely understood.

1.2 Functions and Regulation of Autophagy

1.2.1 Definitions – micro- and macroautophagy

Autophagy, named for the Greek "self eating", is a suite of processes through which cells degrade proteins collected from the cytosol. A study in L929 cells found that a typical cell maintains a population of $2.6x10^9$ proteins, and is capable of synthesising $4x10^6$ proteins per minute.[125] Maintaining this population requires constant degradation of unneeded proteins and organelles. The autophagic pathways are a major mechanism for this degradation, whose end products may be used as a source of amino acids or energy, or may be displayed to the adaptive immune system for immune surveillance of intracellular proteins. Versions of this behaviour are observed in a wide range of fungi, yeasts, plants and animals. The pathways are generally separated into two groups, microautophagy and macroautophagy.

1.2.2 Microautophagy

Microautophagy refers to the degradation of small components from the cytosol, taken up into lysosomes directly via invaginations of the lysosomal membranes. These invaginations bud off to form free vacuoles within the lysosome, and are degraded along with their contents.[79] Microautophagy is known to take two forms, "lead[ing] to the degradation of soluble components or to the selective uptake of entire organelles"[79]. Regulation of the first form of microautophagy appears to be largely dependent on the availability of nutrients to the cell. In yeast, for example, microautophagy is induced in response to nitrogen starvation, as reported by activation of the TOR and EGO signalling complexes. [126]

The second form of microautophagy, the degradation of organelles, appears to be very important. A well-characterised example of this process is the controlled lysosomal engulfment and destruction of peroxisomes in a process dubbed micropexophagy.[127] More recently, investigation is proceeding into the microautophagic degradation of exhausted mitochondria, "mitophagy". The exact regulation of this process is not yet

understood, especially the details of how lysosomes are able to recognise and specifically degrade exhausted mitochondria while allowing fresh mitochondria to survive. It has been shown, however, that fission followed by selective fusion of mitochondria leads to the accumulation of a mitochondrial sub-population with reduced membrane potential and displaying reduced levels of the fusion protein OPA1.[128] In yeast, other genes have been shown to be involved in this recognition and regulation, including Uth1p, Aup1p, Mdm38p and possibly YMe1p.[129] This regulation is quite complex and does not appear to be a simple starvation response. Rather, it appears to be a precisely regulated system that constantly monitors and regulates the mitochondrial population within the cell.[129,130]

1.2.3 Chaperone-mediated Autophagy

Chaperone-mediated autophagy is a major protelysis pathway in most cell types and particularly under conditions of nutrient starvation. Cytosolic proteins are recruited by chaperone molecules and transported to lysosomes, where they are unfolded and imported to the lysosomal lumen for subsequent degradation.

Most known substrates for chaperone-mediated autophagy (CMA) contain a peptide sequence related to the motif KFERQ.[131,132] These motifs may be a directly encoded part of a protein's sequence or the result of a post-translational modification. For example, oxidation and deamidation events that may occur as "wear and tear" during a protein's functions can contribute to creating these motifs.[133]

The constitutively expressed 70kDa heat shock protein hsc70 recognises a range of peptide motifs including the KFERQ motif and can stimulate protein translocation across membranes. However, hsc70 must first be activated by cochaperone molecules such as hsc40, which stimulates the necessary ATPase activity of hsc70. hsc70 and other cochaperones form a complex with a target protein in a reaction with hsc70 interacting protein (hip). hsp90, responsible for preventing unfolded proteins from forming aggregates in the cytosol, may also associate with this complex via the mediation of hsc70-hsp90 organiser protein (hop).[131]

The complexed target protein and chaperone proteins become associated with lysosome associated membrane protein 2A (LAMP-2A; CD107a)) at the lysosomal membrane. The unfolded protein is transported across the membrane into the lysosome in a process that requires ly-hsc70 (an acidic isoform of hsc70) to be present in the lysosome.[131,134]

Chaperone mediated autophagy is commonly upregulated under conditions of nutrient starvation and oxidative stress; loss of the pathway leads to the accumulation of damaged proteins and organelles, and to impaired homeostasis.

1.2.4 Macroautophagy

Macroautophagy is similar to microautophagy in that proteins or organelles are engulfed and eventually catabolised, often yielding amino acids and energy sources for the cell. However, where microautophagy begins with targets being taken up directly by lysosomes, macroautophagy begins with the formation of dedicated double-layered enclosures called "autophagosomes". These autophagosomes later fuse with lysosomes to become "autolysosomes" or receive input from the endosome pathway to become amphisomes.[135] In either case, the decreased pH and degradative enzymes released into the compartment degrade the contents to their constitutive parts. These amino acids, fatty acids, etc. are then typically released to the cytosol where they become available to the cell for use as metabolic components and energy sources. Alternatively, a proportion of the peptides from autophagosomes are displayed to the adaptive immune system to help surveillance of the intracellular environment. Both of these pathways will be discussed below.

1.2.4.1 Autophagosome Formation

Autophagosome formation begins at the phagophore assembly site (PAS). This site has been described as "a hybrid of the forming vesicle… and the core machinery proteins, the exact machinery of which depends on the stage of autophagosome formation."[136] A typical autophagosome has a

diameter of 0.4μm and can capture approx 0.1% of the cytosol.[137] A growing list of proteins are known to be involved in the formation and maturation of the autophagosome. First isolated in yeast and extensively conserved in mammals, these are known as the autophagy related genes (ATGs). A summary of their functions is listed in Table 2.

In yeast this PAS is a perivacuolar site, while in mammalian cells phagophore assembly does not appear to be restricted to a single location. The first stages of autophagosome formation in mammalian cells are known to require phosphatidylinositol 3-phosphate (PI(3)P) and to occur near the endoplasmic reticulum.[138,139] The role of the PI 3-kinases in maintaining the pool of PI(3)P is complex and not entirely understood. While class III PI 3-Kinases are required for the induction of autophagy, class I PI 3-Kinases are able to block induction of autophagy.[138]

Although the exact origin of developing autophagosomes has not been widely agreed upon, evidence has been published recently supporting the hypothesis that the membrane originates from the endoplasmic reticulum. During the early stages of autophagy, a PI(3)P-enriched compartment is formed; this compartment is dynamically connected to the ER.[139] The FYVE domain-containing protein 1 (DFCP1) was isolated based on its ability to bind PI(3)P *in vitro*.[140] During the formation of the PI(3)P-enriched compartment, DFCP1 translocates from the ER to this compartment, apparently via a contiguous membrane bridge, supporting the ER as the source of the forming autophagosome's membrane.[139]

Expansion of the autophagosome membrane then continues, elongating the structure before eventually closing the end and budding from the PAS. The forming autophagosome is structurally supported by ATG9, which may also be involved in trafficking new membrane to the developing structure.[141]

ATG8 (also commonly called LC3) is recruited to the membrane at high levels.[142,143] ATG8/LC3 is constitutively expressed and present in the cytosol of most cells in, until modified from this form (LC3I) to the lipid-conjugated LC3II by a complex of ATG3 and ATG5, after which it becomes embedded in the developing autophagosome membrane. LC3II

may play a structural role in the developing autophagosome, although its best-characterised function is recognising targets marked for degradation via its ubiquitin-like domain.[144,145,146]

Table 2 - Summary of known functions of autophagy genes in mammals

Gene	Protein Function
ATG1, ULK1	A Ser/Thr protein kinase found complexed with its substrate ATG13. Essential for mTOR-mediated autophagy induction.[147]
ATG3	A ubiquitin conjugating-like enzyme that attaches ATG8/LC3 to phosphatidylethanolamine
ATG4	Cleaves ATG8/LC3 ready for its interaction with ATG3
ATG5	Covalently attached to ATG12; this dimer binds ATG16 to form a trimer of unknown function
ATG6 / Beclin 1	A component of the class III PI 3-kcomplex required for initiation of autophagy
ATG7	A homologue of the ubiquitin-activating enzyme; it activates both LC3 and ATG12 before conjugation
ATG8 / LC3	After covalent attachment to a lipid by ATG3, LC3 is embedded into the forming autophagic membrane and assists in targeting proteins for degradation
ATG9	A transmembrane protein involved in delivering membrane to the forming autophagosome
ATG10	A ubiquitin-conjugating-like enzyme that covalently attaches to ATG12 and ATG5
ATG12	Structurally similar to ubiquitin; attaches to ATG5 and ATG16

NB: Information mostly from Rubinsztein *et al.* 2007.[148]

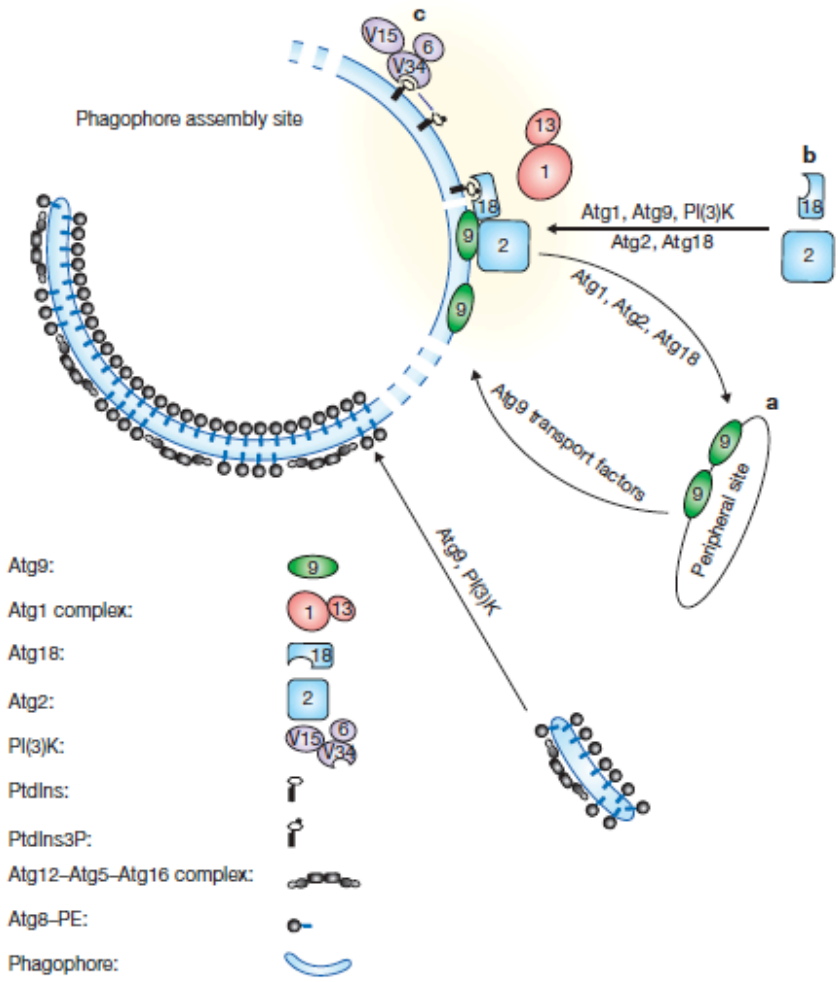

Figure 7 - Phagophore Assembly Site (PAS); figure excerpted from Xie and Klionsky 2007.[136]

1.2.4.2 Selection of autophagosome targets

At first it was assumed that uptake of cytosolic components to these autophagosomes was an entirely non-specific bulk degradation pathway.[149,150] However, more recent work has shown that it can be a precisely targeted process. In yeast, even during bulk autophagy certain proteins (e.g. catalase, Ald6, Lap3) are selectively targeted for autophagy.[151]

In higher eukaryotes, several distinct targeting systems have been identified and appear to show distinct functions.

Large aggregates of proteins can form within a cell as a result of protein misfolding, or simple over-abundance. This misfolding may be due to a transient problem with the synthesis pathways, or part of a more serious condition such as Parkinson's disease or Huntington's disease.

The formation of these inclusion bodies generally requires the multifunctional protein p62 (also known as A170/SQSTM1/sequestrome 1). p62 is able to directly bind LC3 and GABARAP family proteins along with K63-polyubiquitin chains. The structural basis of the binding of p62 to LC3 is well understood, having been solved by a combination of NMR spectroscopy, X-Ray crystallography and other biochemical techniques.[146] Its binding to these targets may serve dual purposes, facilitating the extension of the polyubiquitin chains and shuttling polyubiquitinated proteins for degradation. The degradation of these proteins was originally thought to be via the proteosome,[152] although it now seems more likely that p62 specifically targets K63-ubiquitinated proteins for autophagic degradation. Upon binding its targets, p62 is also able to polymerise to form large aggregates, which become inclusion bodies. Inclusion bodies containing p62 accumulate in autophagy-deficient cells and are reduced following the induction of autophagy.[153,154] This autophagic degradation of protein aggregates also appears to be necessary for clearance of plaques of α-synuclein and huntingtin in Parkinson's and Huntington's diseases, respectively.[148] This may have a protective effect, as deliberate induction of autophagy reduced the toxicity of mutant huntingtin in fly and mouse models of Huntington's disease.[155]

As an example of larger structures being selectively targeted by macroautophagy, yeast (*Saccharomyces cerevisiae*) under starvation conditions selectively degrades mature ribosomes.[156,157] Although some of this degradation may be part of a less specific bulk catabolic pathway, it seems that ribosomal subunits are specifically recognised and incorporated into the autophagosome for degradation, following target-specific ubiquitination and subsequent de-ubiquitination steps. Interestingly this process (referred to as "ribophagy") targets the ribosomal subunits at

different rates, leading to an imbalance. The consequences of – or a possible purpose for – this imbalance are currently unclear.

The increase in understanding of targeting during bulk macroautophagic degradation has led some to suggest that all macroautophagy might be specifically targeted.[151] At present, the evidence published does not seem sufficient to support that claim. It seems likely that at least some proportion of macroautophagy is bulk catabolism or, as will be discussed later, non-specific collection of cytosolic proteins for other uses such as immune surveillance.

1.2.4.3 Autophagy and Starvation

One of macroautophagy's best-characterised functions is as a catabolic pathway used to recycle cytosolic components for use as a source of metabolic precursors. Under nutrient-poor conditions, proteins and organelles are engulfed by autophagosomes and degraded. The breakdown products are then released to the cytoplasm.[158] This behaviour is strongly conserved across eukaryotes, having been observed in yeast (e.g. *Saccharomyces cerevisiae*), plants (e.g. *Acer pseudoplantanus*) and mulicellular animals. For example, *Caenorhabditis elegans* requires a functional macroautophagy pathway to enter the dauer diapause, a reversible developmental arrest brought on by limiting nutrient availability.[159] In mammals, autophagy is required to survive the early neonatal starvation period. This is the period between the sudden interruption of trans-placental nutrient supply at birth and the resumption of supply from milk. During this period, neonatal mice strongly upregulate autophagy in many tissues; knockout mice unable to induce autophagy starve within one day of delivery unless force-fed milk.[160,161]

In cells lacking the pro-apoptotic proteins Bak and Bax, withdrawal of growth factors lead to an inability to use extracellular glucose. In order to survive, cells upregulated macroautophagy and relied on the catabolism of cytosol components to maintain ATP production. Suppression of autophagy by RNAi or drug treatment lead to rapid cell death, confirming that

autophagy is essential for cell survival after growth factor withdrawal.[162] In mammals this regulation of autophagy in response to starvation is largely controlled by the mammalian target of rapamycin (mTOR) and its activators, notably the class I PI 3-kinase and Akt pathway.

1.2.4.4 Regulation of autophagy by mTOR

TOR kinase homologues function in a signal transduction pathway that is conserved from yeast to mammals.[163] This pathway integrates signals from the detection of nutrient and growth factor availability, calcium signalling within the cell and levels of energy (in the form of ATP) available to the cell.

In yeast, the proteins TOR1 and TOR2 are essential for progression through the G1 phase of the cell cycle.[164] These proteins are around 289kDa in size and highly homologous, at around 70% identical. Mammals share a single protein, mTOR, which is conserved up to 60% across the species studied to date.[165] TOR1, TOR2 and mTOR all contain a c-terminal kinase domain similar to Phosphatidylinositol 3-kinase and are, therefore, sometimes referred to as PI kinase-related kinases (PIKK). The target of this kinase is a (Ser/Thr)-Pro motif or a threonine flanked by large hydrophobic residues.[166]

Inhibition of the TOR proteins leads to accumulation of glycogen, repression of genes associated with growing cells and stimulation of genes associated with starvation, even under nutrient rich conditions. Inhibition of the TOR proteins also leads to the induction of autophagy.[167]

mTOR is found in two distinct complexes: mTORC1 and mTORC2. mTORC1 is composed of mTOR, raptor (regulatory associated protein of mTOR), PRAS40 and mLST8/GbL. mTORC2 is composed of mTOR, rictor (rapamycin-insensitive companion of mTOR), mSIN1, protor-1, mLST8/GbL and PRR5.[165]

mTORC2 is primarily involved in actin cytoskeleton organisation and cell survival. mTORC1 is primarily involved in regulating mRNA translation, cell cycle progression and autophagy.[168] Disrupting mTORC1

leads to the formation of new autophagosomes, and allows their elongation and maturation.

TOR and mTOR inhibit the formation of the Ser/Thr protein kinase complex composed of Atg1 Atg13 and Atg17. This effect is due to (m)TOR-dependent phosphorylation of Atg13, which prevents this complex from assembling[169] and prevents the recruitment of class III PI 3-kinase Vps34 to autophagic membranes. Atg1:Atg13 and Vps34 are required for the early stages of autophagosome creation and expansion.[169]

1.2.4.5 Autophagy in viral infections

The role of autophagy in immunity against intracellular pathogens has been discussed previously. Sections 1.1.5.7 (page 22) and 1.1.5.8 (page 23) discuss autophagy's role in intracellular and adaptive responses to pathogens, respectively.

Briefly, several systems exist within the cell to detect intracellular infections, such as the Toll-like receptors and dsRNA-activated kinases (see Figure 3, page 15).

Upon activation, the stress signals produced may lead to upregulation of macroautophagy. An example of this is the activation of dsRNA activated kinase PKR, resulting in phosphorylation of its target, eIF2α, and subsequent induction of macroautophagy.[75] Many viruses have evolved to prevent activation of this pathway. In Herpes Simplex Virus, deleting the protein ICP34.5 allows this induction of autophagy to proceed, resulting in the degradation of viral proteins within autophagosomes and marked reduction in neurovirulence.[74] In contrast, several RNA viruses – poliovirus, equine arterivirus and mouse hepatitis virus – appear to require the formation of autophagosomes (or autophagosome-like structures) for successful formation of replication complexes and therefore successful completion of replication.[77] Further examples and a more detailed discussion can be found in section 1.1.5.7, page 22.

Proteins from within autophagosomes can be passed to an endosome-like compartment known as the MHC Class II Compartment (MIIC or

CIIV). Within these compartments they can be processed for binding to MHCII, and thus presented on the cell surface to cells of the adaptive immune system. For a more detailed description of the molecular pathways and consequences of this activity, see section 1.1.5.8, page 23.

1.2.5 Autophagy and Cancer

1.2.5.1 Autophagy and tumour suppression

Beclin 1 is a key autophagy gene involved in the early stages of autophagosome formation. While it has no enzymatic activity of its own, it is able to bind the class III PI 3-kinase Vps34 and two regulatory proteins, pro-autophagic UVRAG and anti-autophagic Bcl-2.[168]

Beclin 1 is also a haploinsufficient tumour suppressor gene. It was found to be hemiallelically deleted in 40-75% of spontaneous human tumours from breast, ovary and prostate. In experiments in mice, homozygous deletion of the encoding gene BECN1 was embryonic lethal. Heterozygous mice showed reduced ability to induce autophagy and a higher incidence of spontaneous tumours.[170,171] Additionally, the anti-apoptotic oncogene Bcl-2 is known to bind Beclin 1 and inhibit its role in initiating autophagy, providing a possible mechanism for partial downregulation of Beclin 1 activity in some cancers.[172]

Further negative correlations between autophagy induction and cancer have been pointed out. For example, the importance of mTOR control in regulating the growth of cancer cells is well established and cellular proteins known to suppress mTOR (and therefore upregulate autophagy) such as PTEN and TSC are well known as tumour suppressors. Conversely, molecules involved in the activation of mTOR (and therefore downregulation of autophagy) such as class I PI 3-kinases and Akt are commonly upregulated in cancers.[171]

The relationship between autophagy and tumourigenesis is not firmly established. It can be expected that cells lacking efficient autophagy pathways will suffer more damage from various stresses, whether metabolic, chemical or from other sources, *e.g.* UV light exposure. Additionally, the basal level of autophagy is required for quality control of newly synthesised proteins and for homeostasis. Finally, an accumulation of exhausted mitochondria could lead to a build-up of reactive oxygen species within the cell. It has therefore been suggested that cells lacking an efficient

autophagic pathway would be more susceptible to accumulating the DNA damage that eventually leads to tumourigenesis. [173]

However, it has been extensively shown that cells defective for apoptosis or lacking growth signals are able to survive in environments with low nutrient or growth signal availability by relying on autophagy as a source of nutrients. These conditions are typical of those in solid tumours before the development of an adequate vascular structure.[158,160,161,162,171,173]

Additionally, some cancer cell lines are known to rely on autophagic mechanisms to survive challenge with certain chemotherapeutic drugs. It seems possible that selective pressure favours a loss or impairment of autophagy at early stages of tumourigenesis, but a recovery of these abilities in established tumours, although there is currently insufficient evidence to make a strong claim to this effect.

1.2.5.2 Autophagy protects cancer cells from starvation

Due to the increased replication and synthesis activities typical of tumour cells, their need for oxygen and nutrients is often higher than that of normal cells. Additionally, dysplastic development of the tumour tissue often creates an environment through which these metabolic components cannot diffuse efficiently. Developed tumours overcome this challenge by encouraging vascularisation around and sometimes within the tumour. Before this process has completed the tumour is often hypoxic and nutrient-poor, a challenging environment for rapidly dividing cells. Even once an adequate vasculature has been established throughout a tumour, it is still possible that dysregulated cell growth will disrupt the blood supply, again depriving of the tumour of sufficient nutrients and oxygen.[171,174]

The upregulation of autophagy in response to starvation has already been described above. While normal cells without specific growth signals would typically undergo apoptotic death in these conditions, this cell death pathway is frequently disabled in tumour cells. Instead, autophagy has been observed to be upregulated in starved cancer cells from several sources, and these cells survive considerably longer than normal cells when starved of

carbon and nitrogen sources. Inhibition of autophagy by RNAi knockdown of ATG genes or constitutive activation of class I PI 3-K removes this survival ability.[171]

1.2.5.3 Autophagy and chemotherapeutic drugs

Being involved in management of cellular stresses, autophagy plays a role in the reaction of several cancers to challenge with various drugs. As mentioned above, inhibiting autophagy in a mouse lymphoma model sensitised the cancer to transient induction of p53 or alkylating drug therapy.[175] A selection of the drugs known to induce autophagy in cancer cells is shown in Table 3, excerpted from Kondo *et al.* 2006.[176]

Table 3 - Cancer therapies linked to autophagy

Therapy (mechanism)	Cancer Cell Type
Tamoxifen (anti-oestrogen)	Breast
Ionising Radiation (DNA damage)	Breast, prostate, colon, malignant glioma
Arsenic trioxide	Malignant glioma
Temozolomide (DNA alkylation)	Malignant glioma
Resveratrol	Ovarian
Soybean B-group triterpenoid saponins	Colon
Vitamin D analogue	Breast
Rapamycin (mTOR inhibito)	Malignant glioma
Butyrate and suberoylanilide hydroxamic adic (HDAC Inhibitors)	Cervical, with Bcl-X_L overexpression
HDAC, Histone deacetylase; mTOR, mammalian target of rapamycin	

Table data from Kondo *et al.* 2006[176]

Although autophagy is observed in dying cells during treatment, it is not clear in all cases whether this is a route to cell death or a cell survival mechanism. For example, using 3-methyladenine to inhibit formation of new autophagosomes protected malignant glioma cells from treatment with Temozolomide (TMZ). Interestingly, treatment with bafilomycin A1, which

allows autophaghosomes to form but blocks their eventual fusion with lysosomes, increased the toxicity of TMZ in the same cell line.[176] This suggests a complex relationship between autophagy and TMZ in this particular cancer. Inhibition of autophagy by RNAi knockdown of ATG5, Beclin 1 and ATG7 restored the vulnerability of tamoxifen-resistant breast cancer cell lines to tamoxifen treatment.[171]

1.2.6 Inhibiting Autophagy

1.2.6.1 3-Methyladenine

As described previously, the induction of autophagy is dependent on the creation of a compartment enriched with Phosphatidylinositol 3-phosphate (PI(3)P) which recruits PX(Phox Homology) and FYVE-domain containing proteins to membrane compartments. 3-Methyladenine inhibits the activity of Class III PI 3-Kinase Vps34, thus blocking the creation of PI(3)P. This, in turn, blocks the formation of new autophagosomes, inhibiting the macroautophagy pathway.[169]

1.2.6.2 Chloroquinine

Chloroquinine is a lysosomotropic drug which appears to function by raising the lysosomal pH and thus reducing the efficiency of the lysosome's degradative enzymes. A consequence of this is the failure to degrade the contents of targeted autophagosomes efficiently. Blocking this final step in the autophagic pathway leads to an accumulation of defective autophagosomes. More importantly, it can lead to the death of cells reliant on autophagy for survival, e.g. cancer cells in nutrient-poor or ischemic tumour environments.[175] Mice carrying lymphoma rendered resistant to apoptosis by inactivating p53 were treated with Chloroquinine. This treatment significantly inhibited tumour growth, supporting the idea of autophagy being an important survival pathway for some tumour cells. In the same model, Chloroquine treatment also enhanced apoptotic tumour regression induced by transient reactivation of p53 and suppressed subsequent tumour recurrence.[175]

1.2.6.3 Amino Acids

One of the chief products of autophagy, amino acids, act to suppress further formation of autophagosomes.[177,178]

The presence of amino acids – particularly leucine or histidine[179] – stimulates the class III PI 3-kinase Vsp34. Activated Vsp34 upregulates the activity of mTOR, thus downregulating the creation of new

autophagosomes.[92,168]

Additionally, it is clear that at amino acids can inhibit autophagy in an mTOR-independent manner. In CRC12 myotubes, induction of autophagy appeared to be dependent on the production of PI(3)P and its interaction with Beclin-1; this activity was not stopped when mTOR was disrupted using rapamycin. In human colon cancer HK-29 cells, a further pathway was found: amino acids stimulated the inactivation by phosphorylation of the Erk1/2 mitogen-activated protein kinase (MAPK). This inactivation prevents MAPK from stimulating the GTPase-activating protein G alpha interacting protein (GAIP), thus leaving intact the inhibitory effect of trimeric Gi3 protein on autophagy.[92]

1.3 Detecting Autophagy

As a complex, multi-staged process controlled by several distinct pathways, monitoring the overall progression of a cell through autophagy is not a simple task. Many steps of the induction process have been considered as potential targets for an assay of autophagy induction. A recent review by Klionsky *et al.*[180] of targets attempted for use in an assay is reproduced in Table 4.

Many of these events have proven to be too challenging to monitor, to vary between cell lines and the means by which autophagy has been induced, or to lack specificity for the autophagic pathway. Therefore it has become common for groups showing induction or modification of autophagy to utilise several different assays to confirm the extent of autophagic induction and progression.[181,182,183] The more commonly used techniques in recent literature are discussed below.

Table 4 - A selection of assays used to detect autophagy.

Step of Autophagy	Assay	Represents / Requires
1. Induction	Atg8 synthesis	Signalling
	Atg13 dephosphorylation	Tor inactivation
	GFP-LC3	Signalling
	LCI conversion to LC3II	Signalling
	LysoTracker Red	Acidified compartments
	Monodansylcadaverine	Acidified compartments
2. Cargo Recognition / packaging	Ams1 activity	Atg19, Atg11, Cytoskeleton
	Ape1 processing / activity	Atg19, Atg11, Cytoskeleton
	Precursor Ape1 localisation	Atg19, Atg11, Cytoskeleton
3. Vesicle formation	Acridine orange	Vesicle formation machinery
	Active site CtoS	Atg7 activation, Atg3- Atg10 conjugation
	Atg1 kinase activity	Atg1, Atg11, Atg13, Atg17 function
	Atg8-GFP processing	Atg4 cleavage
	Atg12-Atg5 conjugation	Atg7-Atg10 conjugation
	Atg8-PE formation	Atg3 conjugation, Atg4, Atg7
	ATG8-PE membrane association	Atg3 conjugation, Atg4, Atg7
	AP formation / accumulation	Vesicle formation machinery
	Electron microscopy	Vesicle formation machinery
	GFP-Atg8 localisation	Atg3 conjugation, Atg4, Atg7
	GFP-LC3	Vesicle formation machinery
	LC3 C-terminal processing	Atg4 cleavage
	LysoTracker Red	Vesicle formation machinery
	Monodansylcadaverine	Vesicle formation machinery
	Protease-protection	AP/Cvt vesicle completion
	Sequestration of cytosolic markers	AP formation
4. Retrieval	TAKA assay	Atg1, Atg2, Atg13, Atg18, Atg23. Atg27, cytoskeleton
5. Fusion / Breakdown	AB/AP formation and accumulation	Atg15, Pep4, Prb1, Fusion machinery, Vacuolar pH
	Electron microscopy	Atg15, Pep4, Prb1, Fusion machinery, Vacuolar pH
	Fox3 degradation	Pexophagy
	GFP-Atg8 localisation	Atg15, Pep4, Prb1, Fusion

		machinery, Vacuolar pH
	GFP-Atg8/LC3 processing	Membrane delivery, AB lysis
	LC3II turnover	Complete autophagy
	Peroxisomal enzyme inactivation	Pexophagy
	Pex14-GFP processing	Pexophagy
	Pho8Δ60 activity	Bulk delivery
	Protein degradation	Bulk delivery
6. Efflux	Ape1 (or other protein) synthesis	Permease function

Table data from Klionsky et al. 2007[180]

1.3.1 LC3 modification and localisation

As discussed above, the modification of LC3I to LC3II is an essential step in the formation of autophagosomes in mammalian cells. During the extension of the membrane that will become the autophagosome, the modified form – LC3II – becomes embedded in the internal and external surfaces of the autophagic membrane.[136,142,144,145,184] This therefore makes LC3 an appealing target for measuring the formation and accumulation of autophagosomes. Of the homologues available in mammals, LC3B is the most commonly targeted.[185] The two major techniques for measuring the incorporation of LC3 into autophagosomes are Western blotting and confocal microscopy.

The principles of western blotting for conversion of LCI to LCII were recently reviewed by Mizushima and Yoshimori, 2007.[185] Probing a western blot membrane for LC3B yields two bands, at approximately 17 and 15 kDa, representing LC3I and LC3II respectively. This is represented in Figure 8.

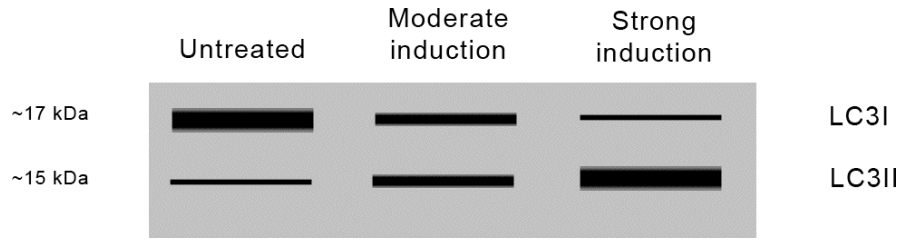

Figure 8 - Diagram of a typical Western blot result for LC3B.

The proportion of LC3I to LC3II in a resting cell varies between cell types; additionally, LC3II within an autophagosome is degraded when fusion with a lysosome converts the autophagosome to an autolysosome.[186] LC3II on the outer surface of the autophagosome may be recycled to LC3I. To further complicate the interpretation of this technique, LC3II may be more sensitive to immunoblotting than LC3I.[145]

Therefore the intensity of the lower band on the Western blot does not directly reflect the extent of autophagy induction in those cells. Rather, the

ratio of LC3I to LC3II in treated cells must be compared to the same ratio in resting cells. This comparison gives an indication of the increase in modification of LC3I to LC3II. This is often taken to be indicative of an increase in the rate of autophagosome formation. However, it is important to note that the same effect could be seen at endogenous levels of autophagy induction if the maturation and subsequent degradation steps are inhibited.

A possible solution to this problem is the inclusion of controls treated with bafilomycin or other agents that block the final stages of autophagy. This allows the effect of a block in autophagosome clearance to be observed and compared with the effect of the experimental conditions. For example, when autophagy is upregulated, a higher LC3II:LC3I ratio would be expected in cells exposed to the treatment and bafilomycin than in the cells treated with bafilomycin alone. Equal LC3II:LC3I ratios between these two samples would suggest that the increase is not due to induction of autophagy, but due to the failure to clear autophagosomes that are being formed at the usual rate.

Confocal microscopy had been used extensively to detect changes in the localisation of LC3. During the construction of an autophagosome, LC3 is recruited from its diffuse distribution in the cytoplasm to be packed relatively densely in the newly formed membrane.[145] Several groups have published work using cells transiently or stably transfected with a plasmid expressing a GFP-LC3 fusion protein under the control of a CMV promoter.[144,187]

This technique must be used with caution, however, as under some conditions over-expressed GFP-LC3 protein has been shown to form aggregates in the cytoplasm. This behaviour is not entirely unexpected, as many other proteins have been shown to form aggregates when overexpressed under various conditions.[188] These aggregates of GFP-LC3 can resemble small autophagosomes under confocal microscopy, but occur independently of autophagy induction.[187] Similar puncta may be formed or enhanced in fixed cells when treated with various detergents to permeabilise membranes in preparation for immunoblotting.[189] Additionally, GFP-LC3

has been shown to associate with organised smooth endoplasmic reticulum membranes independent of autophagy induction; by contrast, unmodified LC3 does not associate with this type of membrane at any stage.[190]

Several antibodies specific to LC3 and suitable for confocal microscopy have recently become commercially available, and have now been used by several groups to visualise endogenous LC3 expression and localisation. An example of this staining, taken from my own data, is shown in Figure 9. As expected from the varying levels of LC3II shown by Western blots, different cell types display differences in LC3 distribution at rest and after induction of autophagy.

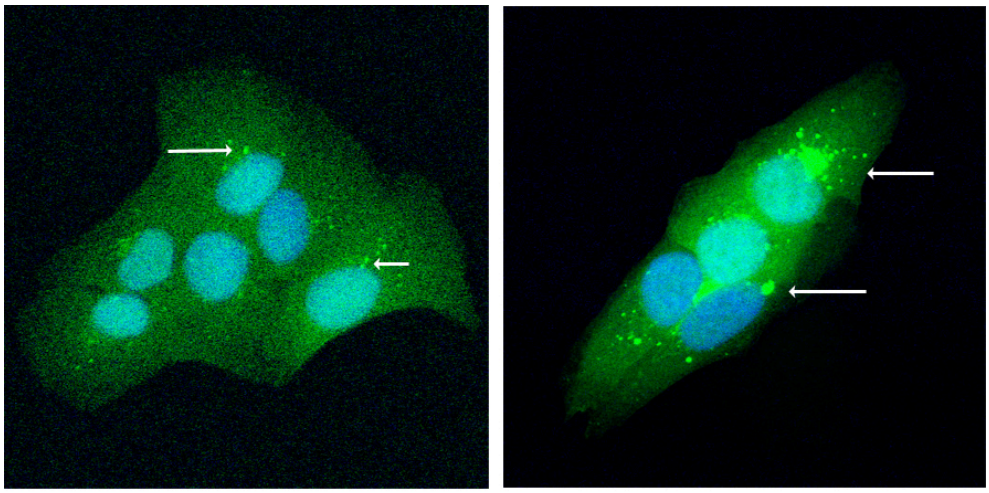

Figure 9 - LC3 immunofluorescence to visualise autophagosomes. Cells in the right column were infected with *dl*331 and fixed after 28 hours.

It should be noted that, as this method visualises the accumulation of autophagosomes based on detecting LC3, it might be expected to lose efficacy in detecting autolysosomes, whose internal LC3 is subject to rapid degradation. Additionally, the number and size of autophagosomes present in a cell do not necessarily reflect the rate of autophagic degradation. It is possible that a cell containing a large number of autophagosomes is forming them at its normal background rate, but the clearance of the autophagosomes is being somehow inhibited.

1.3.2 p62 accumulation

A common fate for misfolded or denatured proteins within the cell is to become insoluble and form aggregates, which may grow to form large inclusion bodies. This is especially true for ubiquitinated proteins and LC3.[188,191] This behaviour is exemplified by the tendency of overexpressed GFP-LC3 to form large punctate structures, as described in the previous section.

The formation of these inclusion bodies requires the multifunctional protein p62 (also known as A170/SQSTM1/sequestrome 1). p62 is able to directly bind LC3 and GABARAP family proteins along with K63-polyubiquitin chains. Its binding to these targets may serve dual purposes, facilitating the extension of the polyubiquitin chains and shuttling polyubiquitinated proteins for degradation. The degradation of these proteins was originally thought to be via the proteosome,[152] although it now seems more likely that p62 specifically targets K63-ubiquitinated proteins for autophagic degradation. Upon binding its targets, p63 is also able to polymerise to form large aggregates, which become inclusion bodies. Inclusion bodies containing p62 accumulate in autophagy-deficient cells and are reduced following the induction of autophagy.[153,154]

Accumulation of p62 has therefore been used as an indicator of inhibited autophagy, although measuring the half-life of p62 after treatment may give more meaningful results. Live-cell imaging of p62 to detect formation, trafficking and degradation of inclusion bodies is also possible; a thorough review of these methods has been published recently.[192]

Similar to p62 is the recently described protein NBR1 (neighbour of BRCA1 gene 1). NBR1 carries LC3- and Ubiquitin-binding domains and is found recruited to inclusion bodies, which are eventually targeted for degradation by autophagy. This behaviour can occur in co-operation with p62, with which it can form oligomers, although p62 is not required for NBR1 to function.[193] This makes NBR1 an appealing target to measure autophagy using similar techniques to p62. However, at the time of writing

no groups have published evidence confirming its utility as a marker of autophagic degradation.

1.3.3 Acridine Orange

When applied to cells, Acridine Orange fluoresces green when in contact with dsDNA, dim orange when bound to ssRNA or bright red when in acidic compartments such as lysosomes or late stage autophagosomes (autolysosomes).[193] The upregulation of autophagy correlates with the appearance within the cells of acidic vesicular organelles (AVOs), presumably lysosomes prepared in readiness for fusion with autophagosomes to form autolysosomes.[180] Several groups have therefore used Acridine Orange staining as a measurement of autophagy upregulation.[182,183,194]

No consensus seems to have been reached on the best application of this technique. Confocal microscopy has been used to count the mean number of AVOs per cell, or to count cells containing more than a threshold level of AVOs. Alternatively, flow cytometry has been used to detect the overall intensity of red signal emitted by each stained cell. These data are then analysed by either counting the number of cells whose signal exceed a given threshold, or by comparing the ratio DNA:AVO (green signal:red signal) of cell populations.

It must be noted that, as early autophagosomes are generally not acidic, this staining is not specific to autophagosomes. While autophagy upregulation does entail the productions of AVOs, these methods are best used in conjunction with a more specific assay for autophagic flux, such as LC3 localisation or processing.

1.3.4 Monodasylcadaverine (MDC) staining

The autofluorescent compound monodasylcadaverine (MDC) was originally suggested as a specific stain for autophagic components in 1995 by Biederbick *et al.*[195] Later work in Chinese hamster ovary (CHO) cells demonstrated that many MDC-stained vesicles are acidic and that MDC

staining typically accumulates in vesicles labelled with GFP-LC3, presumably autophagosomes.[196]

Numerous investigators have since used MDC staining to detect autophagy and reported good specificity and selectivity for this dye in animal[197] and plant[198] cells.

This accumulation is reliant on two separate mechanisms. Firstly, MDC's negative charge causes it to become trapped in acidic vesicles; the resulting change in charge may alter its fluorescence slightly through a pH-dependent Stokes shift. Secondly, MDC shows increased fluorescence in a hydrophobic environment typical of the lipid-rich autophagosome environment. Together, these characteristics cause MDC to localise to, and fluoresce most brightly from, autophagosomes.[199]

However, others have reported problems with MDC's specificity. Bampton *et al*. showed that MDC stains double-membraned acidic lysosomes and endosomes, including but not exclusively autolysosomes. This staining was still visible where autophagy had been inhibited by homozygous ATG5 deletion; additionally, MDC staining did not always co-localise with LC3-positive enclosures in mouse embryonic fibroblasts (MEFs).[200] It is worth noting that this lack of specificity was observed only in living cells, and is presumably due to MDC accumulating in lysosomes and late endosomes due to ion trapping of MDC in the low-pH environments. In fixed cells the pH gradient should no longer be present, causing the MDC to accumulate only in lipid-rich structures such as autophagosomes and other lamellar bodies. Comparison of live and fixed staining of the same field on a coverslip appears to support this, showing that some vesicles stained in living cells are not stained when the same cells are fixed and re-treated with MDC.[201]

Replacing the primary amino group of MDC with the non-polar dansylamylamine to create monodansylamylamine (MDH) removes MDC's tendency to accumulate in low-pH environments, improving its specificity for lipid-rich structures such as autophagic vesicles.[201]

1.3.5 Radiolabelled protein degradation

Autophagy is just one of several distinct pathways responsible for degradation of cellular proteins. However, while the proteosome and various proteases seem to target short-lived proteins, autophagy is generally used to degrade relatively long-lived proteins. This distinction makes it possible to use long-lived protein degradation as a proxy measurement of the overall functioning of the autophagy pathway.[180,202]

The typical approach is to grow cells in media containing one or more radiolabelled amino acid(s), such as [^{14}C]Valine or [^{3}H]Leucine. After an incubation of 10-16 hours, cells are restored to normal growth media and incubated for a suitable time to allow turnover of short-lived proteins. Once the short lived proteins have been degraded and excreted from the cells, the slower degradation of labelled long-lived proteins can be monitored by measuring the change in radioactivity of washed cell pellets.[180,202]

With this technique it is important to note that high amino acid concentrations in growth medium have been shown to inhibit autophagy induction. Of the labelled amino acids commonly used in this technique, [^{14}C]Valine is likely to be the preferable choice, as high Leucine concentrations may be a more powerful inhibitor of autophagy induction.[178,180,202]

2 Materials and Methods

2.1 Cells and media

2.1.1 Tumour cell lines

Cell line	Tissue type	Cultured in
HCT116	**Colorectal**	**E4 + 10% FCS**
MiaPaCa-2	**Pancreatic**	**E4 + 10% FCS**
Suit-2	**Pancreatic**	**E4 + 10% FCS**
PANC-1	**Pancreatic**	**E4 + 10% FCS**
A549	**Alveolar epithelial**	**E4 + 10% FCS**

2.1.2 Normal cells

Normal Human Bronchial Epithelial (NHBE) cells were bought from Cambrex Biosciences. They were cultured following manufacturer's instructions, and fed with BEGM every other day.

Prostate Epithelial Cells (PrEC) were bought from Cambrex Biosciences. They were cultured following manufacturer's instructions, and fed with PrEGM every other day.

2.2 Viruses

Ad5 – Wild-type class C adenovirus

***dl*309** – Based on Ad5, partial E3 deletion, specifically E3 10.4kDa, 14.5kDa and 14.7kDa are deleted; E3 6.7kDa lacks two internal amino acids.[203]

***dl*331** – Originally constructed from *dl*327, an Ad5-based virus with a large deletion having removed the E3 region. In addition to this E3 deletion, *dl*331 has a 29bp deletion in the intragenic promoter of VA-RNAI.[121]

2.3 Virus Production

2.3.1 Acknowledgement

The viruses used in this work – Ad5, *dl*331 and *dl*309 – were bulked up from pre-existing laboratory stocks by Jennelle Francis and Katrina Sweeney, who were also responsible for their purification and initial titres. The following, up to and including the measurement of infectious titre, is a description of their methods.

2.3.2 Initial expansion

For production of Ad5 and *dl*331, A549 cells were grown in E4 + 10% FCS to a confluence of 90%. When producing *dl*309, 293 cells were used instead. Infection medium was made by adding 30μl of purified virus stock to 30ml E4 + 2% FCS. Medium was aspirated from the A549 cells and replaced with the infection medium. After 48 hours of incubation at 37°C, cells are checked for cytopathic effect (CPE). If CPE is not visible, cells were incubated for a further 24 hours.

Once cells have detached, they are harvested. The cell suspension was transferred to a 50ml centrifuge tube and freeze-thawed three times using liquid nitrogen and a water bath at 37°C.

2.3.3 Second expansion

When producing Ad5 and *dl*331, four T-175 flasks of A549 cells were used to seed a CF-10™. When producing *dl*309, 293 cells were used instead. A parallel culture in a single T-175 flask was seeded at the same cell density as the CF-10 and kept under identical conditions. Both cultures were incubated at 37°C for 48 hours. Once the cells in the parallel culture reached 90% confluence, the CF-10™ was infected with the freeze-thawed cell suspension. The infected CF-10 was incubated for 48-72 hours, until extensive cytopathic effect (CPE) was visible and cells were floating. The suspended cells were then collected, pelleted by centrifugation at 2000 rpm and re-suspended in 15ml cold PBS. The cells were pelleted again, then re-suspended in 12ml of cold 10mM Tris.HCl at pH 8.0.

2.3.4 Purification

The concentrated cell suspension was freeze-thawed three times using liquid nitrogen and a 37°C water bath. This lysate was then spun at 6000rpm for 10 minutes to remove cellular debris. The supernatant was layered onto a CsCl concentration

gradient (upper layer at 1.25g/ml, lower layer at 1.4g/ml). Centrifuging this at 25,000rpm for 2 hours banded the purified virus particles between the two CsCl layers.

This purified virus was extracted from the tube and layered onto 4ml of 1.35g/ml CsCl solution. This was then centrifuged at 40,000rpm for 15 hours and the resulting band collected. This purified virus was diluted with TSG buffer (Table 5) to 12ml and injected into a slide-a-lyzer dialysis chamber. This is then stirred in 2 litres of dialysis solution (Table 6) for 24 hours to remove CsCl from the virus stock. The concentrated, purified virus stock is stored at -80°C.

Table 5 - TSG Buffer: Combine 700ml of solution A with 3.5ml of solution B and 300ml Glycerol. Heat together and filter to sterilise.

Solution A		**Solution B**	
Stock Solution	**Final Concentration**	**Stock Solution**	**Final Concentration**
Distilled Water	**---**	**Distilled Water**	**---**
NaCl	**137mM**	**$MgCl_2$**	**98mM**
$NaHPO_4$ (dibasic)	**0.7mM**	**$CaCl_2$**	**136mM**
0.3g KCl	**4mM**		

Table 6 - Dialysis solution to remove CsCl from purified virus stock

Stock Solution	**Final Concentration**
1M Tris.HCl pH7.4	**10mM**
1M $MgCl_2$	**1mM**
5M NaCl	**150mM**
Glycerol	**10%**
Sterile Distilled Water	**---**

2.4 Determination of viral titre

Purified virus stocks were titrated using two methods, to determine particle count and concentration of viable particles.

2.4.1 Particle count

Two dilutions of virus in a lysis buffer were prepared along with a virus-free "blank" solution (Table 7).

Table 7 - Viral solutions used for measurement of particle counts by spectrophotometry

	Blank	**A**	**B**
Virus	**-**	**100µl**	**200µl**
Dialysis Buffer	**200µl**	**100µl**	**-**
Lysis Buffer	**200µl**	**200µl**	**200µl**
Water	**600µl**	**600µl**	**600µl**

These samples were heated to 56°C for 10 minutes then allowed to cool to room temperature. Using the blank sample as a reference, the absorbance of each sample was measured at 260nm and the particle count determined by the formula:

OD_{260} x dilution factor x $1.12x10^{12}$ = number of particles per millilitre.

NB:

$1.2x10^{12}$ is the extinction coefficient.

Samples A and B have dilution factors of 10 and 5 respectively.

2.4.2 Infectious Titre

The number of plaque-forming units (pfu) per millilitre was measured by a limiting dilution assay. 293 cells (or A549 cells for *dl*309) were plated into triplicate 96-well plates at 10,000 cells/well. After overnight incubation, the viral sample was serially diluted down these plates in steps of 10-fold dilution. After 11 days of incubation, wells were examined microscopically for evidence of cytopathic effect (CPE). This includes swollen, detached and dead cells. The number of wells showing CPE at each dilution was entered into the $TCID_{50}$ calculation to determine pfu/ml.[204]

2.5 Virus Replication Assay

2.5.1 Infecting cells and collecting viral lysates

Cells to be assayed were grown to 80% confluence in tissue culture-treated flasks. Cells were then trypsinised and plated in 6-well plates at $3x10^5$ cells per well. Only three wells on each plate were seeded, to minimise risk of splashing medium between wells when harvesting. Three wells were seeded for each combination of virus and timepoint; and additional three wells were seeded for cell number controls.

After incubating for 24 hours in standard conditions, cells from three wells were trypsinised and counted. Based on this cell count, the remaining wells were infected with virus at 100 pt/cell, diluted into 1ml of serum-free medium per well.

Cells were incubated at 37°C in this infection medium for two hours. After this time, the medium was removed, and cell monolayers rinsed with warm PBS. Cells were then covered with 2ml of E4 + 5% FCS and returned to the incubator.

Cells and medium were harvested at 24-hour timepoints, by scraping into cryogenic tubes. These were stored at -80°c until all samples were collected.

2.5.2 Measuring viral yield by $TCID_{50}$ assay

A549 cells were grown to 80% confluence, then trypsinised and re-plated into 96-well plates at 10,000 cells/well. Each well contained 190µl medium. Viral lysates were recovered from storage at -80°C, then freeze-thawed three times using liquid nitrogen and a 37°C water bath. Each sample was diluted 1/100 into 5ml serum-free E4. Each of these diluted viral lysates was then serially diluted in 1/10 steps down three of the replicate 96 well plates (Figure 10).

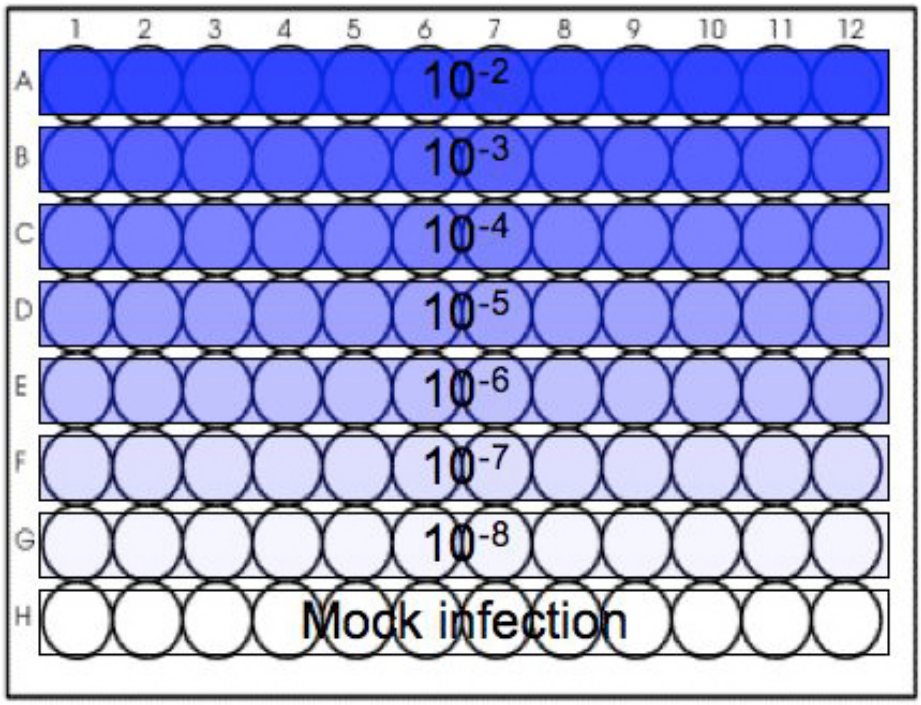

Figure 10 – Plate layout for serial dilution down $TCID_{50}$ plates.

These plates were then incubated for ten days. On the 11th day post-infection, each well was examined for CPE. The total of wells showing CPE in each row was used to calculate the viral yield. The method used was to calculate the dilution at which 50% of wells showed cytopathic effect (CPE). This is the tissue-culture 50% infectious dose, $TCID_{50}$..[204]

2.6 Virus Cytotoxicity Assay

Cells to be assayed were grown to 80% confluence, then trypsinised and re-plated into 96-well plates. Cells were typically seeded at 10,000 cells/well in 90µl of E4 + 5% FCS. Fast-growing cells were seeded at lower densities, chosen so uninfected wells will reach confluence 5 days post-infection.

One edge column of wells contained medium but no cells, to act as a blank for the spectrophotometer. The other edge wells were filled with PBS to prevent evaporation from the sample wells. Triplicate plates were infected with serially diluted virus, leaving a row of uninfected cells to act as a negative control. See Figure 11 for layout.

Six days post-infection, 20µl of MTS was added to each well. Plates were then incubated at 37°C for 2 hours. The optical density of each well was then measured at

490nm using a 96-well plate reader. This was then analysed using a customised Excel spreadsheet and Prism statistical software to calculate the EC_{50} for each virus.

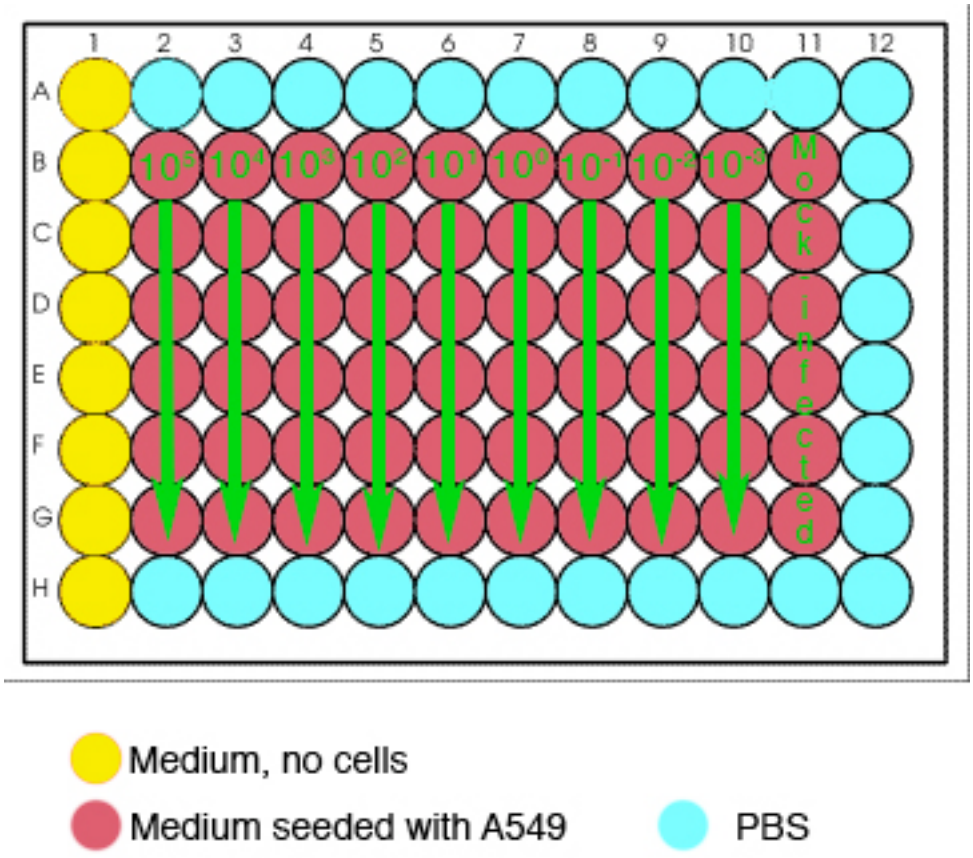

Figure 11 – Viral Toxicity assay plate layout. Green numbers refer to concentration of virus in particles / cell.

2.7 Protein Expression Assay (Western Blotting)

2.7.1 Preparation of whole cell extract

Cells were grown to 80% confluence in 6cm circular dishes, then infected with virus at 100 pt/cell. Cells were harvested by trypsinisation, then re-suspended in E4, 10% FCS to deactivate the trypsin. Cells were then rinsed with PBS, pelleted and the pellets lysed with 200µl of ice-cold RIPA (RadioImmunoPrecipitation Assay) buffer (Table 8), prepared by dissolving one protease inhibitor tablet into 10ml of buffer.

Lysed cells were incubated on ice for 30 minutes with occasional agitation, then centrifuged at 12000rpm for 15 minutes at 4°C to pellet cell debris. The supernatant was then stored at -80°C before assaying for concentration and immunoblotting.

Table 8 - 5x RIPA reducing cell lysis buffer. This must be diluted 1/5 in water, and one protease inhibitor tablet added to 15ml

Reagent	Final concentration
NaCl	**0.75M**
NP40	**5%**
Deoxycholic Acid	**2.5%**
SDS	**0.5%**
Tris pH 8	**0.25M**
Distilled Water	**-**

2.7.2 Preparation of nuclear and cytoplasmic extracts

Nuclear and cytoplasmic protein lysates were extracted using the NuCLEAR Extraction Kit (Sigma UK). Cells were grown in 6cm dishes to 80% confluence, then infected at 100 pt/cell as described above. The manufacturer's protocol was followed to lyse cell membranes, extract nuclei then treat each fraction in preparation for analysis by western blotting.

2.7.3 Concentration of proteins from culture medium

Cells were grown and infected as described in "Preparation of whole cell extract", above. 5ml of medium was collected at each timepoint and stored at -80°C.

When all samples had been collected, medium was filtered by centrifugation through Centricon 10,000D filters. Centrifugation was at 5000g for approximately 80 minutes at 4°c. Filtered medium was discarded; the remaining medium (approx. 1/10th of original volume) was treated as a cell suspension. RIPA buffer carrying protease inhibitors was added to ensure ideal conditions for subsequent electrophoresis.

2.7.4 Bradford Assay

Protein concentration of lysates was assessed using the Bradford Assay. 30µl of each lysates was pipetted into a separate cuvette. Pre-made Bradford Reagent (Bio-Rad) was diluted to 1x concentration. 1ml of this was added to each cuvette, and incubated at room temperature for 5 minutes. After this incubation, absorbance was measured at 595nm. These values were compared to a standard curve of 0, 1, 2, 5, 10 & 20µg of bovine serum albumin (e.g. Figure 12). Protein lysates were then diluted to give a standard protein concentration for every well on a gel.

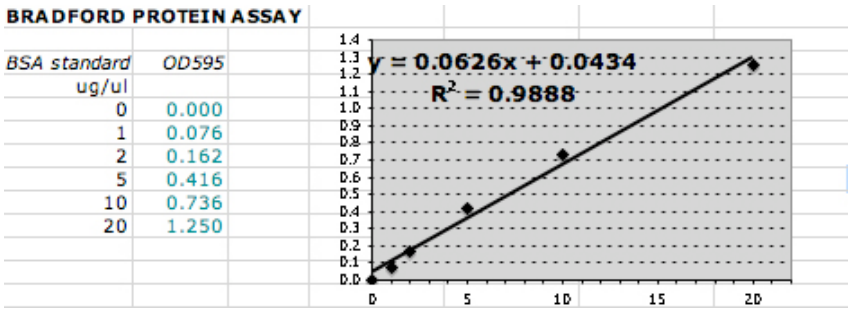

Figure 12 - Typical standard curve from Bradford protein concentration assay.

2.7.5 PAGE and Immunoblotting

Samples were mixed with 5x loading buffer

Table 9) and heated to 100°C for 5 minutes. Poly-acrylamide gels were poured using the mixtures listed in

Table 10. When both layers were set, samples mixed with loading buffer were loaded into wells. Gels were run at 0.2A per gel. Amersham's Rainbow Molecular Weight Marker was used to monitor progress through the gel and to estimate protein sizes.

Table 9 – 5x Loading buffer for PAGE

Reagent	Final concentration
Tris.HCl pH 8	225mM
Glycerol	50%
SDS	5%
Bromophenol Blue	0.05%
DTT	250mM
Water	-

Table 10 – Poly-acrylamide Gel mixtures

Running Gel		Stacking Gel	
Reagent	Volume	Reagent	Volume
Protogel 8 (National Diagnostics)	2.3ml	Protogel 8 (National Diagnostics)	0.39ml
4x Resolving Gel (National Diagnostics)	1.75ml	Stacking Buffer (National Diagnostics)	0.75ml
Distilled Water	2.842ml	Water	1.83ml
TEMED	7µl	TEMED	3µl
10% Ammonium Persulphate	70µl	10% Ammonium persulphate	15µl

After separation by mass, proteins were transferred from gel to PVDF membranes by semi-dry electroblotting. Damp membrane was laid over the gel, and this was then covered with filter paper soaked in transfer buffer. A potential of 50v was then applied for 45 minutes, causing the protein to migrate out of the gel onto the membrane. The membrane was then covered in 5% milk powder in TBS-T for 30 minutes at room temperature or overnight at 4°C to block.

Blocked membrane was then transferred to a falcon tube with 10ml of primary antibody solution (see Table 11) and gently agitated for 1.5 hours. The membrane was then rinsed twice in TBS-T before two longer washing steps of 5 minutes' agitation in TBS-T. Secondary antibody was then washed over the membrane for 45 minutes, followed by another wash as before.

Bound antibody was visualised using an ECL biotin detection kit. The two kit solutions were mixed in equal proportion and used to cover the membrane surface. After one minute, excess solution was shaken off. Photographic film was then exposed to the membrane in a film cassette. After exposure (varying from 30 seconds to 5 minutes), membranes were developed using a Fuji automated developer.

2.7.6 Antibodies

Table 11 - Antibodies used in immunoblotting

Antigen	Raised in	Source	Lot Number
RIG-i	**Rabbit**	**Tadaatsu Imaizumi's lab***	**--**
IFNβ	**Rabbit**	**Santa Cruz Biotechnology**	**A0203**
IFNβ	**Rabbit**	**Abcam**	**199168**
PKR	**Rabbit**	**Santa Cruz Biotechnology**	**G3103**
PKR[pT^{451}]	**Rabbit**	**Abcam**	**257820**
IRF-3	**Rabbit**	**Abcam**	**203324**
eIF2α[pS^{52}]	**Rabbit**	**Invitrogen**	**AHO0802**

*NB: anti-RIG-i antibody was a generous gift from Tadaatsu Imaizumi at the Hirosaki University School of Medicine, Japan.

2.7.7 Membrane Stripping

Stored membranes were stripped of antibody using the membrane stripping buffer described in Table 12. Membranes to be stripped were washed in TBS-T for 10 minutes. Membranes were then submerged in stripping buffer and incubated at 50°C for 30 minutes. After stripping, membranes were washed twice in TBS-T before blocking in 5% powdered milk in TBS-T.

Table 12 - Membrane Stripping Buffer

Reagent	Final Concentration
β-mercaptoethanol	**100 mM**
SDS	**2%**
Tris-HCL pH 6.7	**62.5mM**
Distilled Water	**-**

2.8 mRNA expression assays

2.8.1 RNA extraction

Whole RNA was extracted from cells using TriZOL reagent (Invitrogen). As described above, $3x10^5$ cells were seeded into 6-well plates, incubated overnight and infected at 100 pt/cell. Two wells were seeded and infected for each sample. At appropriate timepoints, medium was aspirated from both wells and 0.75ml of TriZOL pipetted onto each monolayer. These samples were combined and stored at -80°C until all samples had been collected. After thawing to room temperature, manufacturer's instructions were followed to extract and ethanol-precipitate nucleotides from the sample.

2.8.2 Assessment of RNA purity

The yield and purity of extracted nucleotides were assessed using the Nanodrop spectrophotometer. 1.5µl of each sample was used for the measurement; DEPC-treated water was used to blank the device.

The information returned was:

- Absorbance at 260nm (A260)
- Concentration in ng/µl (Calculated from A260)
- A260/230, an indication of phenol or similar compound contamination
- A260/A280, an indication of protein contamination

Generally, an A260/230 of over 1.9 was considered to be pure. Similarly, an A260/A280 over 1.8 was considered pure.

2.8.3 Assessment of RNA integrity

Purified nucleotides (from RNA extractions or PCR products) were visualised using RNAse- free agarose gel electrophoresis, stained with ethidium bromide. Whole RNA was assessed for integrity by running a small sample (3-4µl) in a 1% TBE gel, made with DEPC-treated water. The expected result for intact RNA was two sharp bands representing 28s and 18s rRNAs. Degradation of the RNA sample results in smearing of these bands.

2.8.4 RT-PCR

DNA was digested using RNAse H and buffers supplied by QIAGEN. After inactivation of RNAse, reverse transcription was performed using the Superscript II

enzyme and buffers kit, also supplied by QIAGEN. Random primers were used, to allow transcription of rRNA and VA-RNAI. Reactions were based on a starting template of 2μg total RNA.

PCR to detect IFNβ mRNA was based on the primers listed in Table 11. GAP-DH was used as an endogenous control. The PCR was performed using Taq polymerase and buffers from QIAGEN. Concentrations of reagents used are listed in Table 13; Primer sequences and melting temperatures are listed in Table 14. PCR products were visualised on 2% agarose TBE gels.

Table 13 - Reagent concentrations for PCR

Reagent	**Volume for IFNβ PCR**	**Volume for GAP-DH PCR**
10x PCR Buffer (2.5mM $MgCl_2$)	**5 μl**	**5 μl**
10mM dNTPs	**1 μl**	**1 μl**
Primers mix	**5 μl (to 3 μM each)**	**5 μl (to 3 μM each)**
Taq	**0.25 μl**	**0.25 μl**
H_2O	**28.75 μl**	**28.75 μl**
Template (product of RT reaction)	**5 μl**	**5 μl**
Total volume	**50 μl**	**50 μl**

Table 14 - Primers for PCR to detect IFNβ mRNA

Gene	Forward Primer	Reverse Primer	Melting temperatures (°c)
IFNβ	CACGACAGCTCTTTCCATGA	AGCCAGTGATCGATGAATCT	64.4; 63.9
GAP-DH	GTGAAGGTCGGAGTCAAC	TGGAATTTGCCATGGTG	58.0; 65.5

Table 15 - Thermal cycler programme for IFNβ and GAP-DH PCR

Initial denaturing step	95°c	5 minutes	Once
Denature	95°c	2 minutes	30 cycles
Annealing	56.5°c	45 seconds	
Extension	72°c	45 seconds	
Final extension	72°c	10 minutes	Once

2.8.5 qPCR

Taqman primers and probes for qPCR were ordered from Applied Biosystems after being designed with Applied Biosystems' Primer Express 3 software. Primers and probe for E1A and Hexon were created automatically. VA-RNAI is too short for the oligos to be automatically designed, so primers and probes were manually designed. Melting temperatures and lengths were kept as close as possible to the program's default settings. 18s rRNA was used as an endogenous control, using Taqman Ribosomal RNA Control Reagents. See Table 16 for the sequences and other properties of primers and probes.

Infected cells were harvested by TRIzol extraction, and their nucleotides purified. DNA was digested using Ambion's DNA-*free* DNAse and deactivator system. Using this purified RNA as template, cDNA was produced using Applied Biosystems' High Capacity cDNA Reverse Transcription Kit. Random primers were used to initiate reverse transcription of 2μg RNA.

The purity, concentration and integrity of RNA were confirmed as described above. Pure samples were then used as template for real-time PCR (qPCR). These reactions used Taqman PCR Master Mix, with primer/probe sets and the 18s rRNA detector as an endogenous control (Table 17).

Reaction mixtures were assembled in triplicate, in 96-well optical reaction plates set up in a sterile tissue culture class II safety cabinet. The PCR was run in a 7500 Real-Time PCR unit from Applied Biosystems using the standard cycler settings.

Table 16 - Primers designed for qPCR.

Primer	Sequence	Melting temp.	Secondary Structure	Self-Dimer
E1A Forward	CCAACGAGGAGGCGGTTT	67.4	Very Weak	No
E1A Reverse	TCCTGCACCGCCAACAT	66.8	None	No
Hexon Forward	GAAGACGAAGTAGACGAGCAAGCT	65.9	None	Yes
Hexon Reverse	GCGCCTGCCAAATACG	67.7	None	No
VAI Reverse	CCGTTGTCTGACGTCGCAC	68.2	Weak	No
VAI Reverse	GGGCACTCTTCCGTGGTCT	66.6	Weak	No

These data were reproduced from the manufacturer's Quality Control Sheet.

Table 17 - Reagent volumes for real-time PCR using Taqman primers and probes.

Reagent	Volume in each well	Volume in Master Mix
2x Taqman PCR Master Mix	12.5µl	1000µl
Forward primer (900nM)	2.5µl	200µl
Reverse (900nM)	2.5µl	200µl
Probe (2.5µM)	2.5µl	200µl
20x 18s rRNA detector	1.25µl	100µl
Water	1.5µl	220µl
Template	1µl	-
Total Volume	25µl	1.92ml

2.9 Microarray sample preparation

NHBE cells were grown according to manufacturer's instructions then seeded at $3x10^5$ cells per well in 6-well dishes. After 24 hours, these were infected with *dl*309, *dl*331 or mock-infected at 100 pt/cell. After two hours, the infection media were aspirated and then the monolayers were rinsed with warm HEPES-buffered saline and re-fed with 1.5ml of medium. RNA was harvested from the cells using TRIzol (Invitrogen) at 6, 12, 18, 24, 28 & 32h after infection. Two wells were seeded and infected for each combination of timepoint and virus. RNA from these pairs was pooled into a single sample. Three biological replicates of the experiment were performed at different times. The same lots of cells and viruses were used for all replicates, and cells were grown for the same number of passages before infection.

Total RNA was extracted from the TRIzol following the manufacturer's instructions. The resulting RNA was cleaned using an additional purification step. 1/10 volume of NaOAc (pH 5.2) and 2.5 volumes of ethanol were added to each sample. RNA was precipitated by incubating this sample at -20°C for two hours. The precipitate was pelleted by centrifugation at 15,000g for 20 minutes at 4°C. This pellet was then washed twice with 80% ethanol in DEPC-treated water before drying and re-suspending in 30µl DEPC-treated water. This cleaned RNA was assessed for concentration, purity and integrity as described above.

Preparation of samples for the microarray analysis proceeded following the protocol supplied by Affymetrix. The chips used were Affymetrix's U133 plus 2.0 expression analysis arrays. For each sample, the protocol was begun with 5µg RNA; all proceeding measurements and calculations were based on this quantity. Surplus RNA samples were stored at -80°C. The procedure is outlined in Figure 13.

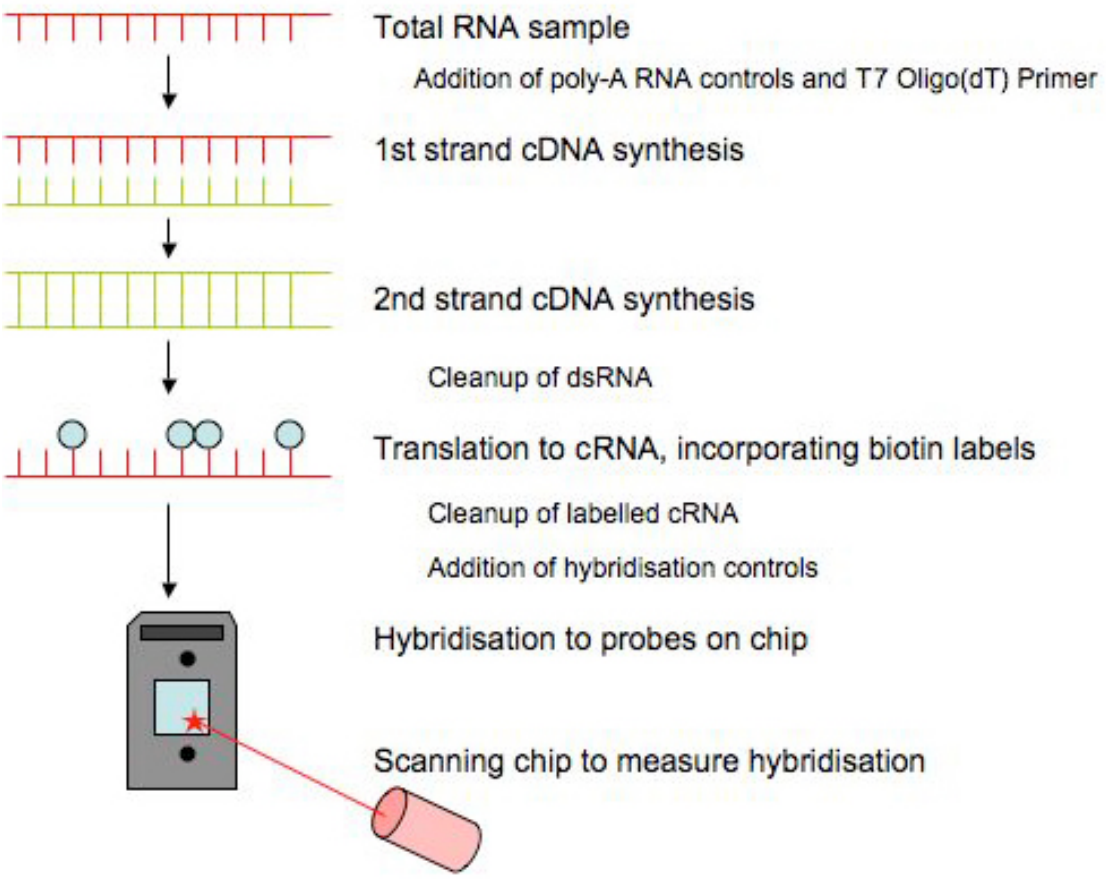

Figure 13 - Outline of microarray sample protocol.

Briefly, the protocol involves the reverse transcription of total RNA using poly-A primers. A second strand of DNA is then synthesised, giving double-stranded cDNA. After cleaning, this cDNA is used as a template for the synthesis of "cRNA" incorporating biotin-labelled nucleotide analogues. After cleaning, the labelled cRNA is hybridised to "probe" DNA sequences embedded on a microchip. The level of hybridisation to each probe is measured by scanning the chip for fluorescence produced by the biotin labels.

These fluorescence data are recorded as an image file, which is then processed to quantify the level of binding to each probe. The final check for hybridisation efficiency and integrity of the sample is by comparison of binding intensities of 3' and 5' ends of control RNAs.

2.9.1 Analysis of Microarray Data

The data analysis and bioinformatics protocol described between this statement and the end of the section "Unsupervised hierarchical clustering" was designed and

carried out by Dr Claude Chelala, who very kindly gave her time and expertise to this section of the project.

Data analysis was performed in the 'R' platform using the Bioconductor software packages (http://www.bioconductor.org). Bioconductor is an open source environment for statistical analysis of genomic data.[205]

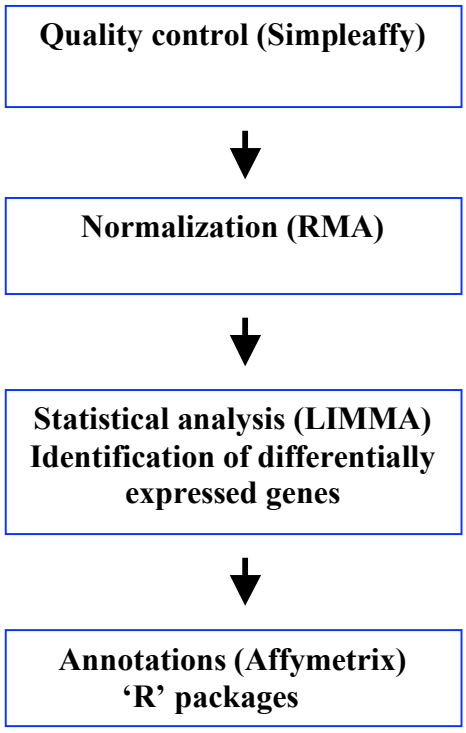

Figure 14 - Four different steps in the Affymetrix data analysis.

2.9.2 Quality control assessment

The expression data were read from the .CEL files using the 'affy' package. As quality control is a crucial step for successful microarray data analysis, scanned images were first analysed using Simpleaffy, a Bioconductor package dedicated for Affymetrix quality control. It uses a number of assessments including: scaling factor, the percentage of probe sets declared 'present' (% P) by the detection call algorithm, and the 3'/5' ratios of the signal intensity values for two housekeeping genes, glyceraldehyde-3-phosphate dehydrogenase (GAPDH) and beta-actin (ACTB).

2.9.3 Normalization

Gene expression data were normalized by computing the Robust Multichip Average (RMA) directly from the Affymetrix .CEL files. RMA consists of three steps: a background adjustment, quantile normalization and finally summarization. After background correction, normalization and summarization by the median polishing, we applied a filter using the standard deviation of gene expression values to select the top 5,000 and top 1,000 genes.

2.9.4 Identification of differentially expressed genes using LIMMA

To identify differentially expressed genes we used LIMMA, a Bioconductor package designed for the differential expression analysis of microarray data.[206] LIMMA fits a linear model to the expression data for each gene and uses an empirical Bayes method to moderate the standard errors of the estimated log-fold changes. It has been shown that LIMMA is particularly useful for analysis of experiments with small number of samples.[207] Gene annotations were obtained from R packages called 'hgu133a' and 'hgu133b'. A double cutoff of False Discovery Rate (FDR) < 0.01 and a fold change ≥ 2 was selected.

2.9.5 Unsupervised Hierarchical Clustering

In order to reveal the relationship between the specimens analyzed, unsupervised hierarchical clustering of samples and gene expression values was performed using the average linkage method and Euclidean distance measurements in R 'hclust' package. Average linkage clustering uses the average similarity of observations between two groups as the measure. This is a multivariate technique that puts samples into unknown groups or clusters suggested by the data itself (and not defined *a priori*). The samples in a given cluster tend to be more similar then samples in different clusters.

2.9.6 qPCR of Genes Selected from Microarray

Cells were grown in 6-well plates and infected with *dl*309 or *dl*331 to 100pt/cell as described previously, and their RNA extracted using the TriZol method, also described previously. After purification and integrity of RNA were checked by Nanodrop and running samples on a nuclease-free agarose gel, samples were reverse-transcribed and this cDNA used as template for qPCR reactions with the following primers:

Table 18 - Affymetrix Gene Validation Primer Sequences

Gene	Primer Sequence	Tm	Product size
E2F1	AGGACGTTGGTGATGTCATAGATG	59°c	78bp
	CGGTGTCGTCGACCTGAACT	60°c	
E2F8	TTCAAGGTGCCAAGGGTTTT	58°c	71bp
	AGCCGCCTCGCCAAA	58°c	
Zinc Finger 239	TCTTCTTGTGTCATTGCTGAGTTG	58°c	78bp
	TTCCTGCGAGTGTTAAGGTTGTC	59°c	
ID2	CTGCTTAGATTGGGCAATTCCT	58°c	86bp
	TGCAGTTGGAAGGTTTTCTTTATATACT	58°c	
DUSP6	AGCCAAGCAATGTACCAAGACA	58°c	66bp
	CGGGCGTTCTACCTGGAA	58°c	
H2al	TTGGCGCGAGCTTTGC	59°c	61bp
	CCATTTATCGTTTCTTCGTCATGT	58°c	
DMRT2	GGACTCGTGCTCCCTTCAAGT	57°c	67bp
	AATGCCACCACCTCAGTTCAA	59°c	
RRAD	TGGGCACATCATCTGTTTGC	59°c	64bp
	TTCGAGAAGGCCTCAGAACTG	58°c	
KRT53	TCCCAGCACACCTCAAAACC	60°c	89bp
	GGCTGCTAACAACGGCTACAT	58°c	
CCNE2	GGTTATTACCAAGCAACCTACATGTC	58°c	117bp
	ATGGTGTTCAACCTGTGCTCTAAA	58°c	
18s	CGCCGCTAGAGGTGAAATTC	58°c	
	CATTCTTGGCAAATGCTTTCG	58°c	

Results of these reactions were normalised against those from commercial 18s rRNA primers.

2.10 Confocal Microscopy

Confocal microscopy was used to detect autophagy in cells, based on visualising the protein LC3 as it is incorporated into autophagosomes.

2.10.1 Transfected cells

U20S cells stably transfected with a plasmid expressing GFP-LC3 fusion protein under control of a CMV promoter were a gift from Dr Claire Barra. These transfected cells were grown on sterile coverslips in the bottom of cell culture plates, then infected with virus at 100pt/cell as described above. At 28 or 48 hours after infection, cells were fixed with 2% paraformaldehyde in PBS for 15 minutes at room temperature. Coverslips with fixed cells attached were then rinsed briefly with PBS before mounting on slides using Invitrogen's "ProLong Gold" with DAPI mounting reagent. The reagent was allowed to set overnight at room temperature, and the mounted slides stored at 4°C in the dark before visualisation by microscope.

2.10.2 Antibody Probing

After fixing with paraformaldehyde as described above, cells were permeabilised with 0.5% Triton X-100 in PBS for 5 minutes at 4°C. This was then removed by briefly rinsing with cold PBS.

Coverslips were immersed in blocking solution (10% FCS in IF Buffer [Table 19]) at room temperature for 1 hour to block non-specific binding of antibodies. This was replaced with primary antibody solution, consisting of primary antibody dissolved in IF Buffer, for 1 hour at room temperature. Coverslips were then washed three times, each for 5 minutes in IF Buffer. Secondary antibodies were dissolved in IF Buffer and used to probe slides for 45 minutes at room temperature, before washing the slides a further three times. Finally, the coverslips were briefly rinsed (approx 1 second immersion) in sterile water to remove excess salts before mounting with ProLong Gold with DAPI, then set overnight and stored at 4°C in the dark.

Table 19 - IF Buffer for preparing slides for immunofluorescent microscopy

NaN_3	7.7mM
BSA	1%
Triton X-100	0.2%
Tween-20	0.05%
PBS	-

2.10.3 Acridine Orange Staining

Cells were grown on coverslips as described above. After allowing attachment, cells were either re-fed with E4, 10% FCS or starved by replacing growth medium with Hank's Buffered Salts Solution for approx. 12 hours. Growth medium or HBSS was removed and the coverslips rinsed twice with PBS to remove traces of phenol red. The coverslips were then immersed in either 1.0μg/ml or 0.1μg/ml acridine orange in PBS for 15 minutes at room temperature. They were then rinsed twice with PBS to remove excess dye, then fixed, mounted and stored as described above.

2.11 Flow Cytometry

2.11.1 For Cell Cycle Analysis

Cells grown in 6-well plates were arrested at the G1/S phase transition by treating with 5μg/ml aphidicolin added to E4, 10% FCS for 16 hours. This arrest was released by removing the treated medium and washing cells twice with warm PBS before infecting the cells with 100pt/cell of *dl*331, *dl*309 or mock-infection, as described above. For each virus, two wells (approx. $6x10^5$ cells total) were treated in parallel and later combined for reading by flow cytometry.

At 24 and 28 hours after infection, medium and any floating cells were removed from each well and saved in labelled FACS tubes. Adherent cells were trypsinised, and the trypsin in each well neutralised using the medium originally taken from that well. These cell suspensions were then pelleted and the medium discarded, thus saving both adherent and floating cells from each well.

Pelleted cells were washed twice with PBS, then fixed in ice-cold 75% Ethanol in water. When adding the ethanol, pellets were constantly agitated to avoid formation of cell clumps. After 30 minutes at 4°C, cells were pelleted again, ethanol decanted and discarded, and the remaining ethanol washed away with PBS. Finally, each sample (estimated as approx. $5x10^5$ fixed cells per sample) was treated with 50µl RNAse A at 0.5µg/ml in PBS and 250µl phosphatidyl inositol (PI) at 2.5 µg/ml in PBS.

2.11.2 For Detection of Autophagy

Cells growing in 6-well plates were infected with virus at 200 pt/cell (infections carried out as described previously), starved in Hank's Buffered Salts Solution for 12 hours or mock-infected and re-fed with E4, 5% FCS. Two wells (approx. $6x10^5$ cells in total) were treated in parallel and combined for each sample. When ready for harvesting, growth medium or HBSS was aspirated and the monoloayer rinsed twice with PBS before being overlaid with acridine orange at 0.1µg/ml, 1.0µg/ml or 5.0µg/ml in PBS. After incubation for 15 minutes at room temperature, the stain was aspirated off and the cells trypsinised. Trypsin/Versene was neutralised with an equal volume of E4, 10% FCS before pelleting the cells. The pellet was then washed twice with PBS to remove traces of phenol red before resuspending the stained, washed cells in 0.5ml PBS ready to run immediately on the flow cytometer.

2.12 Transfection

2.12.1 Plasmids

pAdVAntage plasmid was purchased from Promega. pGEM-7Zf(+) plasmid was a gift from Professor Hurst's lab. It was originally purchased from Promega and has since been amplified, re-purified and checked by digestion.

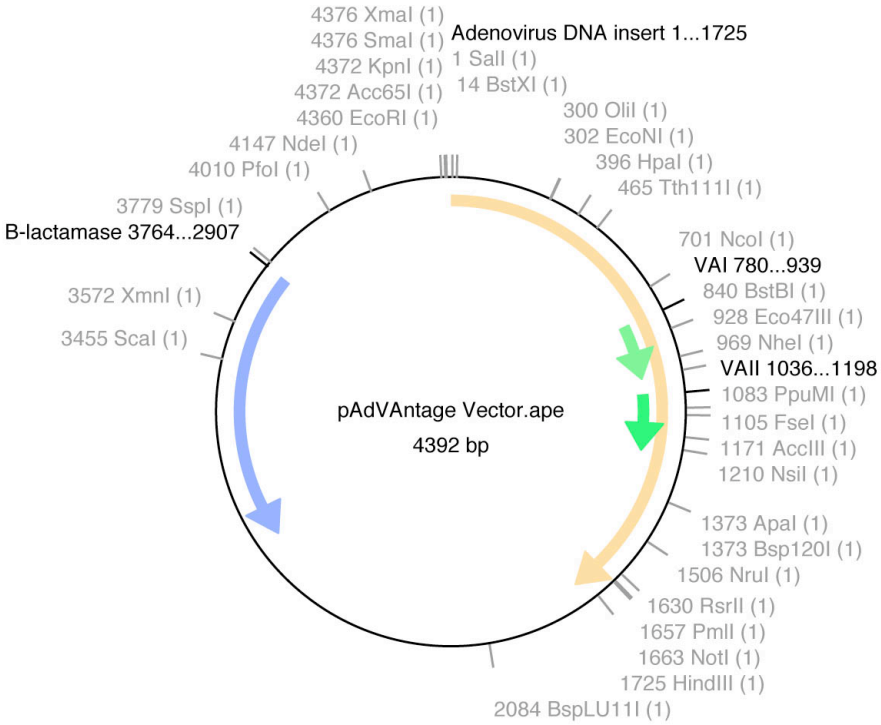
4376 XmaI (1)
4376 SmaI (1)
4372 KpnI (1)
4372 Acc65I (1)
4360 EcoRI (1)
4147 NdeI (1)
4010 PfoI (1)
3779 SspI (1)
B-lactamase 3764...2907
3572 XmnI (1)
3455 ScaI (1)
Adenovirus DNA insert 1...1725
1 SalI (1)
14 BstXI (1)
300 OliI (1)
302 EcoNI (1)
396 HpaI (1)
465 Tth111I (1)
701 NcoI (1)
VAI 780...939
840 BstBI (1)
928 Eco47III (1)
969 NheI (1)
VAII 1036...1198
1083 PpuMI (1)
1105 FseI (1)
1171 AccIII (1)
1210 NsiI (1)
1373 ApaI (1)
1373 Bsp120I (1)
1506 NruI (1)
1630 RsrII (1)
1657 PmlI (1)
1663 NotI (1)
1725 HindIII (1)
2084 BspLU11I (1)
pAdVAntage Vector.ape
4392 bp

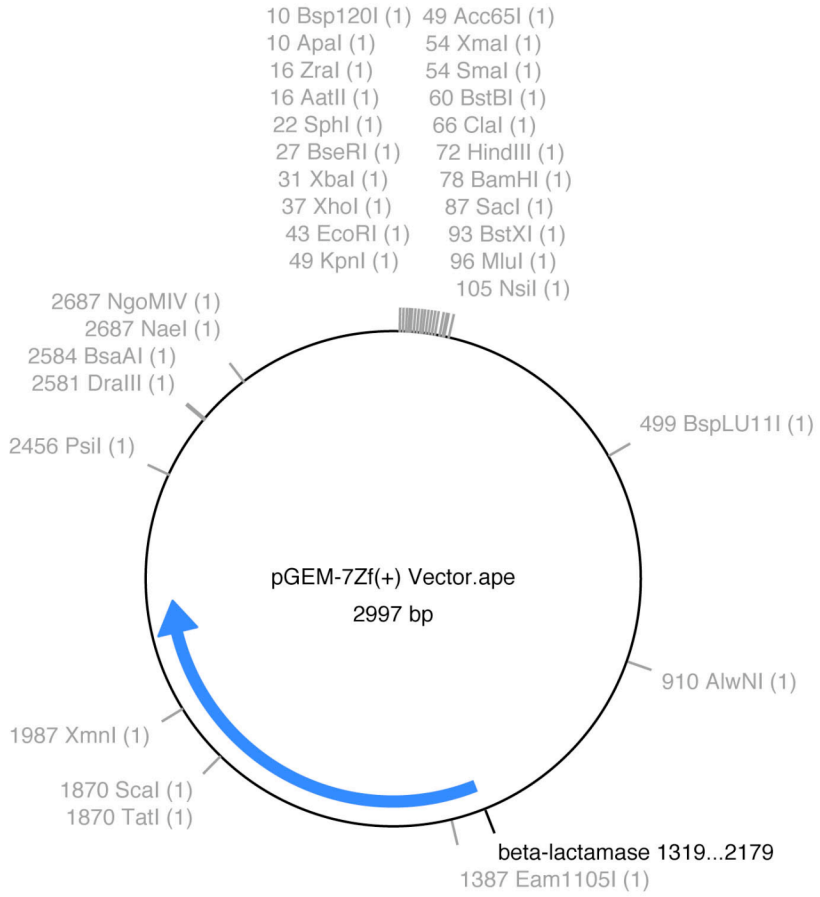
10 Bsp120I (1)
10 ApaI (1)
16 ZraI (1)
16 AatII (1)
22 SphI (1)
27 BseRI (1)
31 XbaI (1)
37 XhoI (1)
43 EcoRI (1)
49 KpnI (1)
49 Acc65I (1)
54 XmaI (1)
54 SmaI (1)
60 BstBI (1)
66 ClaI (1)
72 HindIII (1)
78 BamHI (1)
87 SacI (1)
93 BstXI (1)
96 MluI (1)
105 NsiI (1)
2687 NgoMIV (1)
2687 NaeI (1)
2584 BsaAI (1)
2581 DraIII (1)
2456 PsiI (1)
499 BspLU11I (1)
910 AlwNI (1)
1987 XmnI (1)
1870 ScaI (1)
1870 TatI (1)
beta-lactamase 1319...2179
1387 Eam1105I (1)
pGEM-7Zf(+) Vector.ape
2997 bp

2.12.2 Amplifying plasmids

The plasmid pAdVAntage was bought from Promega and amplified in the lab using Top10 Chemically Competent *E. coli* (Invitrogen):

One 50µl vial of cells was thawed on ice, half of which was transferred to a separate sterile tube for use, the other half re-frozen (-80°C) for future use. 0.5µl of plasmid in sterile water was added to the cells and mixed by flicking the tube. After keeping this mixture on ice for 30 minutes, the cells were heat shocked at 42°C for 30 seconds, then immediately re-chilled on ice. Next, 250µl of pre-warmed SOC medium was added to the cells. The transformed cells in warmed medium were then transferred to a shaking 37°C incubator for 1 hour. The cells were then spread on a plate containing 100µg/ml ampicillin and placed in a dry 37°C incubator overnight.

The following day, four colonies were picked and transferred to 15ml of LB agar with 50µg/ml ampicillin. After approx 16h incubation (overnight) at 37°C, each culture was pelleted and plasmid DNA extracted with a miniprep kit.

Transient transfections were carried out using QIAGEN's Effectene Transfection Reagent, following the manufacturer's guidelines. Specifically, plasmid DNA was diluted in buffer EC then mixed with "Enhancer". After 3 min incubation at room temperature, Effectene reagent was added, the mixture vortexed and then incubated for a further 5 min. This DNA/Effectene mixture was then mixed with a small volume of medium, and then added dropwise to fresh growth medium covering the cell layer. Transfections were typically performed in 6-well plates using the reagent volumes shown in Table 20.

Table 20 - Typical Effectene Transfection Protocol (volumes for 1 well)

Plasmid DNA	0.4µg
Volume of DNA (in Buffer EC)	100µl
Effectene Reagent	10µl
Enhancer	3.2µl
Volume of medium mixed with above	600µl
Final volume of medium in each well	1.6ml

Results

3 VA-RNAI affects Adenovirus replication and cytotoxicity

*3.1 VA-RNAI-deleted virus dl*331 *replicates poorly in normal epithelial cell lines*

Our group has demonstrated that VA-RNAI-deleted adenovirus replicates poorly in normal human cells when compared to wild-type adenovirus. In order to confirm this in my project, replication of *dl*331 was compared to wild-type Ad5 in normal human prostate epithelial cells (PrEC). Similarly to our group's previous findings, *dl*331 showed over a 100-fold reduction in replication efficiency compared to wild-type virus (Figure 15).

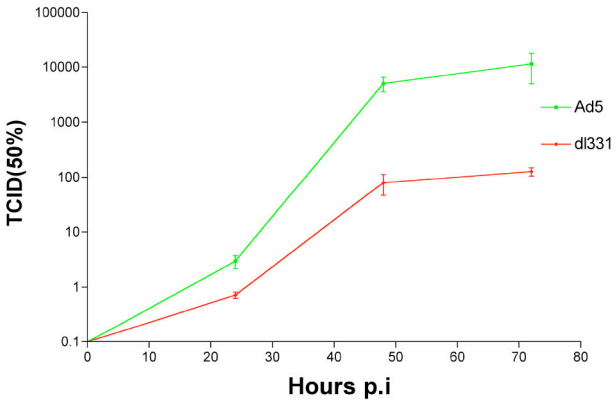

Figure 15 - Replication of *dl*331 and Ad5 in normal human prostate epithelial cells.

*dl*331 was derived from a type 5 adenovirus mutant that had almost the entire E3 region deleted, with no genes remaining intact. As described in the introduction, the E3 region is predominantly responsible for regulation of the whole-body immune response to adenoviral infection. Therefore it is generally regarded as dispensable for infections in cultured cancer cells. However, for growth in normal cells the functions of E3 may become relevant, even in the absence of immune cells. For this reason, wild-type Ad5 is not an ideal control virus for investigating the properties of *dl*331.

Instead, *dl*309 was chosen for use as a control. Like *dl*331, *dl*309 was derived from Ad5 and has a deleted E3 region; the only major difference between *dl*331 and *dl*309 is the presence or absence of VA-RNAI. Therefore, *dl*309 is a more useful control for examining the effect of VA-RNAI deletion.

Bronchial epithelial cells are the first site of infection for Ad5 during the typical route of transmission by aerosol. In order to provide more biologically relevant data, replication of *dl*331 was measured in cultured normal human bronchial epithelial cells (NHBE).

*dl*331 showed greatly reduced replication in NHBE cells when compared to *dl*309. The overall quantity of infectious virus produced in bronchial cells was much lower than that seen in prostate cells (Figure 16). Despite this, both cell lines show a very similar pattern of yields between VA-RNAI-positive and VA-RNAI-negative viruses.

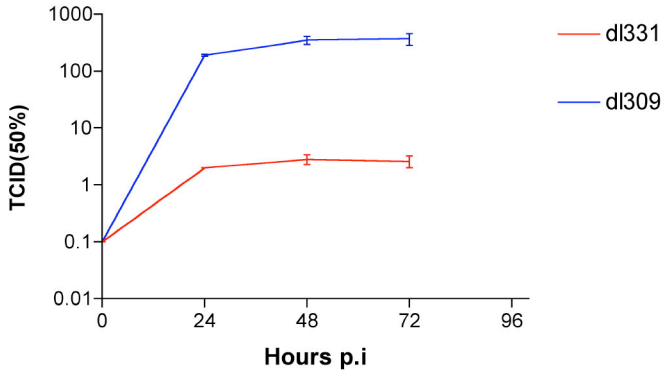

Figure 16 - Replication of *dl*331 and *dl*309 in normal human bronchial epithelial cells.

3.2 VA-RNAI-deleted virus dl*331 replication is rescued in some cancers*

In order to test the hypothesis that cells affected by K-*ras* mutations are able to support replication of VA-RNAI-deleted adenoviruses, two cancer cell lines with ras mutations were infected with *dl*331. The viral yield from each was measured by a limiting dilution assay.

In colon cancer cell line HCT116, *dl*331 replicated with approximately 80% of the efficiency of VA-RNAI-positive *dl*309 (Figure 17). In contrast

to these results, replication of *dl*331 in the metastatic pancreatic cancer cell line Suit-2 support of *dl*331 was more than 10-fold lower than *dl*309 after 96 hours (Figure 18). After 72 hours, PANC-1 cells showed a similar difference in virus replication, *dl*331 reaching approximately 10-fold lower titre than *dl*309 (Figure 19). The highest replication for *dl*331 was seen in pancreatic cell line MiaPaCa2, in which the replication of *dl*331 was almost indistinguishable from *dl*309 at all timepoints (Figure 20).

These results show that while some cancer cell lines support VA-RNAI-deleted viral replication at levels equivalent to VA-RNAI-positive virus, exceptions do exist. All of the cell lines tested here carry a K-*ras* mutation, suggesting that K-*ras* mutation is not sufficient to rescue VA-RNAI's missing functions.

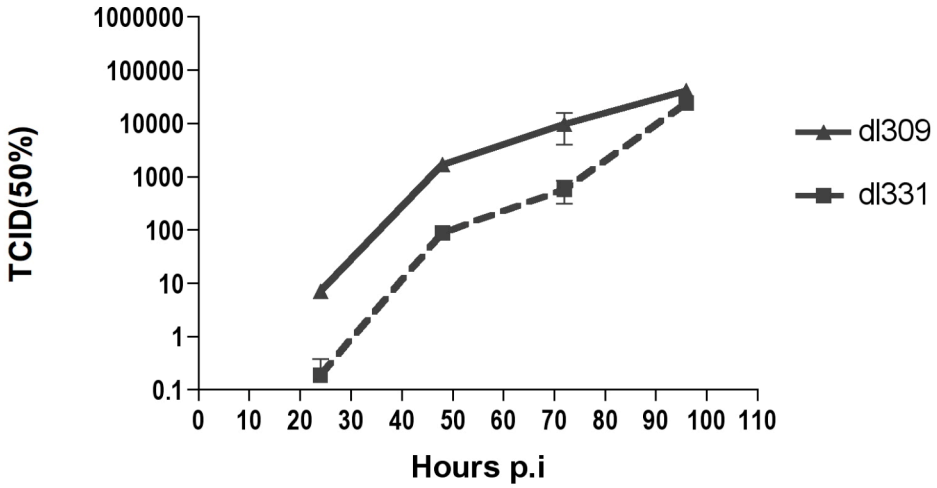

Figure 17 - Replication of *dl*331 and *dl*309 in colon cell line HCT116.

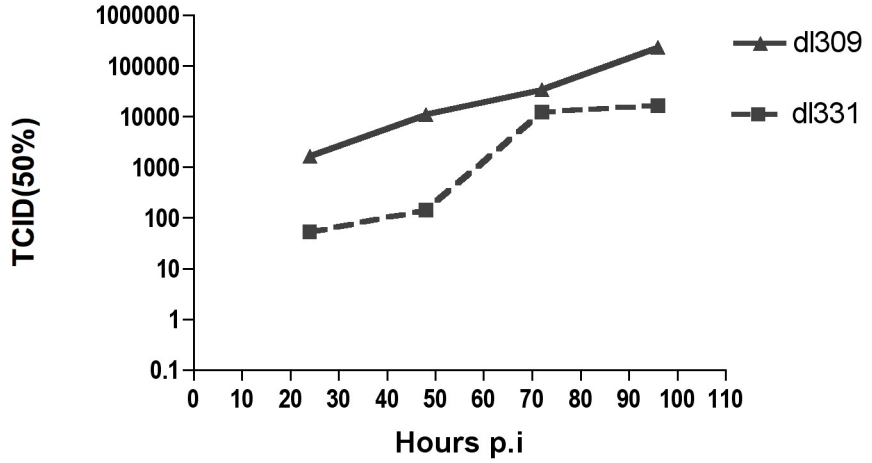

Figure 18 - Replication of *dl*331 and *dl*309 in pancreatic cell line Suit-2.

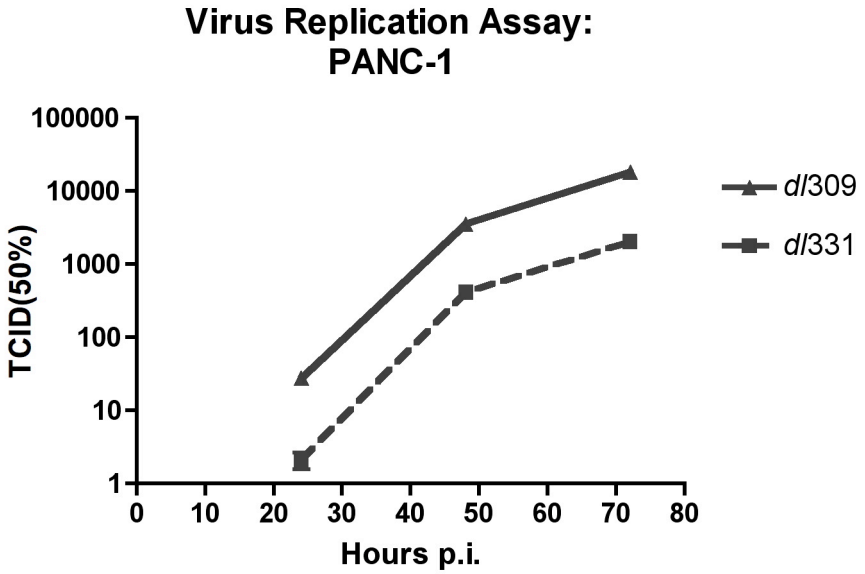

Figure 19 - Replication of *dl*331 and *dl*309 in pancreatic cell line PANC-1.

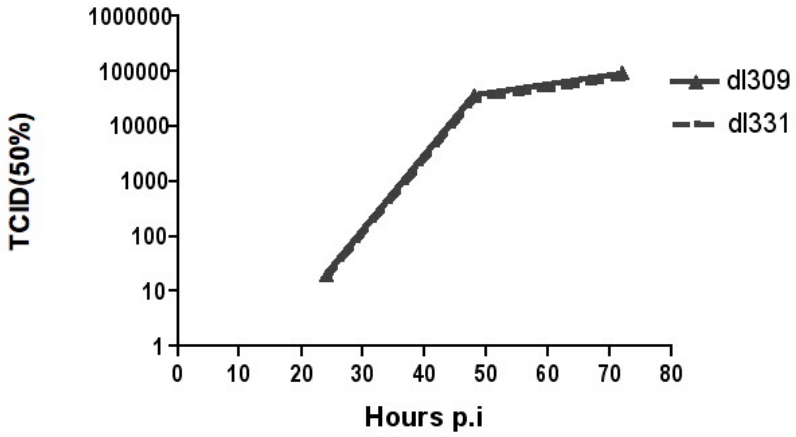

Figure 20 - Replication of *dl*331 and *dl*309 in pancreatic cell line MiaPaCa2.

3.3 Viral toxicity - dl331 is less toxic to cancer cells than control dl309

The toxicity of *dl*331 and *dl*309 was measured in the same cancer cell lines. Following the method for measuring viral toxicity described previously (page 69) The EC_{50} was calculated for each virus in each cell line (Figure 21).

In HCT116, Suit2 and PANC1 cells, the toxicity of *dl*331 was significantly lower than that of *dl*309. In MiaPaCa2 cells, there was no significant difference between the two viruses; indeed, *dl*331 was actually slightly more toxic than *dl*309. This fits with the replication data observed previously. Understanding the root of MiaPaCa2's support for the replication of *dl*331 could provide a valuable insight into the function of VA-RNAI and exploitation of deletion mutants in cancer cells.

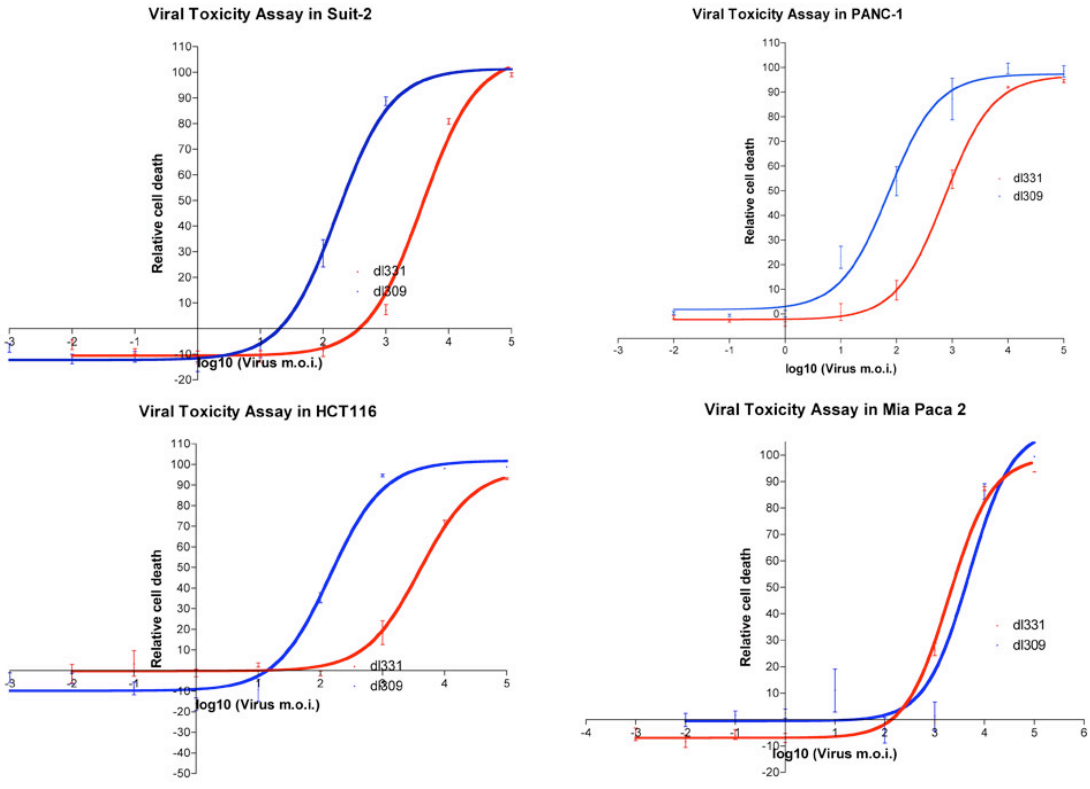

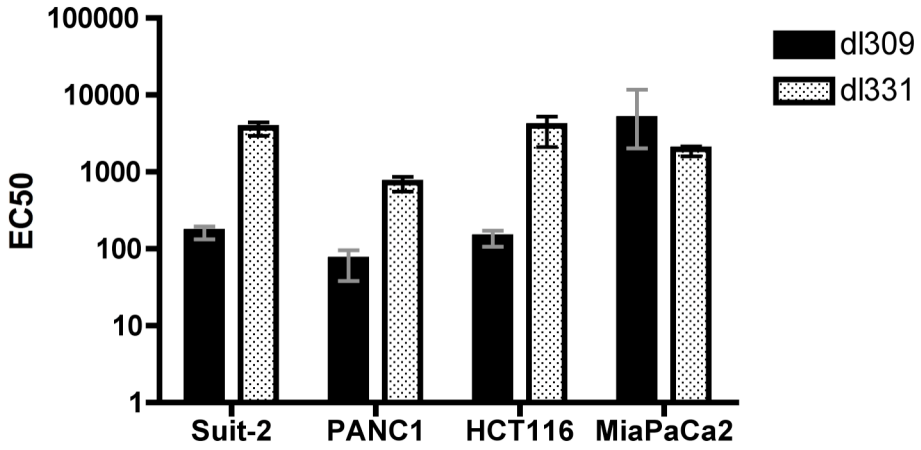

Figure 21 – EC_{50} of *dl*331 and *dl*309 in four cell lines; cells were seeded into 96 well plates and infected with serial dilutions of virus.

Cytotoxicity was measured by MTS assay (top panel), and EC50 values calculated using Prism (bottom panel).

4 Known molecular pathways interacting with VA-RNAI

In an effort to identify the molecular basis of *dl*331's selectivity, several key pathways of the antiviral response were analysed.

4.1 PKR is differentially upregulated in response to infection in Suit-2 cells

HCT116, MiaPaCa2 and Suit-2 cells were infected with *dl*309, *dl*331, Mock-infected or untreated. After 28 hours, protein lysates were harvested, and probed for regulation of Protein Kinase R, PKR. As described earlier, PKR is one of the key regulators of the cellular response to viral infection, and a known target of VA-RNAI.

In Suit-2 cells, infection with *dl*309 and *dl*331 resulted in a small upregulation of PKR when compared to mock or untreated cells. *dl*331 infection induced a slightly higher level of PKR expression than *dl*309 (Figure 22).

MiaPaCa2 cells showed no difference between the two viruses in PKR upregulation, as expected from the two viruses' near-identical replication and toxicity in this cell line. Unexpectedly, a slight decrease in PKR activity is visible after virus infection.

HCT116 cells also show no increase in PKR expression in response to viral infection.

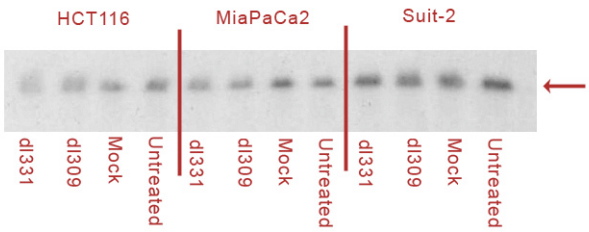

Figure 22 – Western blot for dsRNA-activated protein kinase (PKR) in HCT116, MiaPaCa2 and Suit-2 cells 28 hours after infection with *dl*331 or *dl*309, mock infection or untreated.

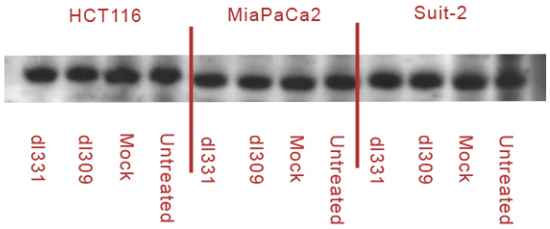

Figure 23 - Western blot loading control; Beta-actin levels in the cell lysates used for the Western blot for PKR (Figure 22)

4.2 PKR activation is differentially regulated by VA-RNAI

As described in the introduction, PKR is upregulated in response to some viral infections but inactive as a kinase until phosphorylated. The lysates described above were re-probed for PKR that had been activated by phosphorylation.

28 hours after infection, Suit-2 cells infected with *dl*331 showed higher levels of activated PKR than those infected with *dl*309 (Figure 24, right column). Unexpectedly, mock-infected Suit-2 cells showed a higher level of phosphorylated PKR than untreated cells and *dl*309-infected cells, suggesting that the infection protocol might stress the cells and that *dl*309 plays an active role in suppressing this stress response.

MiaPaCa2 cells (Figure 24, centre column) show a much smaller increase in PKR activation after infection with *dl*331 and do not show the stress response seen in Suit-2.

HCT116 cells (Figure 24, left column) show a small increase in PKR activation in response to *dl*331 when compared to *dl*309, mock infection or untreated cells.

In these cells the canonical function of VA-RNAI remains intact, as it is necessary to prevent the virus-induced activation of PKR.

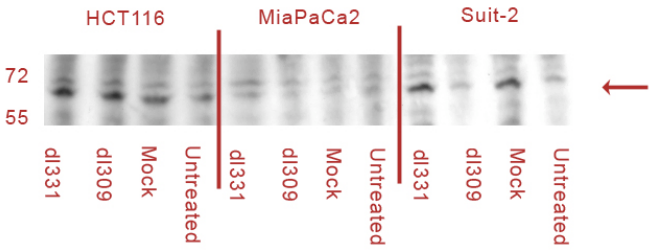

Figure 24 - Western blot for phosphorylated PKR in HCT116, MiaPaCa2 and Suit-2 cells, 28 hours after infection with *dl*331 or *dl*309, mock infected or untreated.

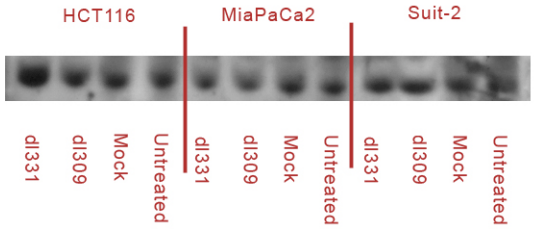

Figure 25 - Western blot loading control; Beta-actin levels in the cell lysates used in the Western blot for pPKR (Figure 24)

4.3 Phosphorylation of eIF2α is affected by VA-RNAI

The previous results confirmed that PKR expression is regulated by VA-RNAI. However, to influence the cell's behaviour PKR must be activated by binding dsRNA. The best-characterised target of PKR is the initiation factor subunit eIF2α, therefore phosphorylation of eIF2α is a useful indicator of PKR activity.

A phosphospecific antibody was used to detect phosphorylation of eIF2α in Suit-2, HCT116, PANC-1 and MiaPaCa2 cells (Figure 26) 28 hours after infection with *dl*309 or *dl*331.

In Suit-2 and HCT116 cells, much more phosphorylated eIF2α is present in response to *dl*331 infection than infection with *dl*309, suggesting that VA-RNAI-RNA is able to prevent PKR activation in these cell lines.

In PANC-1 and MiaPaCa2 cells, no difference between *dl*309 and *dl*331 is discernable. This is as expected for MiaPaCa2 cells: similar levels of eIF2α should allow similar levels of virus replication to proceed. However, PANC-1 cells showed significant differences in virus replication and toxicity despite showing similar levels of eIF2α phosphorylation. Therefore the difference in PANC-1 cells' support for virus replication cannot be accounted for by VA-RNAI's best described function.

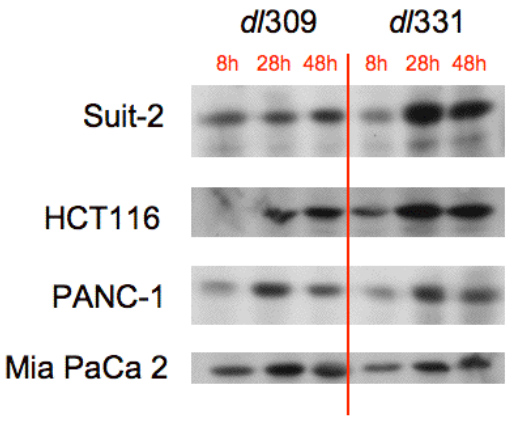

Figure 26 - Western blot for phosphorylated eIF2α in Suit-2, HCT116, PANC-1 and MiaPaCa2 cells, 28 hours after infection with *dl*331 or *dl*309.

4.4 VA-RNAI's interaction with the interferon-β pathway

Several viruses encode proteins or structured RNA molecules that inhibit the activity of PKR, and also inhibit the interferon β response. Examples include HIV TAR RNA and its binding protein, Vaccinia virus's K3L protein and Influenza virus's protein NS1 (reviewed by Gale and Katze[208]). Due to similarities between these molecules and VA-RNAI, its interaction with the IFNβ pathway was investigated. Preliminary data from our group suggested that VA-RNAI might have a role in regulating IFNβ. Previously published work has associated VA-RNAI with both inducing and suppressing IFNβ expression (see Introduction for details). As the interferon response is such a crucial factor in the success of any viral infection, it is important to determine VA-RNAI's actual effect on the pathway. In an attempt to resolve this contradiction, the next antiviral pathway examined was expression of IFN-β.

4.5 VA-RNAI suppresses IFNβ transcription in PANC1

As phosphorylation of eIF2α could not explain the viruses' different replication efficiencies and toxicities in PANC1 cells, the IFNβ secretion pathway was investigated for this cell line. PANC1 cells were infected with either *dl*331 or *dl*309. Total RNA was collected 24 hours later, and IFNβ levels assessed using RT-PCR (Figure 27). The reaction was normalised by controlling cDNA concentration and using constitutively expressed GAP-DH as an endogenous control. The positive control for IFN-β (left column) was approx. 0.5ng of a plasmid encoding the human IFN-β gene. The *dl*331-infected cells showed higher levels of IFNβ expression than those infected with *dl*309. This suggests that the presence of VA-RNAI in *dl*309 is suppressing transcription of IFNβ.

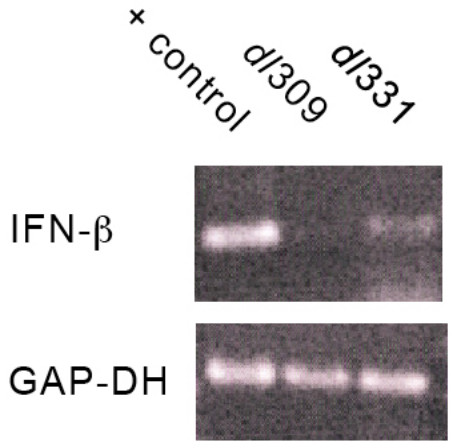

Figure 27 – RT-PCR for IFNβ expression in tumour cell line PANC-1, 24 hours after infection with *dl*331 or *dl*309.

4.6 VA-RNAI does not suppress IFNβ secretion from PANC-1 cells

Following the observation that VA-RNAI suppresses transcription of IFNβ in PANC-1 cells, levels of secreted IFNβ were examined by western blotting (Figure 28). As before, PANC-1 cells were infected with *dl*331 or *dl*309. At 12 or 24 hours after infection, medium was collected from the cells. The proteins were then concentrated by centrifugation through a filtration column. Concentrated media were treated like cell suspensions for PAGE and subsequent blotting for IFNβ.

No difference in levels of secreted IFNβ is apparent. Unexpectedly, medium from mock-infected cells contained IFNβ at levels comparable to virally infected cells. This may be a reaction to some part of the infection protocol itself, although the exact cause has not yet been determined.

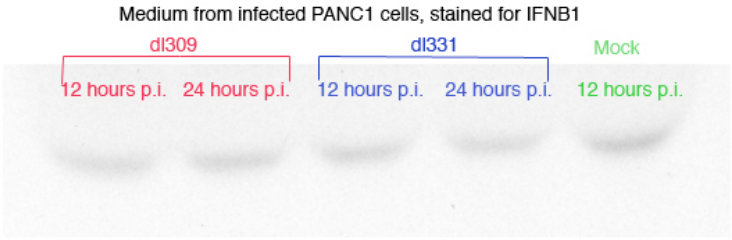

Figure 28 - Western blot for IFNβ secreted by PANC-1 cells 24 hours after infection with *dl*309 or *dl*331.

4.7 VA-RNAI has very little influence on IFNβ transcription in Suit-2 cells

Following the same pattern as the experiment in PANC-1 cells, Suit-2 cells were infected with *dl*331 or *dl*309. Total RNA was harvested at 12 and 24 hours then tested for IFNβ mRNA by RT-PCR.

A small difference in IFN β mRNA levels was visible at 12 hours after infection, with *dl*331 showing slightly higher levels. However, at 24 hours post-infection no difference in levels of IFNβ mRNA was visible by RT-PCR (Figure 29). The reduced replication of *dl*331 in Suit-2 cells cannot be attributed to increased IFNβ expression.

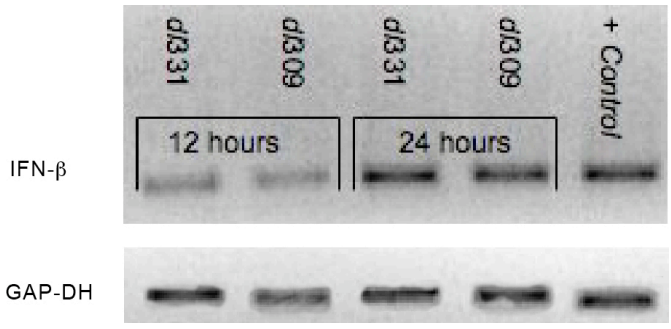

Figure 29 – RT-PCR to detect IFNβ mRNA in Suit-2 cells 12 and 24 hours after infection with *dl*331 or *dl*309.

4.8 VA-RNAI expression leads to upregulation of RIG-I in PANC-1

In preparation for studying RIG-i dimerisation and activation, PANC-1 cells infected with either *dl*331 or *dl*309 were assayed for upregulation of RIG-i. Although constitutively expressed in most cells, RIG-i can be upregulated as an interferon-stimulated gene (ISG). Although not a standard marker, levels of this protein may indicate levels of other ISGs.

Whole cell protein lysates collected 24 hours post-infection were analysed by denaturing PAGE and immunoblotting (Figure 30).

As expected, mock-infected cells showed a basal level of RIG-i expression. Expression of RIG-i was highest in response to Ad5 infection, followed by *dl*309, which expressed RIG-i at approximately basal levels. Unexpectedly, *dl*331-infected cells showed expression levels lower than mock-infected cells. The cause of this is not immediately obvious, although it should be noted that the accumulation of RIG-i may not necessarily indicate its activity.

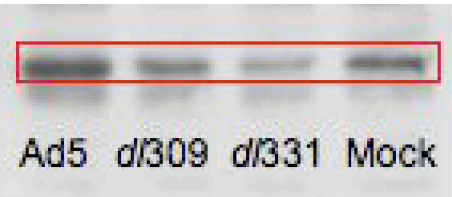

Figure 30 - Western blot of RIG-I expression in PANC-1 cells, 24 hours after infection with *dl*309 or *dl*331 or mock infected.

4.9 VA-RNAI does not influence IRF3 translocation to the nucleus in Suit-2 cells

IRF3 is a key virus-induced inducer of IFNβ (see Introduction for detail). As IRF-3 is induced by signals including the Toll-like receptors and RIG-I, it seemed interesting to determine whether IRF3 activation is influenced by VA-RNAI expression.

Suit-2 cells were infected with *dl*331 or *dl*309. Twenty-four hours later, cytoplasmic and nuclear protein fractions were separately harvested and analysed by PAGE followed by immunoblotting for IRF3 (Figure 31).

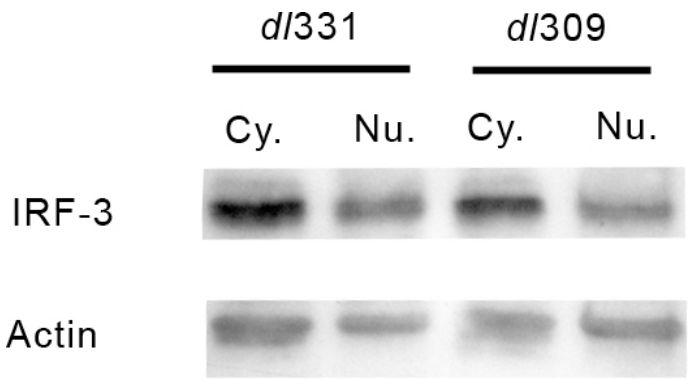

Figure 31 - Western blot for IRF3 in cytoplasmic (Cy) and nuclear (Nu) fractions of Suit-2 cells, 24 hours after infection with *dl*331 and *dl*309.

No difference in levels of IRF-3 translocation was observed between the viruses. This suggests that VA-RNAI does not target the key activators of IFR3, including the Toll-like receptors and dsRNA-induced RNA helicase RIG-i.

4.10 The interferon-β pathway: summary of results

After confirming that *dl*331 acts as a replication-selective oncolytic virus, replication assays confirmed that this activity is not dependent on K-*ras* status as previously believed. VA-RNAI's interaction with the IFNβ pathway appears to be at least partially cell line-dependent.

The pathways believed to be involved in VA-RNAI's activity are complex and frequently mutated or otherwise defective in cancers. In order to escape these complications, the focus of the project moved to work in normal cells. Results from these non-transformed cells can be expected to give a more realistic idea of VA-RNAI's normal function.

5 VA-RNAI Protects Adenovirus From Macroautophagy

5.1 eIF2α phosphorylation is linked to induction of autophagy

As shown previously, VA-RNAI is able to suppress the virus-induced phosphorylation of eIF2α in some cell lines. In yeast and in mammalian cells, phosphorylation of eIF2α in response to various cellular stresses can lead to induction of macroautophagy.[74,75,209] As discussed previously, several other viruses are known to lead to induction of autophagy in mammalian cells. This may lead to degradation of the virus and inhibition of its replication (e.g. HSV1), or may be essential for the viral replication cycle (*e.g.* reovirus). At the time of writing, only very limited information about the interaction of adenovirus with the autophagic pathways is available.

In order to determine whether VA-RNAI has an effect on the induction of autophagy in response to adenovirus infection, the cell lines of interest were infected with *dl*331, *dl*309, Ad5 or mock-infected then assayed for signs of virus-induced autophagy.

*5.2 dl*331 *induces autophagy in U20S cells expressing an GFP-LC3 fusion protein*

As a preliminary experiment to detect the induction of autophagy in response to viral infection, U20S cells stably transfected with GFP-LC3 were infected with *dl*309, *dl*331 or Ad5. At 28 hours after infection, the coverslips were fixed, stained with DAPI and mounted for visualisation on the confocal microscope. The GFP-LC3 fusion protein was visible in the cytoplasm under high gain as a diffuse cloud (green channel). In cells infected with *dl*309, a small number of small, brighter structures were visible in the cytoplasm. Cells infected with *dl*331 contained markedly more of these structures, often much larger than seen in *dl*309-infected cells (Figure 32). These punctate structures strongly resemble the

autophagosomes described previously by other groups, as reviewed by Klionsky *et al.* 2007[180] and described earlier in this thesis's introduction.

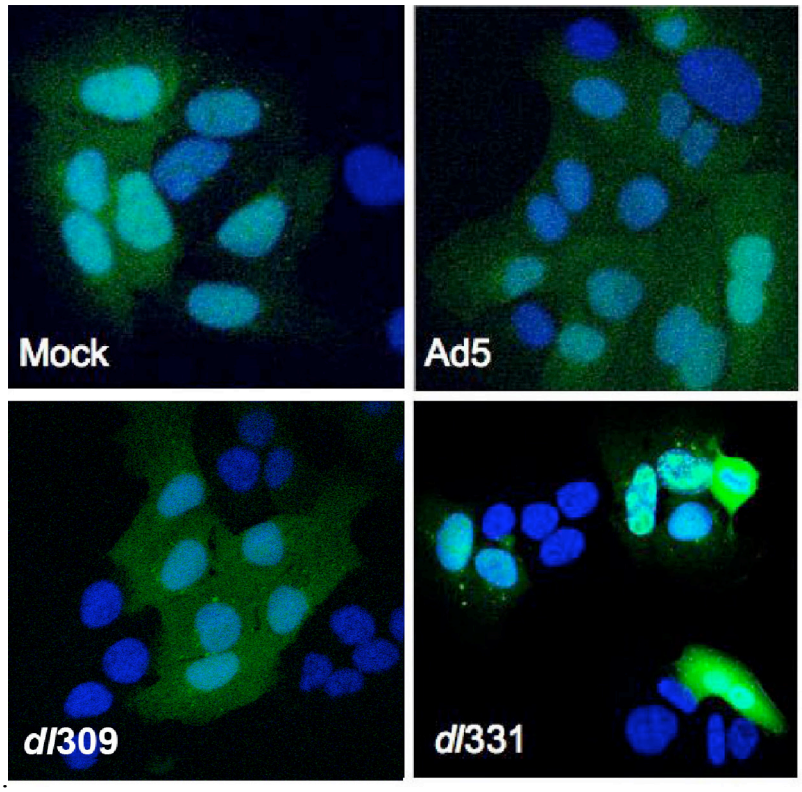

Figure 32 - U20S cells stably transfected with a plasmid expressing GFP-LC3 (shown in green), mock-infected or infected with Ad5, dl309 or dl331.

5.3 Autophagy in virus-infected U20S cells is associated with eIF2α phosphorylation

In order to confirm the link between phosphorylated eIF2α and virus-induced autophagy, U20S cells expressing GFP-LC3 were again infected with *dl*309 or *dl*331, and then fixed after 28 hours. These cells were probed with an antibody against phosphorylated eIF2α before DAPI staining and mounting. As shown in Figure 33, large autophagic vesicles were seen in *dl*331-infected cells, but not in *dl*309-infected cells. Additionally, cells containing autophagosomes (green channel) also have high levels of phosphorylated eIF2α (red channel).

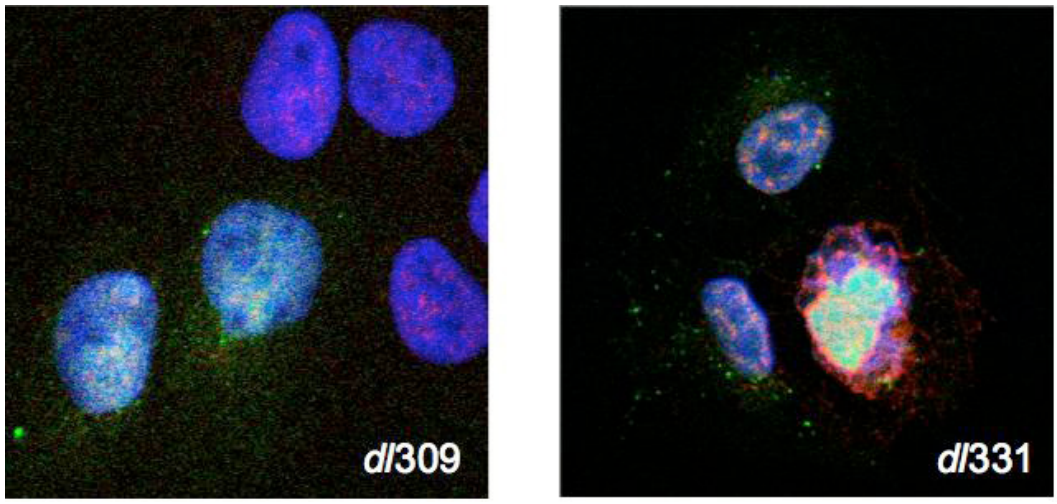

Figure 33 - U20S cells stably transfected with a GFP-LC3 plasmid, infected with dl309 or dl331. GFP-LC3 is green, phosphorylated eIF2alpha is shown in red.

5.4 The autophagy observed in dl*331-infected U20S cells is not an artefact of overexpression*

Overexpression of GFP-LC3 has previously been shown to form aggregate structures resembling autophagosomes, independently of the autophagic pathway.[187] To ensure that the structures detected by microscopy are autophagosomes rather than aggregates of GFP-LC3, this construct was

not used in subsequent experiments. Instead, endogenous LC3 was detected by immunofluorescent microscopy.

Untransfected U20S cells growing on glass coverslips were starved in HBSS for 16 hours or grown in normal conditions, then fixed. After permeabilisation and blocking, the slides were probed with: rabbit anti-LC3 antibody only; rabbit IgG followed by goat anti-rabbit secondary antibody; or both primary and secondary antibodies.

As expected, no signal was seen in cells probed with primary antibody only, confirming that the cells and primary antibody do not autofluoresce under UV light (Figure 34, left panel). Cells probed with secondary antibody only showed minimal background signal, confirming that the secondary antibody does not target any endogenous cellular proteins (Figure 34, middle panel). After probing with both antibodies, cells grown in normal conditions showed a few, small dots in the cytoplasm (Figure 34, right panel). Starved cells stained with both antibodies showed a high number of larger structures, presumably starvation-induced autophagosomes (Figure 35, right panel).

Figure 34 - U20S cells grown in normal conditions, probed with primary (rabbit anti-LC3), secondary (fluorescent goat anti-rabbit) or primary and secondary antibodies.

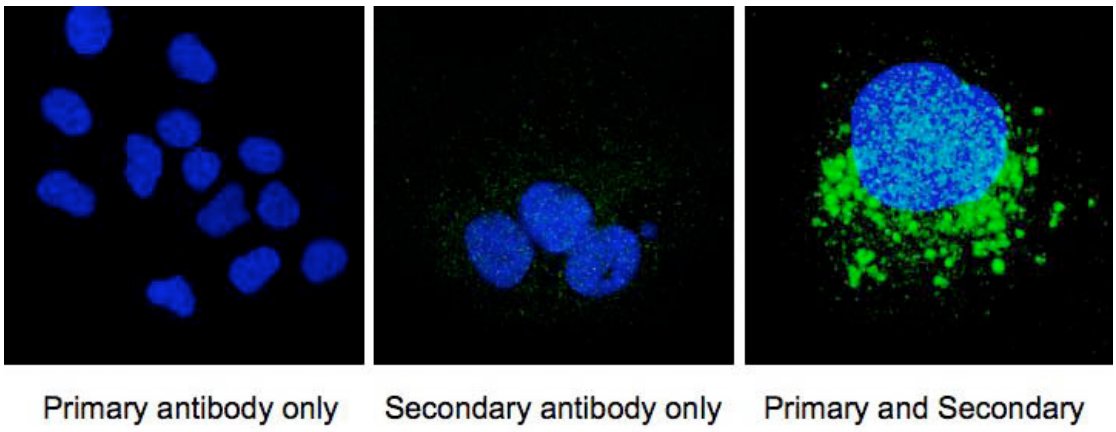

Figure 35- U20S cells starved in HBSS for 16 hours, probed with primary (rabbit anti-LC3), secondary (fluorescent goat anti-rabbit), or primary and secondary antibodies.

These experiments confirmed that infection with *dl*331 but not *dl*309 could induce autophagy in transfected and normal U20S cells. They also showed that autophagy induction correlates with eIF2α phosphorylation. Therefore in this cell line, it seems that VA-RNAI is able to prevent virus-induced autophagy via the eIF2α pathway.

5.5 Viral induction of autophagy corresponds to eIF2α phosphorylation in cell lines

Next, cells from the original panel of cell lines were infected with *dl*331 or *dl*309, fixed after 28 hours and probed for LC3, following the same protocol as described above.

For each combination of cell line and virus, ten fields were photographed using the confocal microscope's 40x lens. Each set of ten fields contained a total of 250-350 cells. These cells were examined and visible autophagosomes counted to quantify the induction of autophagy in response to each infection (Figure 36).

For Suit-2 cells, infection with *dl*309 led to a small but significant ($p<0.0001$) upregulation of autophagy when compared to mock-infected cells. Infection with *dl*331 increased autophagosome formation almost three-fold when compared to *dl*309 ($p<0.0001$), confirming that VA-RNAI is necessary to suppress induction of autophagy in this cell line.

MiaPaCa2 cells infected with either *dl*309 or *dl*331 showed a significant increase in autophagosomes over mock-infected cells ($P\leq0.002$). As expected, however, no significant difference was found between the two viruses.

HCT116 cells infected with *dl*331 showed a slight increase in autophagosome formation over cells infected with *dl*309; however, this did not reach significance. Similarly, no significant difference was seen between *dl*309- and mock-infected cells.

Representative images of infected cells probed for LC3 are shown in Figure 37.

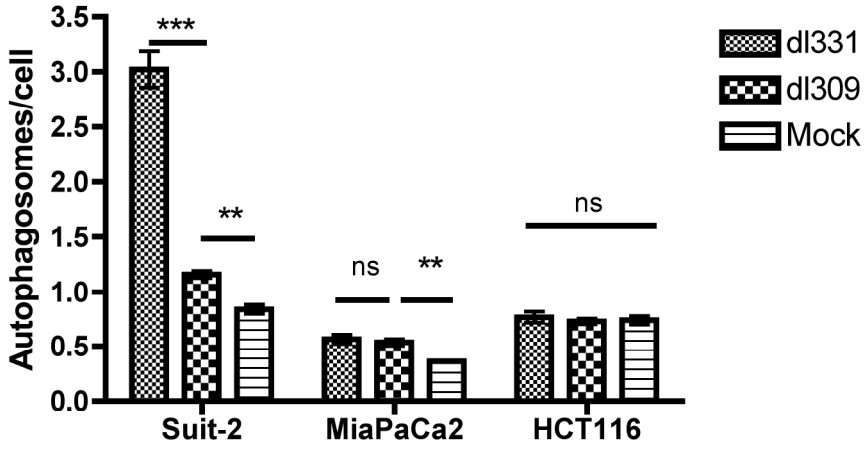

Figure 36 - Induction of autophagy 28 hours after infection with *dl*331, *dl*309 or mock infection. Autophagosomes were detected using immunofluorescence with an antibody against LC3, as described above. Autophagosomes were counted in approximately 300 cells for each combination of cell line and infection.

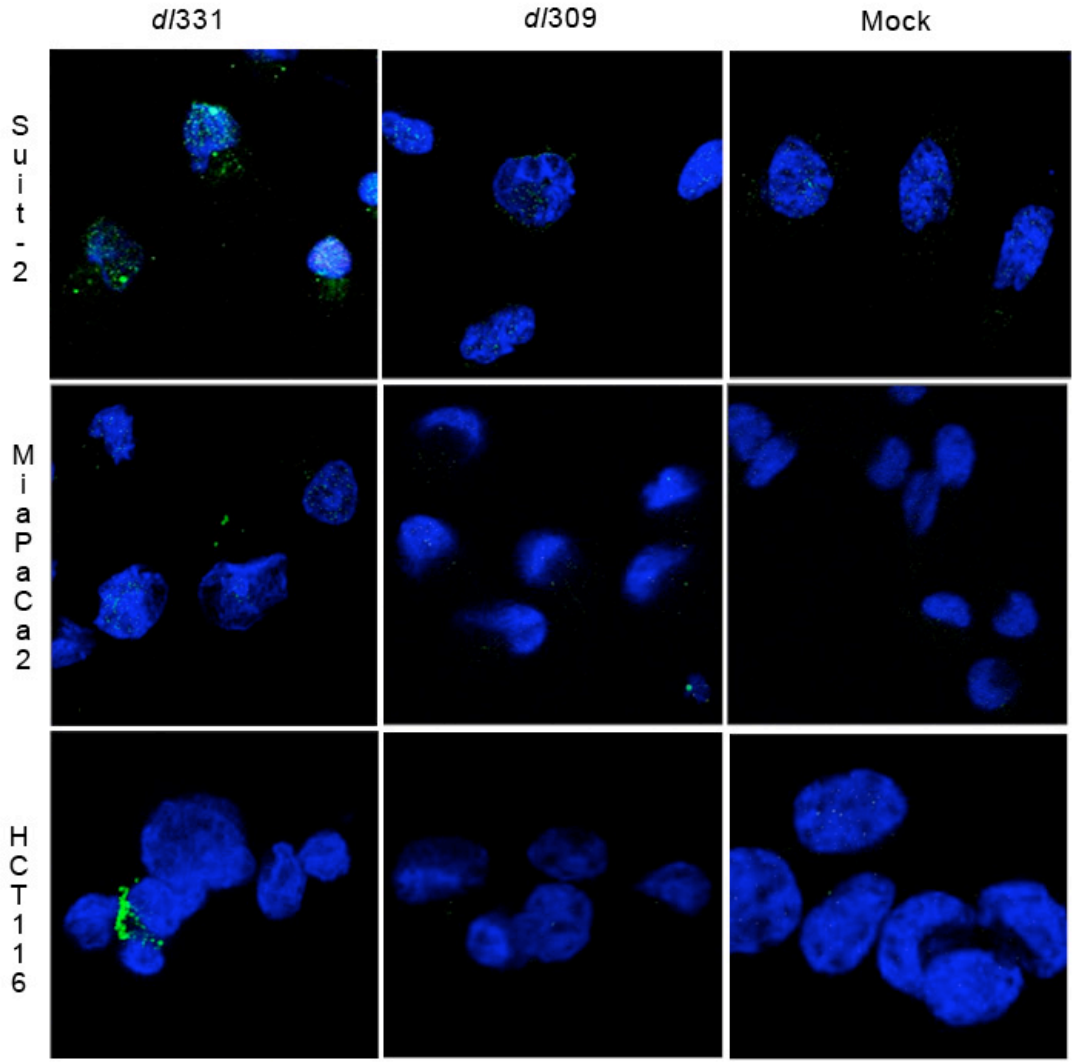

Figure 37 – LC3 protein expression in Suit-2, MiaPaCa 2 and HCT116 cells 28 hours after infection with *dl*331, *dl*309 or PBS (mock infection). As described earlier, autophagy was detected using immunofluorescence with an antibody targeting LC3 (shown in green).

*5.6 Infection with dl*331 *leads to more cells strongly expressing E1A than infection with dl*309

Even in Suit-2 cells, not all cells infected with *dl*331 showed induction of autophagy. This could be due to incomplete infection of cells on the slide, or due to a proportion of successfully infected cells failing to undergo autophagy. Suit-2 and MiaPaCa2 cell lines showed the most and least

induction of autophagy respectively, so were chosen to examine whether induction of autophagy correlates with infection.

5.6.1 By confocal microscopy

After fixation and permeabilisation, the cells were then probed with antibodies against both LC3 and adenovirus E1A. E1A was chosen as it is expected to be present at high levels in the cell very soon (typically within four hours) after infection. Representative images of these cells are shown in Figure 38. The pattern of autophagy induction matched that previously observed, with vesicles only induced at high levels by *dl*331 in Suit-2 cells. Unexpectedly, only a minority of cells stained positive for high levels of E1A in any combination of cell line and virus. In Suit-2 cells infected with *dl*331, those cells containing high levels of E1A uniformly contained high numbers of autophagic vesicles.

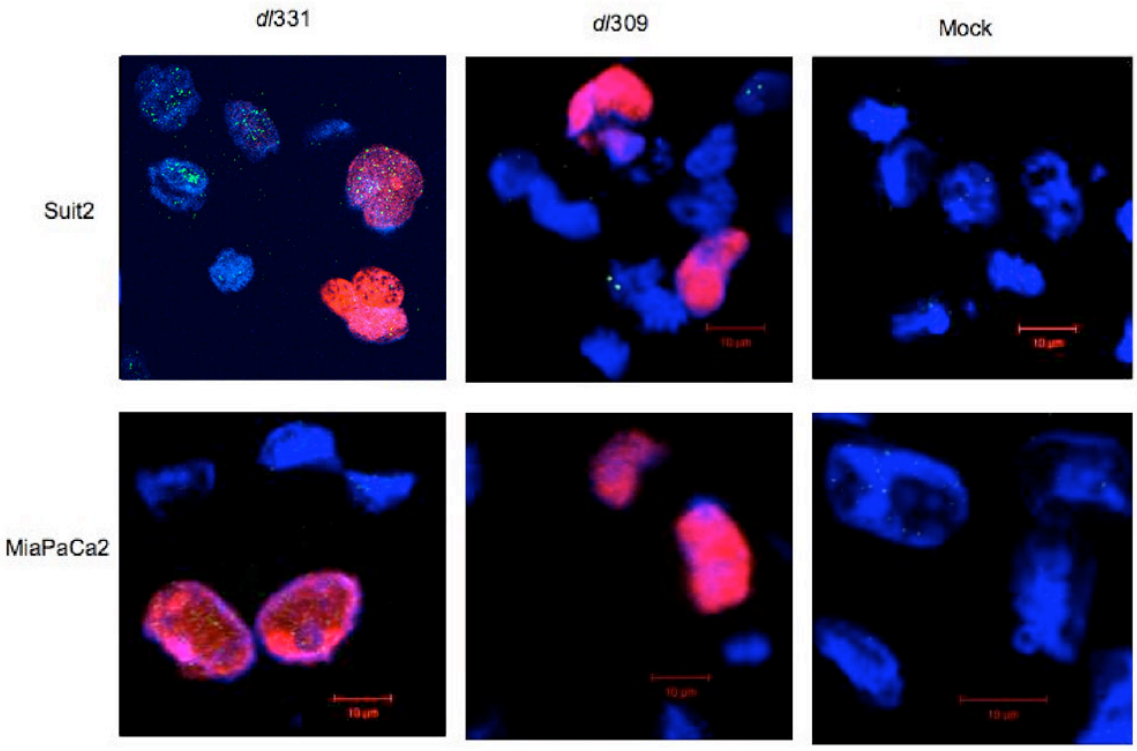

Figure 38 - Suit-2 or MiaPaCa2 cells 28 hours after infection with *dl*331, *dl*309 or PBS (mock infection). Immunofluorescence was used with antibodies targeting LC3 (green), and adenovirus E1A (red).

Cells expressing markedly high levels of E1A compared to the majority were identified visually and counted. Unexpectedly, Suit-2 cells showed significantly more high-expressing cells after infection with *dl*331 than *dl*309 (p=0.0009). HCT116 and MiaPaCa2 cells also showed slight increases, although this did not reach significance in either cell line.

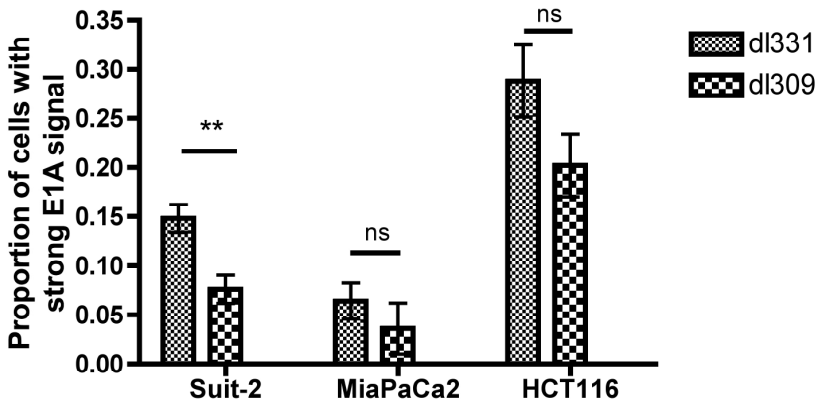

Figure 39 - Proportion of cell population expressing high levels of E1A 28 hours after infection. Ten fields totalling approximately 300 cells were counted for each combination of cell line and virus. "" represents a significant difference, in this case p=0.0009.**

5.6.2 By Western blotting

Cell lysates harvested from infected cells confirm that E1A protein accumulates to higher levels in *dl*331-infected cells than in cells infected with *dl*309 (Figure 40).

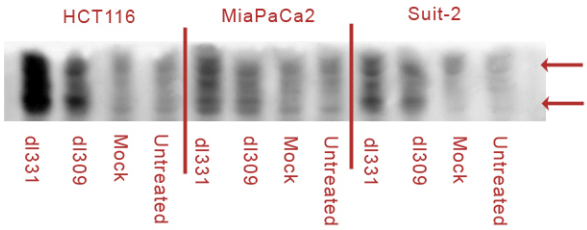

Figure 40 - Western blot for adenovirus E1A in HCT116, MiaPaCa2 and Suit-2 cells, 28 hours after infection with *dl*331 or *dl*309, mock infected or untreated.

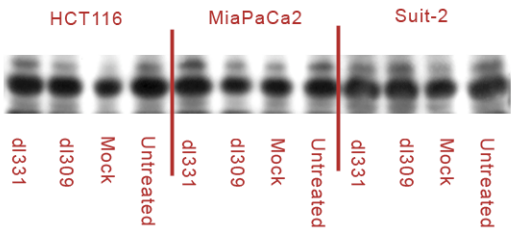

Figure 41 - Western blot loading control; Beta-actin levels in the cell lysate used for the Western blot for E1A (Figure 40).

5.7 Adenovirus E1A co-localises with autophagosomes

While only a minority of cell undergoing autophagy stained strongly for E1A, a weaker signal was still visible in almost all of them. In these cases, most of the detectable viral protein was co-localised with the autophagosomes (Figure 42**)**.

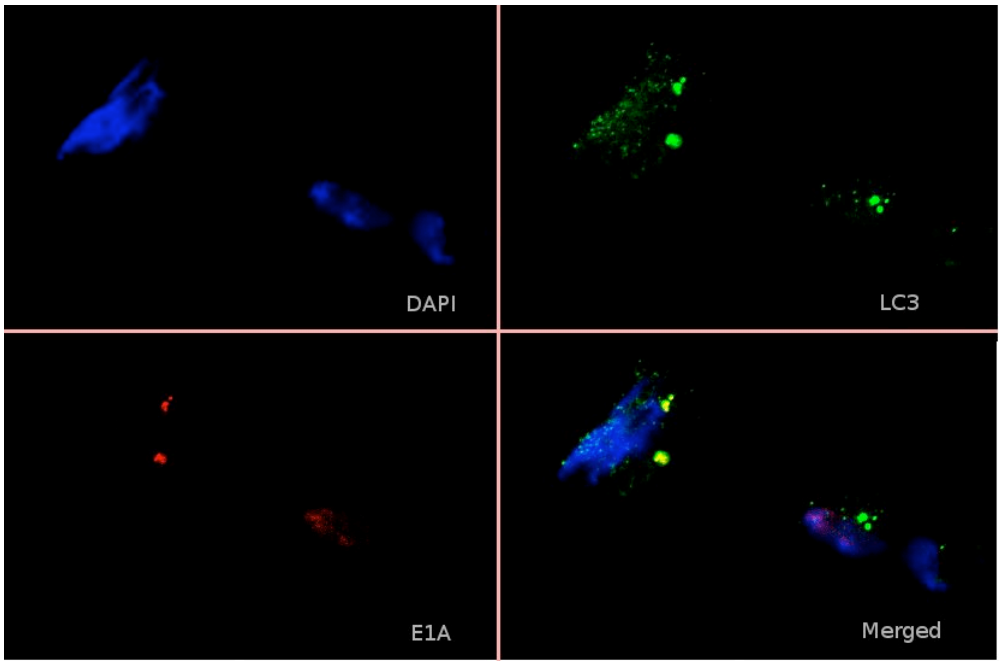

Figure 42 – Co-localisation of Adenovirus E1A with autophagosomes. Suit-2 cells infected with dl331, probed for LC3 (green) and E1A (red).

As discussed earlier, several viruses are known to exploit autophagosomes during their replication cycle. However, given VA-RNAI's function in blocking virus-induced autophagy, it seems more likely that this co-localisation indicates the degradation of viral proteins through the autophagic pathway.

*5.8 VA-RNA expression from plasmid rescues dl*331 *from virus-induced autophagy*

5.8.1 Expression of VA-RNAs from plasmid

In order to confirm that deletion of VA-RNAI is responsible for the difference in autophagy induction between *dl*331 and *dl*309, cells were transiently transfected with a plasmid expressing VA-RNAI (pAdVAntage) or a control plasmid (pGEM 5zf(+)) before infection. Quantitative RT-PCR was used to confirm continued expression of VA-RNAI in cells 48 hours after transfection (Figure 43).

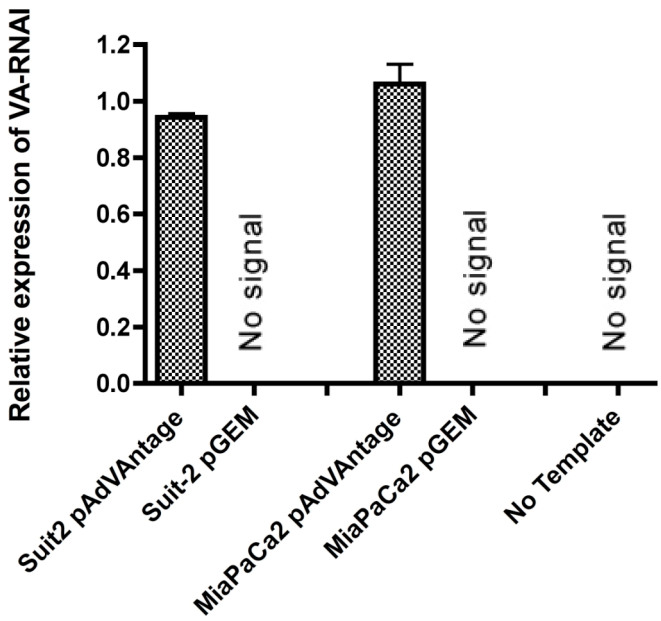

Figure 43 - Expression of VA-RNAI from cells transfected with pAdVAntage or the vector control pGEM 5zf(+), 48 hours after transfection.

5.8.2 Using confocal microscopy to detect autophagy

Suit-2 cells were transiently transfected with the VA-RNA expressing plasmid pAdVAntage or the vector control plasmid pGEM, then infected with *dl*309 or *dl*331. Twenty-eight hours after infection, cells were fixed and probed with antibodies against LC3 (green) and adenovirus E1A (red).

As expected from previous results, cells transfected with the control plasmid showed higher levels of autophagy after infection with VA-RNAI-deleted virus *dl*331 than after infection with the control *dl*309 (Figure 44, top row).

In cells expressing VA-RNAI from the pAdVAntage plasmid, no induction of autophagy was seen after infection with either virus (Figure 44, bottom row). This result confirms that the VA-RNAs alone are sufficient to suppress virus-induced autophagy in this cell line.

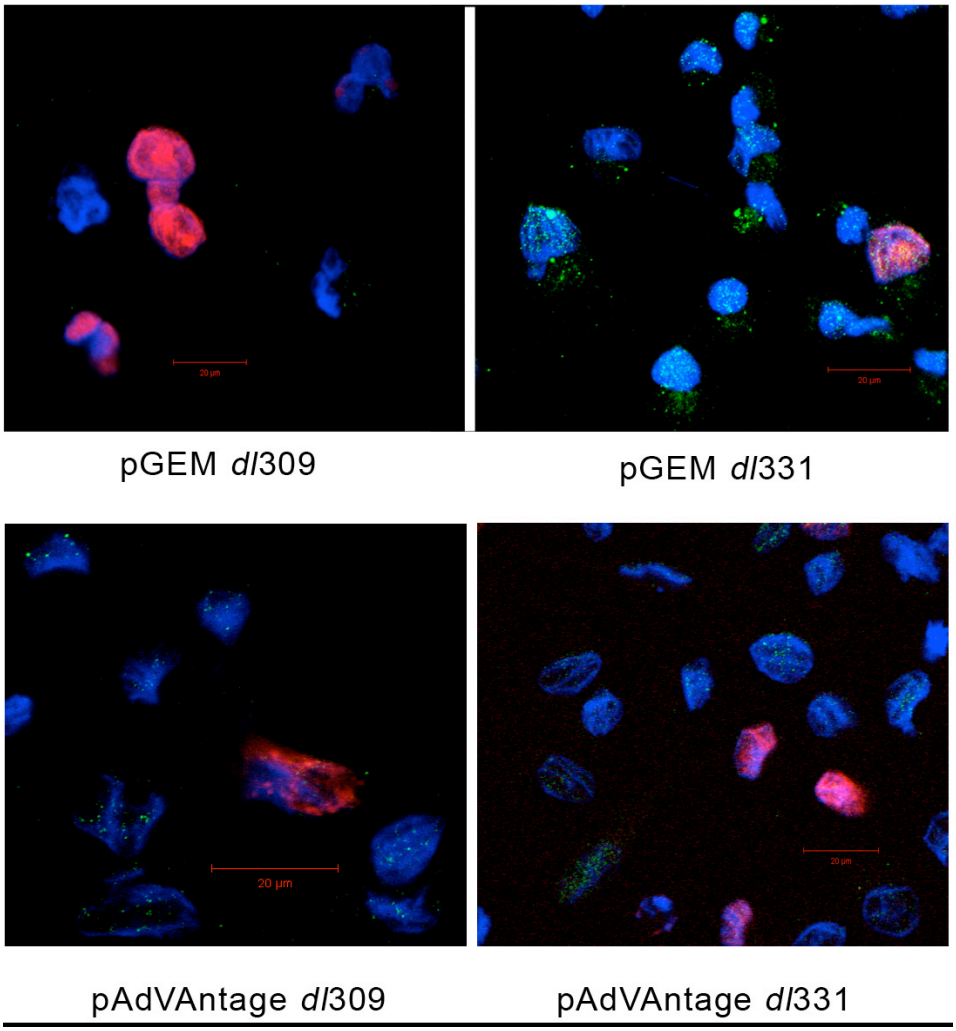

Figure 44 - Expression of VA-RNAs from the plasmid pAdVAntage prevented virus-induced autophagy in Suit-2 cells. Suit-2 cells were transfected with pGEM or pAdVAntage then, after 24 hours, infected with *dl*331 or *dl*309. 28 hours after infection, cells were fixed and probed with antibodies against LC3 (green) and adenovirus E1A (red).

5.8.3 Use of Acridine Orange to detect autophagy

As discussed earlier, the dye Acridine Orange (AO) is often used to stain cells for detection of acidic vesicular organelles. While this is not a direct measure of autophagy, late stage autophagosomes do merge with lysosomes to form acidic "autolysosomes" and should cause AO to fluoresce. This provides an alternative method for quantification of autophagy in a cell population.

To confirm that AO selectively stains acidic vesicular organelles and that AVOs are seen more in autophagic cells, Suit-2 cells were starved for

28 hours before fixing and staining with AO. Examination of the cells by confocal microscopy confirmed an increase in red fluorescent puncta in starved Suit-2 cells (Figure 45). This agrees with the expected result, the red puncta presumably being acidic vesicular organelles and possibly autophagosomes. Due to an incompatibility between the AO staining and LC3 immunofluorescence protocols, it was not possible to test how well the AO puncta co-localises with LC3-positive autophagic vesicles.

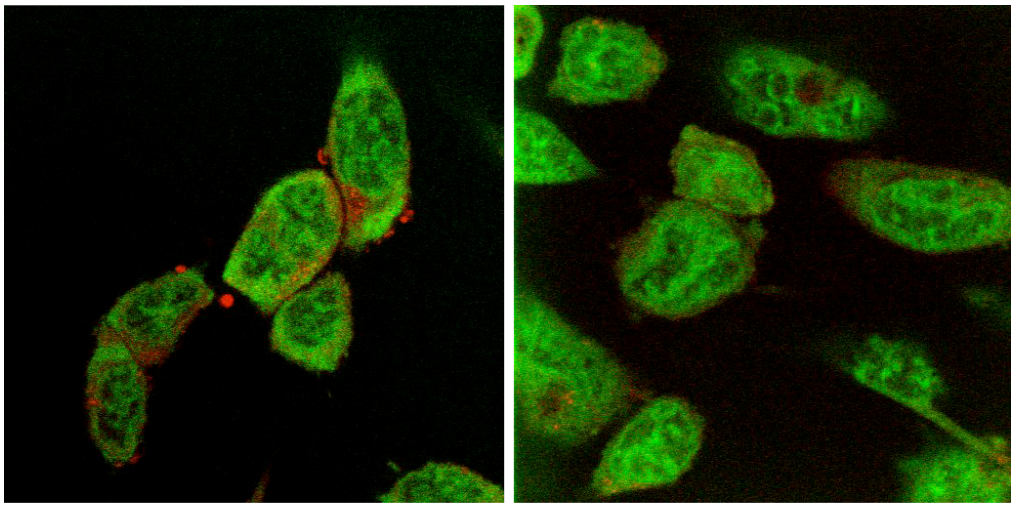

Figure 45 - Confirmation that acridine orange (AO) fluoresces red in acidic vesicular organelles. Suit-2 cells were starved for 24 hours before fixing and staining with acridine orange solution.

5.8.4 Flow cytometry of Acridine Orange-labelled cells confirms the results from confocal microscopy

Twenty-eight hours after infection, living cells were stained with acridine orange in the manner described previously (page 87) and then analysed by flow cytometry.

For each cell line, mock-infected cells were used to establish a baseline for red fluorescence from acidified acridine orange. Because the lowest expression was expected from cells expressing VA-RNAI and VA-RNAII, this baseline was set using cells transfected with the pAdVAntage plasmid. Based on this, a threshold was set at which approximately 10% of cells would be detected.

In Suit-2 cells (Figure 46), expression of VA-RNAI and VA-RNAII from the plasmid pAdVAntage prevented any increase in red fluorescence in infected cells. Cells transfected with the control plasmid pGEM had a higher background level of fluorescence than those transfected with pAdVAntage. Infection with *dl*309 increased red fluorescence above this high background; as expected, infection with *dl*331 produced the largest increase. These results confirm that expression of VA-RNAI is a strong suppressor of virus-induced autophagy in Suit-2 cells.

MiaPaCa2 cells (Figure 47) transfected with pAdVAntage show a similar resistance to the formation of acidic vesicular organelles (AVOs) following viral infection. As expected from the confocal microscopy data (Figure 36, page 114), MiaPaCa2 cells not expressing VA-RNAI did show a small increase in AVOs. Somewhat unexpectedly, infection with *dl*331 led to a higher induction than *dl*309. While VA-RNAI does not seem to play a role in suppressing eIF2α phosphorylation or subsequent autophagosome formation in this cell line, it does appear to suppress the formation of AVOs induced via some other pathway.

The results from HCT116 cells (Figure 48) matched those expected from the confocal microscopy data, with no increase in red fluorescence resulting from either viral infection, with or without expression of the VA-RNAs.

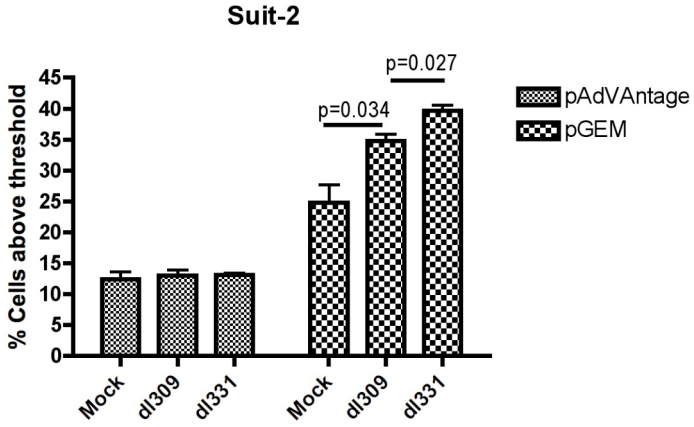

Figure 46 - Suppression of AVO formation by VA-RNAI in Suit-2 cells.

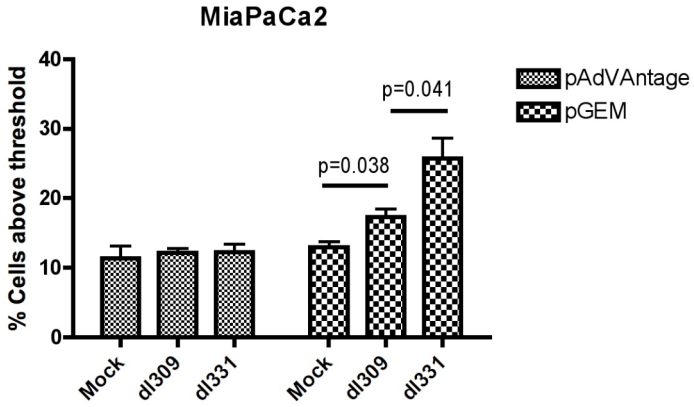

Figure 47 - Suppression of AVO formation by VA-RNAI in MiaPaCa2 cells

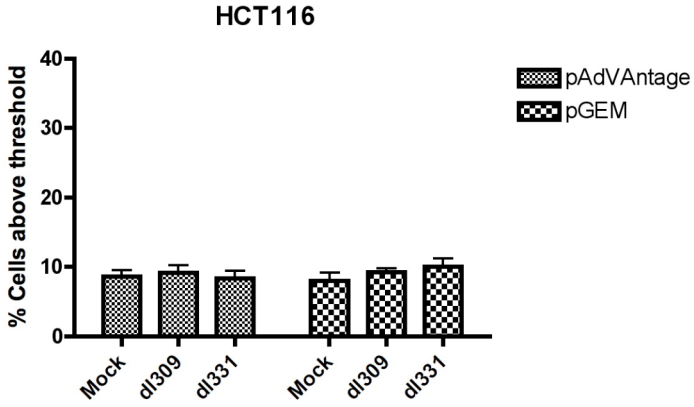

Figure 48 - Suppression of AVO formation by VA-RNAI in HCT116 cells

<u>Figure 46, Figure 47 & Figure 48</u>

Cells were transfected with pAdVAntage or pGEM then, 24 hours after transfection, infected with *dl*331 or *dl*309 or mock infected. Formation of AVOs was detected using the lysosomotropic dye acridine orange. Mean results of three experiments were subjected to two-tailed unpaired t-tests; significant differences are indicated.

5.9 VA-RNA expression affects autophagy-related proteins

5.9.1 VA-RNA expression prevents conversion of LC3I to LC3II in Suit-2 cells

As described previously, cells were transfected with pAdVAntage or control plasmid pGEM. Twenty-four hours after transfection, cells were infected with *dl*331, *dl*309 or mock-infected. Cell lysates were harvested twenty-eight hours after infection.

In cells transfected with the control plasmid pGEM, no increase in the conversion on LC3I to LC3II was seen in response to infection in HCT116 cells (Figure 49, left column) or MiaPaCa2 cells (Figure 49, centre column). In Suit-2 cells, levels of both LC3I and LC3II increased in response to *dl*331, compared to *dl*309 and mock infections (Figure 49, right column). While an increase in LC3II:LC3I ratio can indicate an increase in autophagosome formation (subject to the caveats described in the introduction; see page 56), the cause of this increase in both LC3I and LC3II is less clear.

This accumulation of LC3I and LC3II was not observed in cells transfected with pAdVAntage (Figure 50).

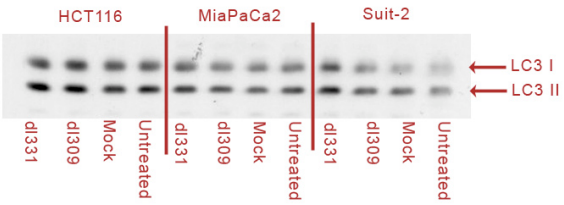

Figure 49 – Ratio of LC3I : LC3II in cells transfected with control plasmid pGEM. Cells were transfected then, 24 hours later, infected with *dl*331 or *dl*309, mock infected or not treated. Lysates were harvested 24 hours after infection.

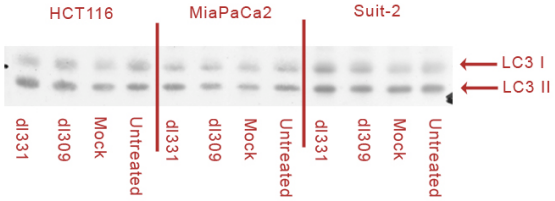

Figure 50 - Ratio of LC3I : LC3II in cells transfected with pAdVAntage. Cells were transfected then, 24 hours later, infected with *dl*331 or *dl*309, mock infected or not treated. Lysates were harvested 24 hours after infection.

5.9.2 VA-RNA expression prevents accumulation of Beclin 1 in MiaPaCa2 cells

Although constitutively present in cells and regulated by its association with other proteins, Beclin 1 has been reported to accumulate in some cells in response to pro-autophagic signals. It may therefore be useful as an alternative marker of the induction of autophagy.

In HCT116 cells transfected with control plasmid pGEM, Beclin 1 expression was unaffected by viral infection (Figure 51, left column). MiaPaCa2 cells transfected with pGEM showed increased expression in response to *dl*331 when compared to *dl*309 or mock infection (Figure 51, middle column). Unexpectedly, Suit-2 cells transfected with pGEM showed higher expression of Beclin-1 in response to *dl*309 than *dl*331. (Figure 51, right column).

As expected, HCT116 and Suit-2 cells transfected with pAdVAntage showed no difference in Beclin 1 expression in response to viral infection (Figure 53, left and right columns respectively). MiaPaCa2 cells transfected with pAdVAntage still showed a higher level of Beclin-1 expression in response to *dl*331 infection (Figure 53, centre column).

This failure of VA-RNAI expression to restore the host reaction to *dl*331 to its reaction to *dl*309 suggests that there may be some additional difference between the two viruses. However, as this difference in Beclin-1 expression is the only one so far not found to be dependent on VA-RNAI expression, it is extremely difficult to hypothesise on what may be causing it.

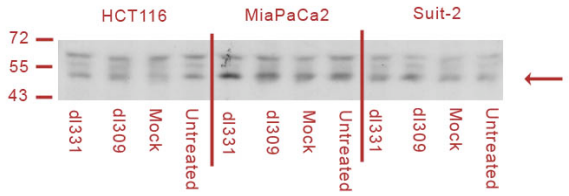

Figure 51 - Accumulation of Beclin-1 in cells transfected with control plasmid pGEM.

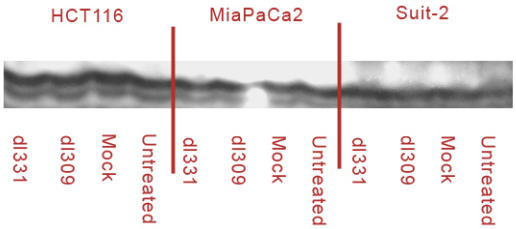

Figure 52 - Western blot loading control; KU70 levels in the cell lysates used in the Western blot for Beclin-1 (Figure 51)

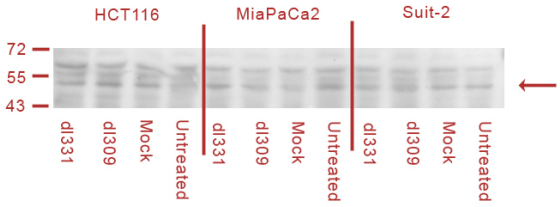

Figure 53 - Accumulation of Beclin 1 in cells transfected with pAdVAntage

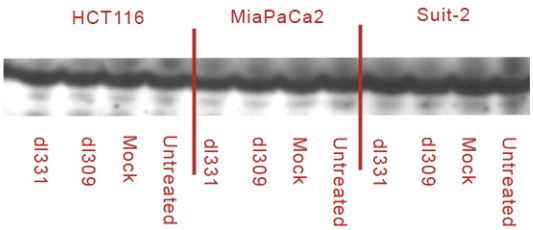

Figure 54 - Western blot loading control; KU70 levels in the cell lysates used in the Western blot for Beclin 1 (Figure 53)

Figure 51, Figure 52, Figure 53, Figure 54

Cells were transfected with pGEM or pAdVAntage then, 24 hours later, infected with *dl*331 or *dl*309, mock infected or not treated. Cell lysates were harvested 28 hours after infection.

5.10 VA-RNA expression from plasmid also rescues Suit-2 cells from starvation-induced autophagy

As described in the introduction, the centre of a solid tumour is often a challenging environment for cancer cells. Cancer cells' typically high levels of metabolic activity increase their requirements for nutrients and oxygen, while inadequate vascularisation severely limits the supply. Cancer cells have previously been shown to survive this starvation or lack of growth factors through the induction of autophagy. Given this potential importance of starvation-induced autophagy for a developing tumour's survival, the effect of VA-RNAI expression on starvation-induced autophagy was investigated.

Suit-2 and MiaPaCa2 cells growing on glass coverslips were starved by replacing their growth medium with Hanks Balanced Salt Solution (HBSS) for 24 hours. As in previous confocal microscopy experiments, they were then fixed and probed with LC3 antibody followed by a green fluorescent secondary antibody, before DAPI staining and mounting onto slides.

Representative images of starved cells are shown in Figure 55. As expected, starvation led to a dramatic upregulation of autophagy in untransfected Suit-2 cells and those transfected with the control plasmid pGEM. Suit-2 cells transfected with pAdVAntage and therefore expressing VA-RNAI were protected from starvation-induced autophagy. MiaPaCa2 cells did not show significant upregulation of autophagy after starvation, with or without VA-RNAI expression.

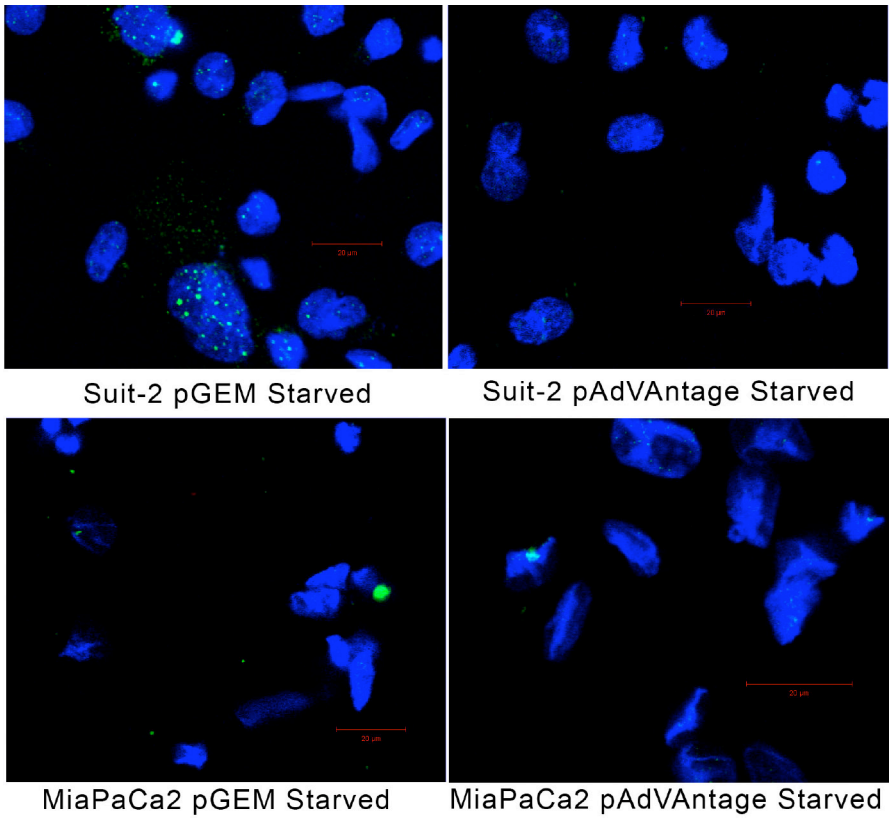

Figure 55 - Suit-2 and MiaPaCa2 cells transfected with pAdVAntage or control plasmid pGEM then starved for 24 hours. Cells were then fixed and probed for LC3 (shown in green).

6 VA-RNAs as a potential therapeutic agent

6.1 VA-RNAs sensitise Suit-2 cells to 5-FU treatment

As described in the introduction, several cancer cell lines appear to rely on autophagy to survive treatment with certain chemotherapeutic drugs. One such agent is the pyrimidine analogue 5-fluorouracil (5-FU) which, after modifications within the cell, becomes incorporated into replicating DNA, causing single- and perhaps double-strand breaks. Examples of this include the inhibition of autophagy having been shown to enhance the cytotoxicity of 5-FU in human colon cancer cells and rat oral keratinocytes.[210,211] Autophagy's role in aiding recovery from DNA damage is presumed to help cancer cells survive this crisis.

Previous results have shown that VA-RNAI is a powerful inhibitor of virus- and starvation-induced autophagy in Suit-2 cells but has little effect in MiaPaCa2 cells. Therefore the effect of VA-RNAI expression on the cytotoxicity of 5-FU was tested.

Cells were grown in 6-well plates until approximately 80% confluent then transfected with the commercial plasmid pAdVAntage or the vector control pGEM-7zf(+), following the Effectene transfection protocol described previously. After overnight incubation, cells were re-seeded into 96-well plates at a density of 2000 cells/well.

As described for the viral cytotoxicity assay (diagrammed in Figure 11), the plate layout included outer wells filled with PBS to minimise loss through evaporation and a column containing medium but no cells, to serve as a blank for the spectrophotometer.

Four rows of ten wells were seeded with each transfected line. Cells in the leftmost well of each row were treated with 5-fluorouracil at 2.5mg/ml, and this mixture diluted tenfold across the 10 wells of each row. To control for cytotoxic effects of the drug's carrier solution, duplicate plates were prepared and treated with serial dilutions of the carrier solution, 6.79mg/ml NaOH in sterile distilled water.

After a further five days' incubation, the cytotoxicity was measured by MTS assay. Curve fitting and calculation of EC_{50} values was performed using Prism statistical software.

In Suit-2 cells, expression of VA-RNAs from the plasmid halved the dose of 5-FU required to kill 50% of cells (EC_{50}) when compared to the control plasmid pGEM or untransfected cells (p=0.018) (Figure 56). The cell killing by the vehicle, NaOH dissolved in PBS, was identical in the three conditions, confirming that this was a sensitisation to 5-FU specifically, rather than a general weakening of the cells.

In MiaPaCa2 cells, expression of VA-RNAs from the plasmid did not produce any difference in EC_{50} of 5-FU. Unexpectedly, transfection with either plasmid may have sensitised the cells relative to untransfected cells, although this did not reach significance (p=0.053).

There was no detectible cytotoxicity from NaOH in MiaPaCa2 cells. However, while it is possible that transfecting MiaPaCa2 with any plasmid creates a specific sensitivity to 5-FU treatment, it could also be the case that transfection simply makes the cells less robust generally, but that the difference in NaOH sensitivity was simply too small for this assay to detect.

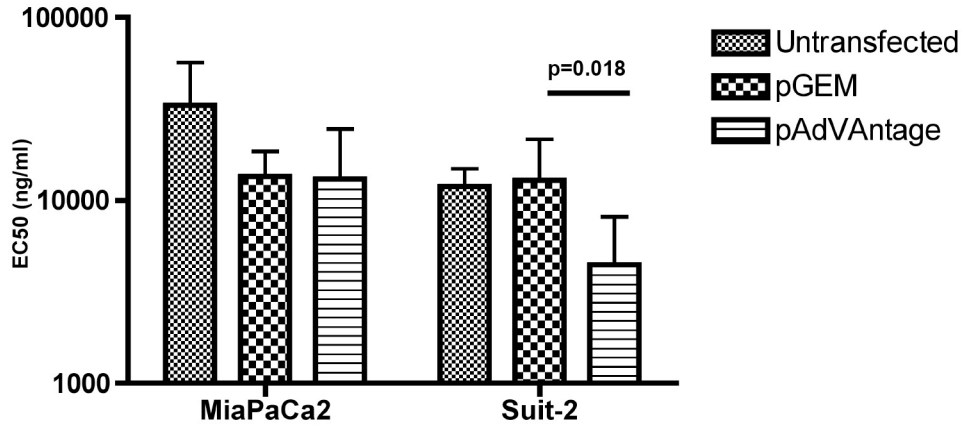

Figure 56 - VA-RNAI expression sensitised Suit-2 cells to treatment with the pyrimidine analogue 5-FU.

7 Affymetrix microarray analysis of gene expression in response to VA-RNAI

7.1 Gene expression profile in NHBE cells after infection with dl309 and dl331

None of the results gathered so far have shown a plausible mechanism for VA-RNAI's ability to protect viral replication from the intracellular immune response. Additionally, this type of work performed in tumour cells is of limited use due to the frequent mutation of pathways involved in the anti-viral response. It is difficult to be certain whether interactions between VA-RNAI and the cell are truly representative of its normal mechanism. For example, the cell line-specific upregulation of IFNβ may be the result of cell lines' different mutations in the complex pathways involved.

In order to resolve this problem and to shed new light on the normal course of Adenovirus infection in its host bronchial epithelial cells, a microarray analysis was employed. NHBE cells infected with *dl*331 or *dl*309 and mock-infected cells were harvested for total RNA at regular timepoints after infection. Based on data from the timecourse experiment above, timepoints for analysis were selected before, after and during upregulation of VA-RNAI.

7.1.1 Kinetics of VA-RNAI expression in normal cells

In order to study further the effects of VA-RNAI expression on normal cells' response to the virus, two normal epithelial cell cultures were selected. These were normal human prostate epithelial cells (PrEC) and Ad5's normal target, normal human bronchial epithelial cells (NHBE). These cells were infected with *dl*331 or *dl*309; total RNA was harvested at regular timepoints after infection.

Firstly, levels of VA-RNAI expression at each timepoint was measured by quantitative RT-PCR, normalised against 18s rRNA (Figure 58). Efficiency of the Taqman primer / probe combination was tested by analysing a standard curve (Figure 57). Although efficiency was relatively

low at 66%, this is sufficient to reliably observe large changes in VA-RNAI's expression levels over time.

VA-RNAI was detected at a constant low level from 4 to 12 hours post-infection. Expression then climbed rapidly between 18 – 24 hours before reaching a plateau at 28 hours post-infection. This suggests that in the course of a normal infection, VA-RNAI expression is upregulated at approximately 18 hours post-infection and it is not subsequently degraded. Because VA-RNAI is transcribed by RNA polymerase III, this timing of expression does not necessarily coincide with other genes in the L1 co-termination region.

As expected, cells infected with *dl*331 did not express detectable levels of VA-RNAI at any point in the timecourse.

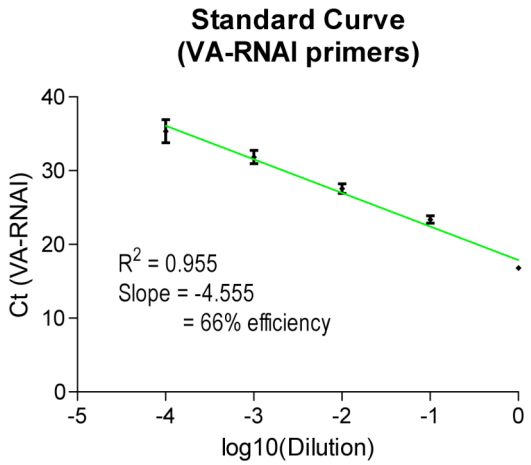

Figure 57 - Standard curve of Taqman primer / probe combination for VA-RNAI. The template for this reaction was total RNA extracted from NHBE cells 24 hours after infection with *dl*309.

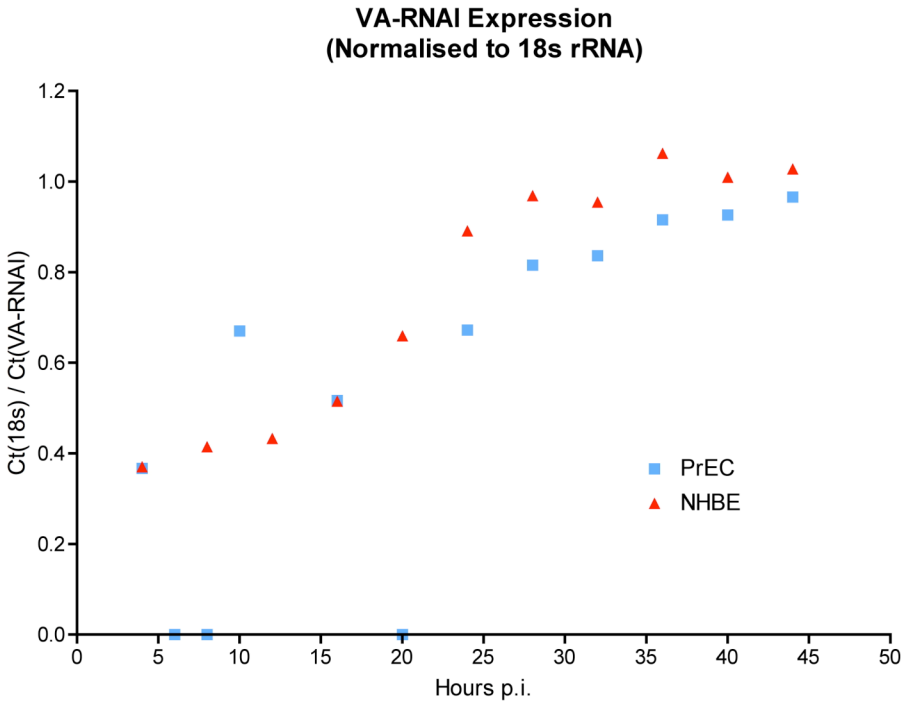

Figure 58 - Expression levels of VA-RNAI in PrEC and NHBE cells infected with dl309. Data were normalised to levels of 18s rRNA.

7.1.2 RNA quality and integrity

Before analysis by microarray, all RNA preparations were checked for concentration, purity and integrity. Concentration and purity were assessed using the Nanodrop spectrophotometer. A sample of results from this analysis is presented in Table 21.

Table 21 - Typical results from Nanodrop analysis of whole RNA samples.

Sample Name	ng RNA / µl	Absorbance at 260nm	A260 / A230	A260 / A280
Mock 24h	1305.0	32.626	2.14	1.99
*dl*309 24h	1256.8	31.421	2.23	1.98
*dl*331 24h	1305.1	32.629	1.96	2.00
Mock 28h	1153.4	28.836	2.22	1.97
*dl*309 28h	950.22	23.755	1.75	1.95
*dl*331 28h	1219.0	30.476	2.23	1.99
*dl*309 6h (rpt)	1099.6	27.492	2.20	1.97
*dl*331 6h (rpt)	1237.4	30.936	2.23	1.97
DEPC-Water (Blank)	0.05	0.001	-0.18	0.59

NB: "rpt" indicates that a sample is from the second biological repeat of this experiment.

The ratio A260 / A280 gives an indication of protein contamination levels in a sample. A value of 1.8 upwards is generally considered pure. The ratio A260 / A230 indicates contamination with phenol and similar organic compounds. A value of 1.9 is generally considered completely pure.

After establishing that samples are sufficiently concentrated and pure, the RNA's integrity is checked by electrophoresis through a nuclease-free agarose gel and visualisation with ethidium bromide. A sample gel image (matching the samples in Table 21) is shown in Figure 59. The abundant 28s and 18s rRNA molecules form sharp bands in the gel, indicating that the RNA is intact; if degradation had occurred, the rRNA would be smeared down the gel.

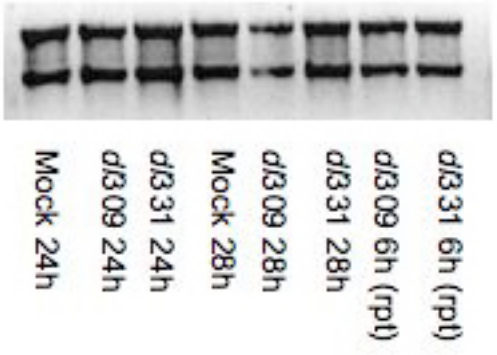

Figure 59 - Example of RNA samples run on an agarose gel to check integrity. Visible bands are 18s and 16s rRNA. Samples marked "rpt" are from the second biological repeat of this experiment.

The Affymetrix microarray chips contain inbuilt quality controls. Known quantities of control oligonucleotides are added to the RNA samples at the earliest stage of the preparation protocol to act as hybridisation controls, allowing the chips' intensities to be normalised. In addition, the chips contain probes designed to hybridise to several sites along specific cellular cRNA molecules. The binding intensities of these controls are plotted against their position along the cRNA molecules. The gradient of this graph indicates how much degradation the cRNA has suffered.

The results of this control are shown in Figure 60. All of the chips show a similar gradient, indicating similar levels of RNA degradation. Therefore any observed changes in gene expression levels are likely to be due to cellular changes rather than differential RNA degradation between samples.

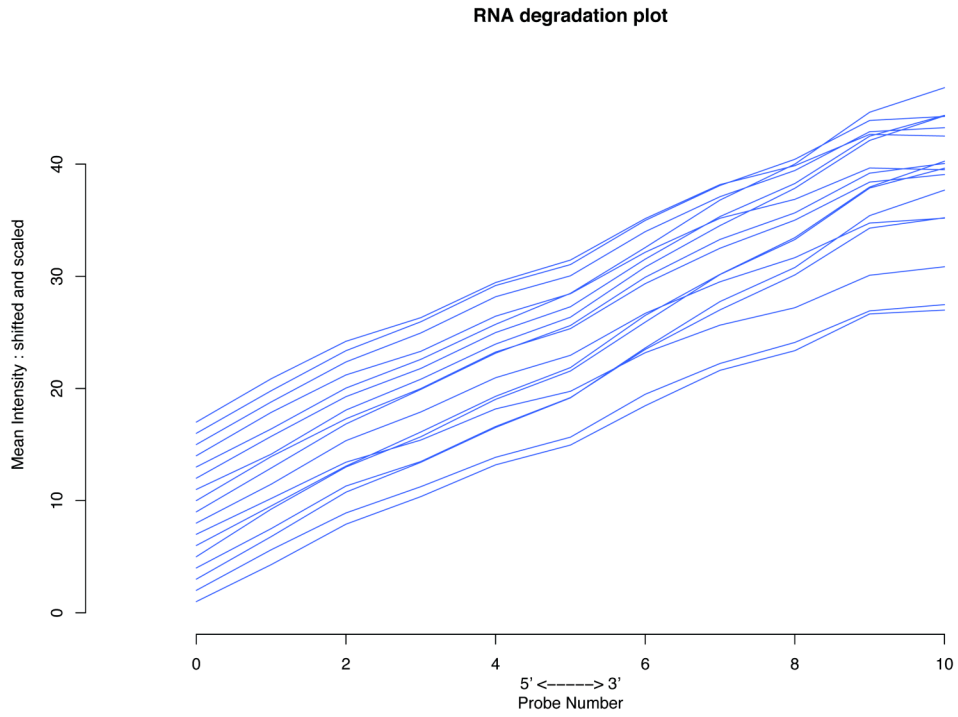

Figure 60 - RNA degradation controls. Each line represents the mean values for a single chip.

7.1.3 Unsupervised clustering

The first stage of data analysis after the quality control checks was preliminary automated clustering of the data. Two clusters are reproduced here, based on the top 5000 (Figure 61) and top 1000 (Figure 62) most variable genes. In both analyses, cells infected by the two viruses tend to cluster together at 6, 12 and 20 hours post-infection. At 24 and 28 hours post-infection, *dl*331 and *dl*309 separate from each other (labelled "V331.[timepoint]" and "V309.[timepoint]" respectively). This suggests that between 20-24 hours the two viruses begin to evoke different patterns of cellular gene expression. This coincides with the accumulation of VAI, which was earlier shown to reach its highest levels between 20-24 hours (Figure 58).

Looking at the cluster produced by the top 5000 genes, it seems that some of the most active genes are unrelated to the viral infections. The mock-infected samples (labelled "WT.[timepoint]") cluster with the virus-infected samples at 12 and 20 hours, indicating shared changes in gene expression. This may be due to the cells differentiating as they grew, or

responding in unison to stress induced by the infection protocol. However, as the infection progresses this becomes less significant: as time goes by, the mock-infected cells are separated from the virus-infected cells by increasing degrees.

This effect is also apparent when focusing on the top 1000 genes. Here, the 6 and 12 hours timepoints of both virus- and mock-infections all cluster together, away from the later timepoints. However, for the later timepoints the mock-infected cells form a subgroup separate from the virus-infected cells. This suggests that more of the shared changes in expression between virus- and mock-infected have been discarded in this model.

Finally, both analyses reveal a large difference between the mock- and virus-infected cells at 6 hours post-infection. This is presumably due to the cellular response to the endocytosis and eventual escape of viral particles. These events could be expected to provoke a large response from the cell, and occur before viral genes to suppress the host response have been expressed. It would be interesting to repeat this experiment using replication-incompetent viral particles to confirm this.

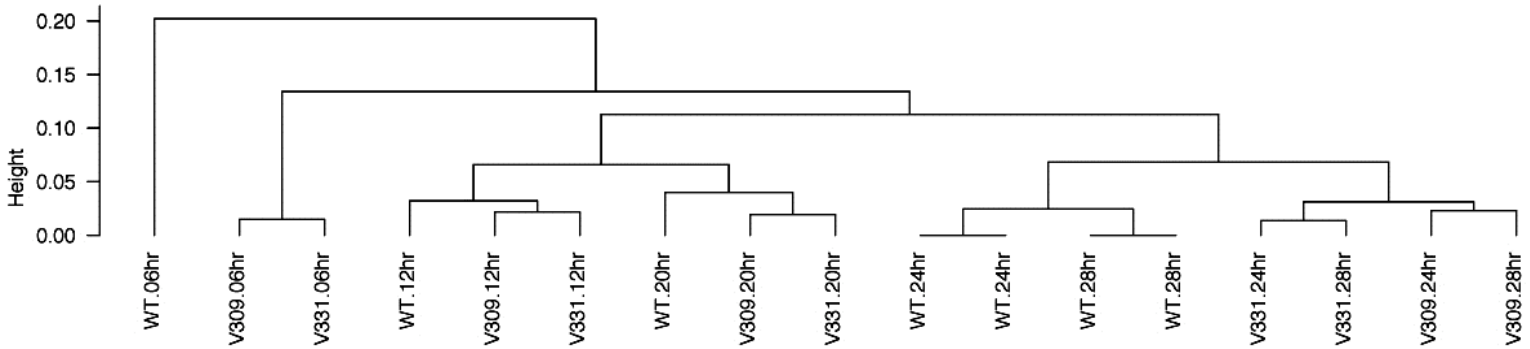

Figure 61 - Clustering of microarray data based on top 5000 genes. "WT" are mock-infected, "V331" = *dl*331, "V309" = *dl*309.

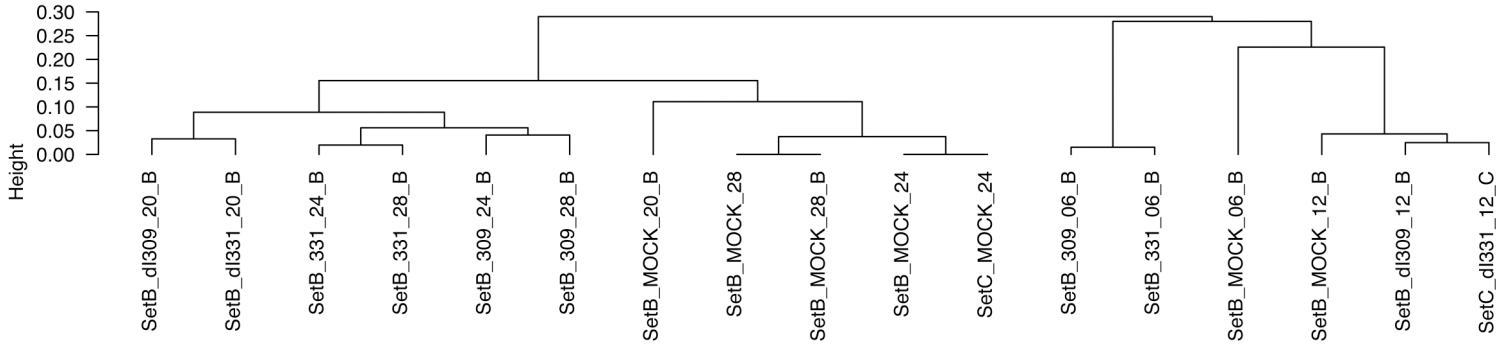

Figure 62 - Clustering of microarray data, based on top 1000 genes. "WT" are mock-infected, "V331" = *dl*331, "V309" = *dl*309.

The next stage of analysis was to take the top 5000 genes and compare their expression between different conditions. The first analysis examined genes whose expression had changed more than twofold since the previous timepoint. For example: for each infection levels of IFNB1 at 20 hours were compared to levels of IFNB1 at 12 hours; if a two-fold or greater difference was observed, the gene was scored as positive. The total numbers of genes whose expression had changed since the last timepoint is reported in the Venn diagrams in Figure 64.

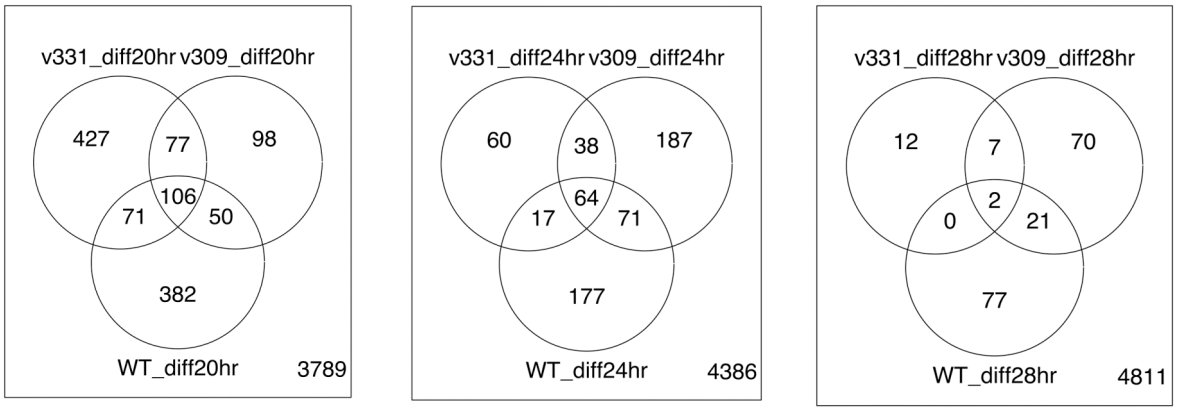

Figure 64 - Venn Diagrams showing differential gene expression between infections. Mock-infected cells are marked "WT". The timepoints shown are 20, 24 and 28 hours.

These diagrams show that the expression of a large number of genes is changed between 12 and 20 hours. 106 of these are common to *dl*331, *dl*309 and mock-infected cells. A total of (427+98=) 525 genes respond differently to *dl*331 and *dl*309. Overall change in gene expression continues at a similar rate between 20 and 24 hours; 614 genes change over these 4 hours, compared with 1211 in the previous 8 hours. Similarly, genes that respond uniquely to either dl309 or dl331 appear at a similar rate: 247 in 4 hours compared to 525 in the previous 8. The most marked difference is seen between 24 and 28 hours, during which time only 189 genes are detected to change. Interestingly, this reduction in rate of gene regulation is also seen in the mock-infected cells. This suggests that this could be a consequence of continuing cellular differentiation, or some other response to tissue culture conditions.

An alternative analysis is to compare *dl*331- and *dl*309-infected cells directly, with changes due to culture conditions taken into account. This is based on a similar comparison to that used above, with gene expression levels at one timepoint being subtracted from those at the previous timepoint. In addition, the resulting list of genes from *dl*309 and *dl*331 are compared to mock-infected cells; this should remove most gene changes due purely to culture conditions. The resulting diagrams are shown in Figure 65.

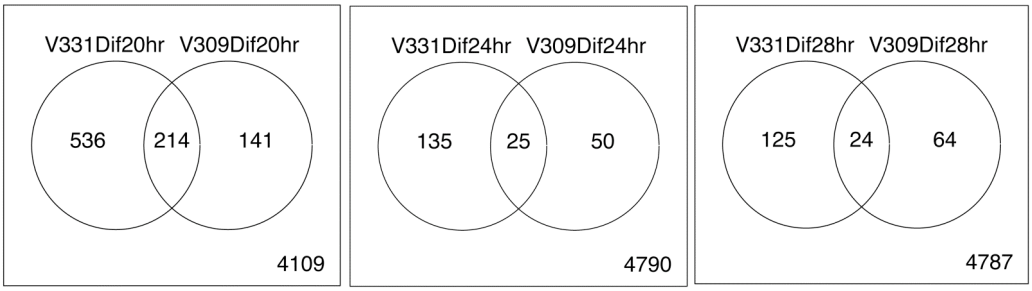

Figure 65 - Venn diagrams showing differential gene expression between *dl*331 and *dl*309 infected cells, normalised against mock-infected cells.

This analysis produces much more manageable numbers of genes. Interestingly, the number of genes that change between 12 and 20 hours is disproportionately high when compared to either 20-24 or 24-28 hours: 891 in 8 hours, compared to 210 or 213 in 4 hours.

The proportion of genes that are similarly regulated in response to infection with *dl*309 and *dl*331 also changes over time. At 20 hours, 214 genes respond similarly to the two viruses, 24% of the total changes. In contrast, during 20-24 hours and 24-28 hours this figure is reduced to 11%. This fits with the idea of VA-RNAI's influence on the cell increasing between 20-24 hours, increasing the differences observed between the two viruses.

7.1.4 Candidate Genes

These analyses produced lists of genes whose expression changed after upregulation of VA-RNAI. Two of these lists are reproduced in the

Appendix, in supplementary tables 1 and 2. These genes were filtered based on the criteria of:

- Being regulated early after VA-RNAI expression (change in expression between 20-24 hours after infection);
- This up- or down regulation is sustained through 24 and 28 hours after infection;
- A greater than 1.5-fold change in expression in response to the virus.

From these lists of genes regulated in response to expression of VA-RNAI, several genes were selected for further investigation. This selection was based on a combination of the magnitude and duration of the differential regulation and the known functions of the gene.

Name	**Symbol**	**Function**
E2F Transcription Factor 1	E2F1	Associated with driving Go-G1 transition
E2F Transcription Factor 8	E2F8	Associated with driving Go-G1 transition
Cyclin E2	CCNE2	Associated with G1-S transition
Inhibitor of Differentiation Factor 2	ID2	Disrupts Rb proteins to allow cell cycle progression
(Histone family member 2 al)	H2al	A structural histone protein; one of many histone proteins strongly upregulated.

The upregulation of these genes and an additional five Histone cluster genes after infection with *dl*331 suggest a link between VA-RNAI and control of the cell cycle. Specifically, the upregulation of VA-RNAI at 28 hours after infection appears to selectively suppress transcription of host genes involved in cell cycle progression. This is somewhat counterintuitive, as Adenovirus requires the cell to enter S phase for successful replication and eventual viral release.

7.1.5 Validation of gene expression data by qPCR

Although gene expression analysis by microarray has become a robust process, the large number of genes whose expression are measured on the chip increases the expected number of false positive results. While extensive internal controls and statistical techniques are used to minimise this possibility, it is nevertheless prudent to confirm the results using an independent assay.

NHBE cells from the same batch as those used for preparing the microarray samples were infected with *dl*331, *dl*309 or mock-infected, and the RNA harvested at 24 hours, using the same protocol and reagents as for the microarray experiment.

PCR primers were designed against the five selected genes (see Methods section for primer sequences), and quantitative RT-PCR used to measure gene regulation in response to viral infection. The results observed (Figure 66) broadly match the expected pattern, with all five genes being upregulated to some degree in *dl*331-infected cells, when compared to those infected with *dl*309 or mock infected.

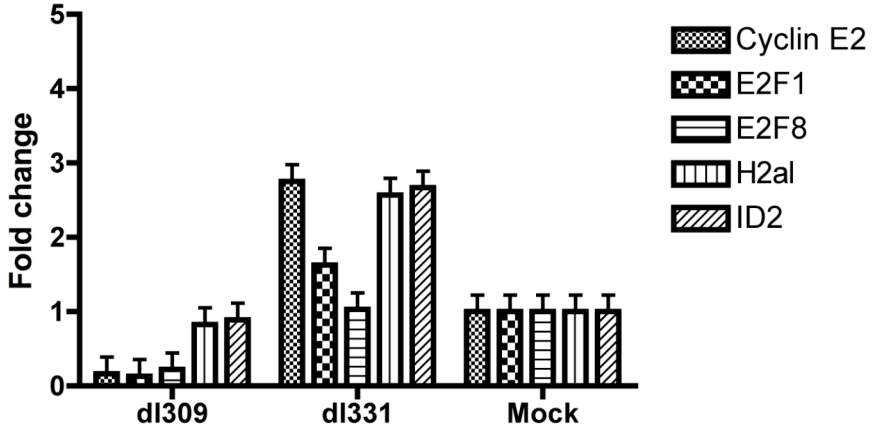

Figure 66 - Regulation of host gene expression in infected NHBE cells. Cells were infected with *dl*331 or *dl*309 or mock infected, then total RNA harvested 28 hours after infection. Gene expression was analysed by RT-qPCR and normalised against 18s rRNA.

Gene	p Value (comparing *dl*331 and *dl*309)
Cyclin E2	p<0.0001
E2F1	p=0.0015
E2F8	p=0.0337
H2al	p=0.0006
ID2	p=0.0005

Table 22 – Unpaired two-tailed t-test results for gene expression regulation in infected NHBE cells; see Figure 66 for data and explanation of protocol.

7.1.6 Regulation of cell cycle-associated genes is similar between Suit-2 cells and NHBE cells

Preliminary to investigating this finding further, these results were validated in Suit-2 and MiaPaCa2 cell lines. PCR primers were designed for these five genes (see Methods section for parameters and sequences). RNA was then harvested from cells 28 hours after infection, reverse transcribed and the resulting cDNA used as template for real-time PCR. 18s rRNA was used as an endogenous control.

Results representative of two experiments are shown in Figure 67 and Figure 68. Each gene is normalised to its expression level in mock-infected cells, allowing comparison of gene induction by *dl*309 and *dl*331. Gene expression in Suit-2 cells appears to follow the trend established in the microarray data, with expression of the cell-cycle associated genes being elevated in *dl*331-infected cells. Although this trend was seen in two biological repeats of this experiment, in each case only Cyclin E2 (CCNE2) reached statistical significance between the two viruses, ($p=0.0012$ in the experiment shown here).

Unsurprisingly, MiaPaCa2 cells did not follow this trend and showed no significant differences in regulation of these host genes between viruses. Interestingly, no difference was observed between the mock-infected cells and cells infected with either virus. Possibly, the cells' constant growth state masks the virus' early attempts to manipulate the cell cycle.

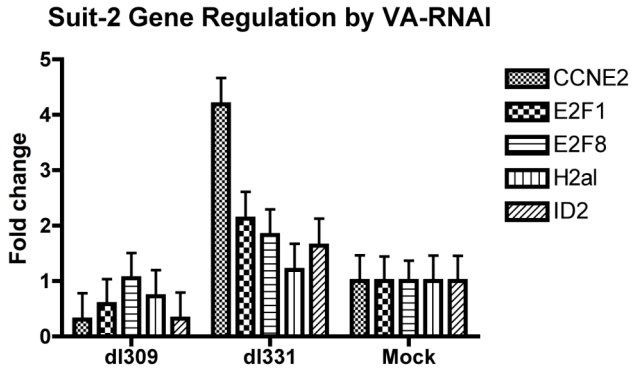

Figure 67 - Regulation of host gene expression in infected Suit-2 cells. Cells were infected with *dl*331 or *dl*309 or mock infected, then total RNA harvested 28 hours after infection. Gene expression was analysed by RT-qPCR and normalised against 18s rRNA. Statistical significance values are shown below, in Table 23.

Gene	p Value (Comparing *dl*331 with *dl*309)
Cyclin E2	p<0.0001
E2F1	p=0.0012
E2F8	p=0.0387
H2al	p=0.1707
ID2	p=0.0031

Table 23 – Unpaired two-tailed t-test results for gene expression regulation in infected NHBE cells; see Figure 66 for data and explanation of protocol.

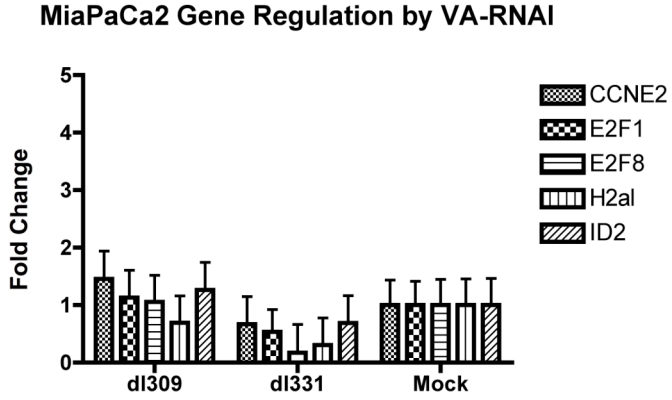

Figure 68 - Regulation of host gene expression in infected MiaPaCa2 cells. Cells were infected with *dl*331 or *dl*309 or mock infected, then total RNA harvested 28 hours after infection. Gene expression was analysed by RT-qPCR and normalised against 18s rRNA. The differences observed were not statistically significant.

To validate further the expression of these genes in cancer cell lines, protein lysates harvested from infected cells were probed for ID2, one of the genes apparently suppressed by VA-RNAI expression (Figure 69). In lysates from Suit-2 cells, a small increase in ID2 is discernible in cells infected with *dl*331, when compared to those infected with *dl*309. Indeed, Suit-2 cells infected with *dl*309 express marginally less ID2 than mock-infected cells.

Unexpectedly, lysates from MiaPaCa2 cells infected with *dl*331 also appear to contain more ID2 than those from cells infected with *dl*309. Lysates from HCT116, however, do not show any discernible change in ID2 levels in response to infection with either virus.

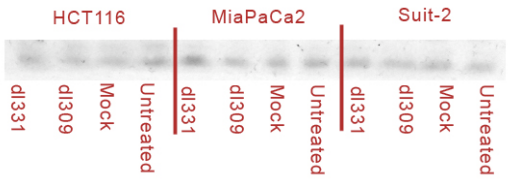

Figure 69 - Western blot for ID2 in Suit-2, MiaPaCa2 and HCT116 cells. Cells were infected with *dl*331 or *dl*309, and lysates collected after 28 hours.

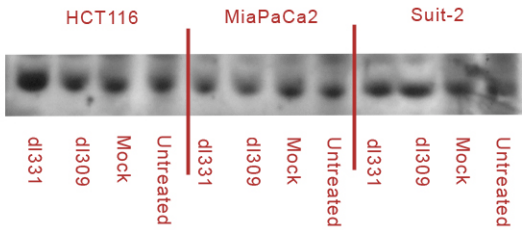

Figure 70 - Western blot loading control; Beta-actin levels in the lysates used in the Western blot for ID2 (Figure 69).

7.1.7 Expression of VA-RNAI alone does not induce cell cycle-associated genes

The downregulation of genes promoting cell cycle progression seems like an unintuitive step for the virus. It was important to determine whether this behaviour is a direct response from the cell to VA-RNAI expression, or

a (possibly unintended) consequence of VA-RNAI's role in modulating the host cell's response against the virus.

Results are shown in Figure 71 and Figure 72. No significant differences in the expression of the genes examined was found in either cell line; the overall trend seen in previous experiments was also absent. This result confirms that VA-RNAI's influence on these genes' expression is part of its role in suppressing the host cell's antiviral response, and not a direct response from the cell to accumulation of VA-RNAI.

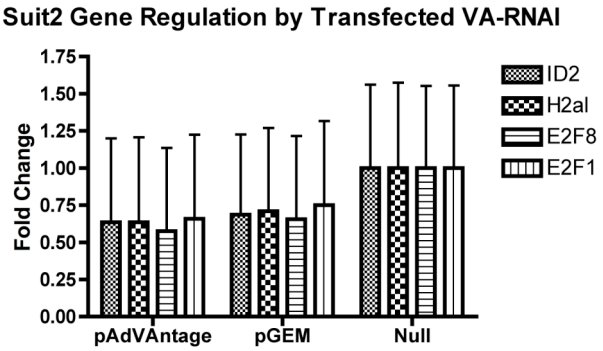

Figure 71 - Regulation of host gene expression in transfected Suit-2 cells. Cells were transfected with pAdVAntage, pGEM 7Z(f)+ or untransfected. 28 hours later, total RNA was collected and gene expression analysed by RT-qPCR.

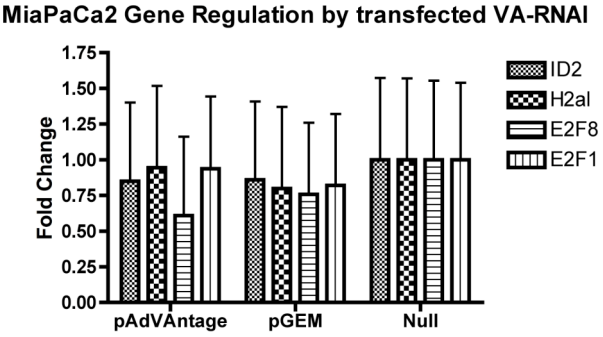

Figure 72 - Regulation of host gene expression in transfected MiaPaCa2 cells. Cells were transfected with pAdVAntage, pGEM 7Z(f)+ or untransfected. 28 hours later, total RNA was collected and gene expression analysed by RT-qPCR.

7.1.8 VA-RNAI expression does influence cell cycle progression in Suit-2 cells

After establishing that VA-RNAI causes several key genes in the cell cycle regulatory pathway to be upregulated and that this pattern is at least partly reproduced in Suit-2 cells, cell cycle analysis was performed on infected Suit-2 and MiaPaCa2 cells. Cells were synchronised by growing in the presence of aphidicolin for 16 hours, then released from cell cycle arrest and immediately infected.

Unexpectedly, analysis of harvested Suit-2 cells shows a transient but significant increase in S-phase cells 24 hours after infection with *dl*309

relative to *dl*331 (p=0.0167), with cells infected with *dl*331 showed a profile very similar to mock-infected cells. This increase in S-phase cells after infection with *dl*309 but not *dl*331 is surprising, given the upregulation of cell-cycle progressing genes originally seen in the microarray results for NHBE and seen as a trend in Suit-2 cells.

In contrast, MiaPaCa2 cells do not show a significantly different cell cycle profile between the two viruses. This too is consistent with the microarray and qPCR results. While it is at odds with the elevated ID2 level shown in *dl*331-infected cells, the level of ID2 is not the only factor controlling the transition into S-phase.

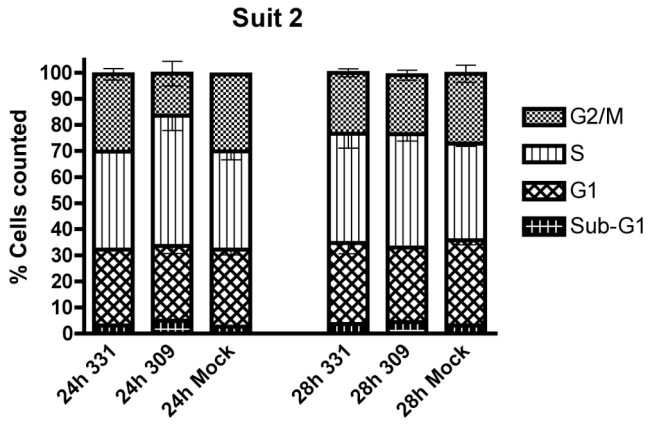

Figure 73 - Cell cycle analysis of Suit-2 cells infected with *dl*331, *dl*309 or mock infected, then harvested after 24 or 28 hours. At 24 hours, infection with *dl*309 leads to higher induction of S-phase than *dl*331 (p=0.0167)

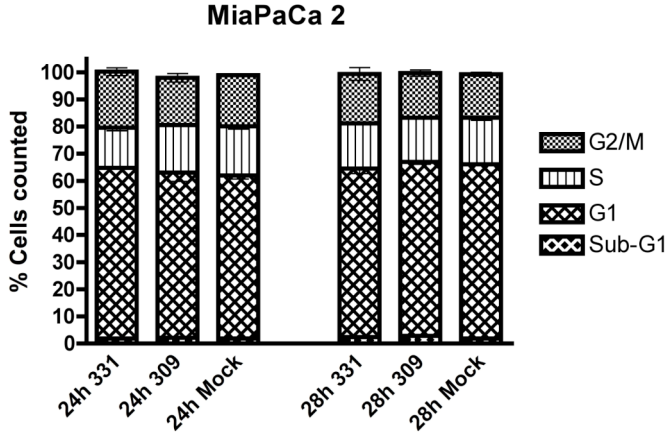

Figure 74 - Cell cycle analysis of MiaPaCa2 cells infected with *dl*331, *dl*309 or mock infected, then harvested after 24 or 28 hours.

8 Discussion

Several types of modified adenovirus have been trialled as cancer therapies. Success as a monotherapy has been very limited so far.[115,116,212] However, the combination of cancer-selective viruses with conventional therapies shows some clinical efficacy. As our understanding of the interactions between adenovirus and cancers improves, new generations of adenovirus are showing increasing promise in animal studies and early clinical trials.

The use of VA-RNAI-deleted adenovirus for cancer therapy has shown some success during *in vivo* studies.[104,124] However, the basis of these viruses' selectivity is not completely clear. Understanding this may make further enhancements of the virus possible, whether by suggesting techniques to improve selectivity or by informing a choice of "payload" gene to enhance toxicity. In the longer term, understanding the basis of the virus' selectivity will allow clinicians to match the virus to susceptible tumour types.

8.1 VA-RNAI deleted virus is selective for some cancer cell lines; this is not solely dependent on ras mutation

The initial aim was to confirm that VA-RNAI-deleted adenovirus *dl*331 selectively replicates in some cancer cell lines. In two lines of non-transformed epithelial cells (NHBE and PrEC), *dl*331 replication was reduced more than 100-fold when compared with VA-RNA-intact control virus. By contrast, *dl*331 replication in cancer cell lines PANC-1 and HCT116 was comparable to wild-type virus.

It has previously been suggested that *dl*331's efficient replication in cancer cells is due to a mutation in K-*ras* complementing VA-RNAI's function, or that a simple over-expression of *ras* is sufficient.[112,124] It was theorised that the *ras* status of cell lines supporting replication of VA-RNAI deleted viruses contributed to suppressing the phosphorylation of eIF2α and thus obviating VA-RNAI's best-characterised function. This theory is not limited to the virus-host interactions of adenoviruses. Reovirus infection

leads to the activation by phosphorylation of PKR, apparently in a *ras*-controlled manner.[213] In a closer analogy to *dl*331, an influenza virus with the eIF2α phosphatase NS1 deleted (*dl*NS1) shows a similar pattern of selective replication, also apparently rescued by over-expression or mutation of *ras*.[214] Similarly, an HSV-1-derived oncolytic mutant, R3616, was found to replicate preferentially in cell lines where the *ras* pathway was upregulated.[215]

PKR shows a reduced ability to autophosphorylate in murine cells with oncogenic *ras*, although whether this is a direct effect of *ras* itself or a currently unknown downstream effector remains unclear.[216] Although the mechanism has not been determined, this supports the idea that the selectivity of VA-RNAI-deleted viruses for cancer cells is based on the common *ras* mutation.

However, *dl*331 showed poor replication in K-*ras* mutated Suit-2 and PANC-1 cells. This confirmed that *dl*331 is not solely selective for K-*ras* mutated cells, re-opening the question of which cancer-associated mutation(s) are responsible for rescuing *dl*331's replication. This result agrees with the findings of Schümann and Dobblestein, published after this work was begun, who were able to manipulate the *ras* status of cell lines to test its effect on the selectivity of VA-RNA-deleted adenoviruses.[106]

Cytotoxicity studies in cancer cell lines showed that *dl*331 causes less cell death than *dl*309 per plaque-forming unit in three of the four cell lines tested, correlating with the virus replication results. This impaired cell killing activity is a potential weakness of *dl*331 as a cancer therapy. However, once the basis of the virus's selectivity is better understood, it may be possible to increase the virus's toxicity to cancer cells. Several approaches to increasing toxicity of an oncolytic virus have been explored previously.

A virus can be armed with the ability to express directly cytotoxic or pro-apoptotic proteins such as p53. A related technique is to make the virus express a prodrug-converting enzyme such as nitroreductase to create an alkylating agent,[217] or thymidine kinase to sensitise cells to nucleoside

analogues such as ganciclovir.[218] The power of RNA interference (RNAi) techniques to silence expression of key oncogenes makes shRNA an appealing payload. Oncolytic adenoviruses have been constructed to carry shRNA targeting *ras*,[219] *hTERT*[220] and the mRNA encoding the tumour antigen Ki-67.[221] In each case, the virus was successful in inducing apoptosis in infected cells, leading to the significant inhibition of xenograft tumour growth in nude mice. Similar results were achieved using an oncolytic adenovirus expressing shRNA targeting survivin to induce apoptosis.[222]

VA-RNAI is known to be targeted by the Exportin 5 and DICER pathways necessary for the function of shRNAs[98,111,223] and possibly to down-regulate siRNA and microRNA biogenesis.[224] It therefore seems plausible that VA-RNAI-deleted adenoviruses could become selective and unusually efficient shRNA delivery vectors.

Endogenous genes may also be modified to enhance anti-tumour efficacy. For example, previous studies have shown some success at enhancing virus toxicity *in vitro* by deleting the anti-apoptotic genes E1A CR2 or E1B-19kD.[212]

While these techniques have shown considerable promise, as is common for gene therapy and oncolytic therapy approaches, efficient delivery to solid tumours remains challenging.

8.2 VA-RNAI influences eIF2α phosphorylation but this alone cannot explain its function

VA-RNAI expression did suppress PKR upregulation and phosphorylation – presumed to be indicative of its activation – in Suit-2 and, to a lesser extent, HCT116 cells. No difference in PKR expression or phosphorylation was observed in MiaPaCa2 cells. This matched the pattern suggested by the replication and toxicity results, in that upregulation and activation of PKR correlates with poor viral replication and toxicity. Presumably the unknown factor associated with *ras* mentioned above is present at high levels in MiaPaCa2 cells.

As expected, phosphorylation of PKR's target eIF2α was regulated by PKR activation in Suit-2 and HCT116 cells. Also as expected, MiaPaCa2 cells, which showed no increase in PKR activation, showed no increase in eIF2α phosphorylation. These data follow the pattern expected from VA-RNAI's canonical function of protecting the virus from an intracellular response by blocking eIF2α phosphorylation.

Unexpectedly, although VA-RNAI expression did significantly increase replication and toxicity in PANC-1 cells, it was not linked with eIF2α phosphorylation. This confirmed published results that support for viral replication is not necessarily controlled by VA-RNAI's inhibition of eIF2α phosphorylation.[106] Since this section of the work was performed, Zhang and Samuel have published evidence supporting the idea that PKR activity is not the sole mechanism of VA-RNAI activity. In agreement with the results shown here, their data confirm that knockdown of PKR is not sufficient to restore the replication efficiency of *dl*331.[225]

One or more of PKR's other proposed targets (e.g. STAT1 or the upregulation of *c-fos*, *c-jun* and NF-κB[212]) may be involved in the intracellular antiviral response, and therefore a target of VA-RNAI's modulatory response. However, it also seems very likely that another pathway entirely is involved in VA-RNAI's protection of the virus. Independent of PKR, the viral infection of a cell can trigger the production of various other defensive signals, most notably type I interferons and products of their signalling cascade such as TNF-α and NF-κB.

8.3 VA-RNAI's activity is not reliant on control of interferon production

IFNβ transcription was suppressed by VA-RNAI in PANC-1 cells, but not in Suit-2, HCT116 or MiaPaCa2 cells. This suppression of IFNβ at 24 hours post-infection did not result in an observable change in IFNβ secretion. Possibly the observed suppression of IFNβ transcription in PANC-1 cells was a transient effect, too brief to have a large impact on accumulation of secreted IFNβ. Alternatively, transcript availability of

IFNβ might not be the limiting factor. Instead, translation of IFNβ could be limited along with all other host genes by the virus-imposed switch to cap-independent translation resulting from L4-100k's interaction with the host kinase and translation initiation factor eIF4E.[226]

Similarly, expression of the dsRNA-sensing RIG-i did not seem to be influenced by the presence of VA-RNAI. There was, however, an increase in RIG-i expression 24 hours after infection with Ad5 when compared to the other infections (mock, *dl*309 and *dl*331). This upregulation was not seen in either of the mutant viruses. This difference seems likely to be due to *dl*331 and *dl*309's shared deletions in the E3 region. Unfortunately, without detailed further study that is outside the scope of this project, it is impossible to ascertain exactly which genes are involved.

As described in the Introduction, intracellular pathogens may be detected by their binding to pathogen-associated molecular pattern receptors (PAMPs or PRRs) such as the Toll-like receptors (TLRs). TLRs are more typically expressed in inflammatory and antigen-presenting cells than in somatic tissues.[227] Activation of the TLRs is a powerful stimulus for the production of type I interferons and, during infections in dendritic cells, IL6 and other inflammatory cytokines.[228]

These receptors tend to be found in endosomes and, as such, may be fed peptide fragments by the autophagic and other degradative pathways. TLR3 and TLR9 recognise dsRNA and unmethylated CpG motifs typical of viral DNA, respectively. TLR2 is also involved in detecting adenoviral infections in some cell types, although its ligand has not been identified. In order to determine whether their activation level is changed by expression of VA-RNAI, the subcellular localisation of IRF3, a signalling molecule immediately downstream of these receptors, was monitored. Expression of VA-RNAI did not alter the proportion of IRF3 localised to the nucleus in Suit-2, the cell line that showed the most consistent difference between *dl*331 and *dl*309. It therefore seems unlikely that TLR signalling is one of the determining factors in a cell line's support for replication of VA-RNAI-deleted virus.

The failure of VA-RNAI to activate TLR3 is somewhat surprising given that VA-RNAI has specifically evolved to be bound by the dsRNA-binding domains of PKR and other dsRNA-sensing molecules.

A low activation of TLR9 might be expected from an adenovirus infection, given the adenovirus genome's low incidence of stimulating CpG motifs.[48]

8.4 VA-RNAI and macroautophagy

8.4.1 Virus-induced eIF2α phosphorylation correlates with induction of macroautophagy

Although my data have shown that the PKR - eIF2α pathway cannot be the sole mechanism for VA-RNAI's activity, the established link between eIF2α phosphorylation and the induction of autophagy presented an attractive hypothesis. Specifically, that a novel function of VA-RNAI could be an inhibitor of macroautophagy in infected cells, protecting the virus from degradation and exposure to the adaptive immune system.

Confocal microscopy of U20S cells expressing a GFP-LC3 fusion protein confirmed that autophagy is upregulated in cells infected with *dl*331 when compared to those infected with *dl*309 or mock infected. These cells were probed with an antibody against phosphorylated eIF2α, and stronger signal was seen in cells infected with *dl*331 that *dl*309, confirming that VA-RNAI inhibits eIF2α phosphorylation in those cells. Additionally, high levels of phospho-eIF2α within a given cell correlated with high numbers of autophagosomes visible within that same cell; this supported the hypothesis that increased levels of autophagy would result from increased eIF2α phosphorylation.

The mechanism of eIF2α's induction of macroautophagy is currently unknown. Continued accumulation of eIF2α leads to a downregulation of cap-dependent translation within the cell, eventually leading to an increase in translation of ATF4 and, later, CHOP, also called GADD153. These act as pro-apoptotic signals, pushing the cell toward death.[229,230] However apoptosis and autophagy appear to be mutually incompatible pathways;

each programme appears to down-regulate the other. It has therefore been suggested that the timing of eIF2α phosphorylation may play a role in determining its result, whether in terms of concurrence with other stress signals or simply duration of the signal.[230]

In the case of a cell infected with *dl*331, the virus expresses several proteins to suppress induction of apoptosis. It seems plausible that these viral anti-apoptotic proteins play a determinative role in pushing the cell's response to this stress signal toward autophagy rather than apoptosis, although further experimentation would be necessary to confirm this.

eIF2α is also strongly associated with the collection of malformed proteins into endoplasmic reticulum quality control compartments (ERQC). ERQCs are pericentriolar enclosures in which misfolded or simply unfolded proteins are collected as part of the UPR.[231,232] However, the role of eIF2α in aiding the formation of these enclosures does not seem related to its role in autophagy, as the contents are not processed into autophagosomes.[232] Indeed, by lowering the unfolded protein load in the cell, this activity of eIF2α seems likely to be removing a pro-autophagic signal from the cellular environment.

Due to the concerns over GFP-LC3 becoming incorporated into aggresomes or becoming associated with membranes of the endoplasmic reticulum, fluorescent immunohistochemistry was used to confirm these result with endogenous levels of LC3 expression. The selectivity and specificity of both the primary and secondary antibodies were confirmed.

VA-RNAI expression was necessary to suppress virus-induced autophagy in Suit-2 cells, although this suppression was not complete; although cells infected with *dl*309 had significantly fewer autophagosomes per cell than those infected by *dl*331, mock-infected cells had fewer still.

MiaPaCa2 cells showed a small but significant upregulation of autophagy in response to both viruses when compared to mock-infected cells. No difference in the number of autophagosomes per cell was observed between the two viruses.

Western blotting for LC3 yeilded ambiguous results, showing an increase in both LC3I and LC3II in *dl*331-infected cells compared to *dl*309- and mock-infected cells. This does not match the expected pattern from induction of autophagy. While it is possible that this represents an upregulation of LC3II expression and its conversion to LC3II for incorporation into autophagosomes, this cannot be confirmed without further control experiments including performing a loading control for the Western blot and the use of bafilomycin as described in the Introduction.

Unexpectedly, VA-RNAI expression was not sufficient to prevent the accumulation of Beclin 1 in MiaPaCa2 cells after infection with *dl*331, while infection with *dl*309 led to no such accumulation. This could indicate that there is some difference between the two viruses beyond the deletion of the VA-RNAI promoter in *dl*331. The complete sequence for *dl*331 has never been published, so such a small uncharted difference is possible. However, as this putative difference in the activity of the virus is very limited and cell-line dependent, it seems likely that this unexpected behaviour is due to the cell line more than the virus. For example, the prolonged and high expression of the VA-RNAs from the plasmid could be somehow priming the MiaPaCa2 cells to respond differently when a new source of the RNAs is established. Alternatively, the difference could be due to the rate of production of VA-RNAs, which might be expected to be higher in cells expressing it from the virus in addition to the plasmids. Unfortunately, at this stage the true cause of this difference is unknown and so these hypotheses remain purely speculative.

Taken together, the results from Suit-2 and MiaPaCa2 cells appear to confirm the hypothesis that induction of autophagy is largely dependent on eIF2α phosphorylation status. The small increase in autophagy in the circumstances where extensive eIF2α phosphorylation is not expected (Suit-2 infected with *dl*309; both MiaPaCa2 infections) could be accounted for by some other shared pathway involved in autophagy induction. For example, the PI3-K dependent active transport of adenovirus into the cell could be expected to have an effect on mTOR regulation.[233]

8.4.2 HCT116 cells appear totally resistant to autophagy

Unexpectedly, HCT116 cells showed no induction of autophagy in response to infection with either virus. Later attempts to induce autophagy in HCT116 by starvation also failed, confirming that this deficiency is not due to viral autophagy inhibitors being unusually efficient in this cell line.

Western blots probing for LC3 and Beclin 1 confirmed that these pro-autophagic proteins are present at levels similar to those seen in Suit-2 and MiaPaCa2. The modified form of LC3 – LC3II – was detected by Western blot in HCT116 cells, confirming the presence and activity of ATG3 and ATG8, the proteins responsible for this modification. However, the conversion of LC3I to LC3II was not influenced by viral infection, suggesting that the deficiency could lie in one of the autophagy-inducing genes.

As described in the Introduction, it is not uncommon for tumourigenesis to involve the loss or suppression of pro-autophagic genes. However, it is unclear what the relevant mutation in HCT116 cells might be. This cell line has homozygous wild-type (pro-autophagic) PTEN[234] and does not appear to have abnormally high expression of (anti-autophagic) Bcl-2.[235] Unfortunately, no additional reports of autophagy gene expression in HCT116 cells are currently available in the literature. The resistant nature of this cell line against induction of autophagy is interesting, and certainly warrants further investigation.

8.4.3 Infection with *dl*331 leads to more cells strongly expressing E1A than infection with *dl*309

In Suit-2, MiaPaCa2 and HCT116 cells, only a minority of cells (between 30% and 5%) showed high levels of expression of adenovirus E1A. When viewed with a higher gain, all cells examined expressed some of the viral protein, confirming that this effect was not due to only a subset of cells becoming infected.

Unexpectedly, a greater proportion of cells were high-expressing in *dl*331-infected cultures than in those infected with *dl*309, although this only reached statistical significance in Suit-2 cells ($p<0.005$).

As E1A is expected to accumulate rapidly at the early times in infection and then decrease to lower levels, the high-expressing cells could be in the early stages of a second wave of infection. In this case there are two possible explanations. Firstly, *dl*331 may have infected the cells less efficiently than *dl*309, leaving a larger population of uninfected cells to be targeted by the progeny virus when it is eventually released. This seems unlikely: VA-RNAI is not carried in the viral capsid and therefore its deletion from the genome should make no difference to the efficiency or speed of cell entry and early gene expression. The second possibility is that *dl*331 has a faster replication and release cycle than *dl*309. There is no obvious reason why such a difference would exist. A small shortening of the viral genome could lead to a dramatic increase in the speed at which genome copies accumulate, due to the PCR-like exponential increase in genome copies tending to amplify very minor differences in initial template availability. However, the genomes of *dl*331 and *dl*309 are very similar in length: the two viruses share deletion of the E3 region, and *dl*331 has an additional deletion of only 29 base pairs, in the intragenic promoter region of VA-RNAI.[121] It therefore seems implausible to expect a faster replication cycle for *dl*331 than *dl*309 based on a difference in genome length.

Expression of VA-RNAI appears to contribute to an effect limiting the accumulation of E1A in infected cells. Expression of proteins from the adenovirus major late transcription unit (MLTU) down-regulates expression of the early genes including E1A.[236] As VA-RNAI expression is known to influence the expression patterns of other late genes,[121] it is conceivable that VA-RNAI expression has an indirect effect on the expression of E1A during late stages of infection.

It has previously been shown that the difference between mRNA levels of E1A from Ad2 and Ad5 could be partially determined by the relative efficiency of their export from the nucleus.[121,237] Although this has yet to be confirmed, it seems possible that VA-RNAI's near-saturation of the Exportin-5 nuclear mRNA export pathway could influence the export and stability of E1A mRNA at late times in infection.

8.4.4 Adenovirus E1A co-localises with autophagosomes

Although only a minority of cells expressed high levels of E1A, all examined cells expressed E1A at a lower level. In cells with visible autophagosomes, E1A was often seen to co-localise with the autophagosomes. Several RNA viruses have been shown to rely on co-localisation with autophagosomes or autophagosome-like structures for successful replication and exit from the cell, including coronaviruses, picornaviruses and murine hepatitis virus. However, DNA-based viruses that have been seen to associate with autophagosomes, such as Herpes Simplex Virus, do not seem to benefit from the association. Indeed, HSV-1 is known to be degraded inside autophagosomes.[74]

The HSV-1 neurovirulence protein ICP34.5 has been mentioned previously in this discussion as being analogous to VA-RNAI, as it redirects the host protein phosphatase 1α (PP1α) to dephosphorylate eIF2α. Work with an ICP34.5 deletion mutant has recently shed light on the importance of autophagy to HSV-1 infection. In cell culture, inhibiting autophagy via knockdown of ATG5 was not sufficient to restore the replication efficiency of the mutant virus to that of wild-type virus,[238] suggesting that autophagy does not play a major role in controlling HSV-1 replication. However, *in vivo* work with the same virus showed that inhibiting autophagy significantly enhanced the neurovirulence of the mutant virus in mice.[239] It remains unclear whether this is due to changes in regulation and importance of autophagy between cell culture and *in vivo* experiments, or due to cell-type specific variation in the same factors.

The results from these studies of HSV-1 raise the question of whether E1A's co-localisation with autophagosomes represents its sequestration for degradation and, if so, whether more proteins – or even entire viral particles – are similarly captured. The consequences of this interaction for the virus are unclear, as the cited work in HSV-1 demonstrated that the relationship between autophagy and viral load can be heavily dependent on some combination of cell type and environment.

8.4.5 VA-RNAI expression prevents starvation-induced autophagy in Suit-2 cells

As described in the Introduction, solid tumours are often nutrient-poor and hypoxic environments. Broadly, this is due to an insufficiently developed or blocked vasculature, incapable of supplying sufficient fresh blood to densely packed and highly metabolically active cancer cells. Many tumour cells survive these conditions through the upregulation of macroautophagy, as a source of metabolites and ATP.

VA-RNAI's ability to block virus-induced autophagy in Suit-2 cells prompted the question of whether it could also block this tumour survival pathway. Starving untreated Suit-2 cells or Suit-2 cells transfected with a control plasmid induced high levels of autophagy. Cells expressing VA-RNAI and the related VA-RNAII from a commercial plasmid were unable to induce autophagy. Interestingly, these cells showed noticeably more cell rounding and detachment indicative of cell death than those which had not had autophagy blocked.

This presents a dilemma in the use of VA-RNAI-deleted viruses in cancer therapy. While the deletion does provide selectivity for certain cancer cell lines, expression of VA-RNAI could actually be advantageous in an oncolytic virus, by sensitising the tumour cells to nutrient deprivation so typical of the tumour environment.

MiaPaCa2 cells did not show an increase in autophagy after starvation. Given that starvation-induced autophagy is regulated by the same pathway as virus-induced autophagy, this is not surprising. In the future, it could be fascinating to discover why MiaPaCa2 are so resistant to the induction of autophagy, and whether this is solely due to its resistance against eIF2α phosphorylation.

8.4.6 VA-RNAI suppresses induction of AVOs

The limitations of staining cells with acridine orange were described in the Introduction. Briefly, this dye is lysosomotropic and fluoresces red when in an acidic environment and so is not truly specific for monitoring autophagy.

The examination of starved Suit-2 cells demonstrated that brightly fluorescing red acridine orange was localised in roughly spherical compartments reminiscent of autophagosomes. Unfortunately, an incompatibility between protocols for acridine orange staining and immunofluorescence prevented a check for co-localisation of AO and LC3.

Flow cytometry analysis of stained Suit-2 cells reflected the pattern expected from the confocal microscopy. Expression of VA-RNAI from the virus partially suppressed the virus-induced formation of acidic vesicular organelles (AVOs). Expression of VA-RNAI from the plasmid completely suppressed virus-induced AVOs. This stronger inhibitory effect is presumably due to a higher expression level from the plasmid, especially during the early stages of viral infection when VA-RNAI would typically be at low levels or entirely absent.

The results for MiaPaCa2 were more unexpected. Expression of VA-RNAI from the plasmid matched the confocal data by completely suppressing virus-induced AVOs. However, while some induction of AVOs was expected based on the confocal data, infection with *dl*331 led to a higher increase in AVOs than infection with *dl*309. Thus, although VA-RNAI expression is not required to prevent phosphorylation of eIF2α or to inhibit virus-induced autophagy, it is required to prevent the creation of new acidified compartments within the cells.

One possible explanation for this behaviour is the virus-dependent induction of the unfolded protein response. This involves the creation of double-membraned, low-pH compartments, which are effectively extensions of the endoplasmic reticulum. Induction of this pathway is dependant on phosphorylation of eIF2α, typically via PERK activation. The discriminating factor that determines whether eIF2α activation will lead to the UPR or to autophagy is currently unknown, although it has been speculated that the duration of the signal may be important. [209,230,232]

8.4.7 VA-RNAI in cancer therapy

VA-RNAI sensitised Suit-2 cells to treatment with the common chemodrug 5-FU. Cancer cells have previously been shown to rely on

autophagy as a mechanism to survive treatment with 5-FU.[210,211] Given 5-FU's mechanism as a chain-terminating nucleoside analogue, presumably the autophagy pathway is called upon for its role in surviving single- and double-strand breaks in DNA.[240,241]

The finding that VA-RNAI is able to sensitise Suit-2 cells to treatment with 5-FU raises the question of its mechanism. The route by which DNA damage leads to the induction of autophagy is not well known, although some details have been elucidated. Promisingly, inhibition of poly(ADP-ribose) polymerase (PARP) activity can prevent autophagy induction.[242] PARP is an indirect target of active PKR via activation of cellular protease CPP32,[243] presenting a clue to a possible mechanism by which VA-RNAI could influence the activation of this pathway.

Taken together, the findings regarding VA-RNAI's activities up to this point present a dilemma. While the exact basis of their selectivity remains unknown, VA-RNAI deletion mutants of adenovirus have well-established selectivity for some cancers. However, its ability to block virus-induced, starvation-induced and apparently 5-FU-induced autophagy suggest that VA-RNAI could be a powerful anti-tumour agent, suppressing a key survival pathway for the tumour.

Based on these results, it would be fascinating to see VA-RNAI trialled as an anti-cancer agent, delivered to cells to sensitise them to starvation or lack of growth hormone, to viral infection or to treatment with 5-FU. Other treatments that induce autophagy, e.g. radiotherapy, would also warrant investigation. Currently, VA-RNAI shares the problems of other gene therapy "payload" toxic genes, most notably delivery.

8.5 Microarray analysis of infected normal cells

The cell line-dependent effects of VA-RNAI on factors such as eIF2α phosphorylation, IFNβ synthesis and autophagy induction highlight the limitations of working with cancer cell lines. It is extremely difficult to be sure whether observed effects and interactions are truly representative of the virus' interactions with normal cells and therefore typical behaviour for the virus, or unique to a certain combination of mutations in a given cancer cell

line. In order to overcome this problem – and to learn more about normal cells' response to viral infection – whole RNA from infected cells was subjected to microarray analysis.

Firstly, levels of VA-RNAI expression were measured at regular intervals during infection. In the two epithelial cell types tested, VA-RNAI was detected at low levels until approximately 18 hours after infection. At this time, levels of VAI rapidly increased until reaching a plateau at 28 hours. This plateau in VA-RNAI accumulation coincided with extensive cytopathic effect beginning to appear in the infected cells. Therefore it may be that VA-RNAI production is not downregulated at the end of infection, merely that synthesis is stopped due to cell death. Alternatively, cellular RNAses could begin to degrade VA-RNAI. However, maintaining a constant quantity of VA-RNAI over several hours could only happen if the production and degradation of VA-RNAI were closely balanced. This seems unlikely to occur by chance.

Based on the known timing of VA-RNAI expression, several timepoints in the infection were chosen for analysis of cellular gene expression using an expression microarray. Two timepoints were chosen before high VA-RNAI expression, at 6 and 12 hours. The purpose of these was to chart the cells' initial response to viral infection. Comparing the VA-RNAI-deleted and control virus infections will confirm whether VA-RNAI only takes effect after the upregulation at 18 hours. Additionally, comparing the infected cells with mock-infected cells will provide invaluable – and so far unique – data on how the early genes of Adenovirus interact with healthy bronchial epithelial cells.

Later timepoints were also chosen: 18, 24 and 28 hours, to coincide with the upregulation and stabilisation of VA-RNAI levels. Comparison of gene expression data from *dl*331 and *dl*309 infected cells will provide extensive information on the cellular response prompted by VA-RNAI.

Automated clustering of the microarray data revealed some information. The six-hour timepoint shows the two viruses clustered together with the mock-infected cells. This indicates that the intracellular

response has not yet had made an obvious impact on cellular gene expression. From twelve hours onwards the mock-infected cells are grouped, separate from the virus-infected cells. This highlights the increasing scale of gene expression changes within the infected cells. The virus-infected cells are paired by timepoint. This confirms that the genes expressed in response to the infection are changing over time, and that this process is largely unaffected by VA-RNAI expression.

More detailed analysis of the data yielded lists of genes whose expression varied over time. Comparison of the regulation of these genes in response to the viral infections resulted in final lists of genes that are differentially expressed at the time that VA-RNAI accumulates to high levels within the cell, and sustained until the last timepoint. Many of these genes were involved in cell cycle regulation, and so a subset of these were chosen for further validation.

E2F1, E2F8, Cyclin E2, ID2 and the histone component H2al are all strongly associated with progression through the cell cycle. Their upregulation in cells infected with *dl*331 is somewhat counter-intuitive, as the consequences of VA-RNAI deletion – protein synthesis arrest, autophagy – could be expected to lead to the inhibition of cell cycle progression.

Nevertheless, quantitative RT-PCR showed that all five of these genes were significantly upregulated in Suit-2 cells infected with *dl*331 when compared to those infected with *dl*309. MiaPaCa2 cells showed no significant upregulation in any of these genes; indeed, all five were reported as slightly lower values in *dl*331-infected cells, although these differences were not significant. The differential regulation of these genes is a consequence of VA-RNA's modulation of the host response to the virus, as evidenced by the lack of differential gene regulation in cells expressing VA-RNAs from the plasmid pAdVAntage but not infected with either virus.

At the protein level, the key cell cycle control gene inhibitor of differentiation 2 (ID2) was upregulated in response to *dl*331 when compared to *dl*309 in Suit-2 cells. As expected, no such regulation was seen in

MiaPaCa2 cells. In general, ID2 expression is expected to favour proliferation, inhibit cellular differentiation and aid tumour angiogenesis.[244] Little has been reported regarding its interaction with viruses, although it is found to be commonly over-expressed in EBV-associated Hodgkin's lymphoma, where it is hypothesised to play a role in preventing terminal differentiation of the B lymphocytes.[244] Its over-expression has also been reported in association with portal vein invasion of hepatitis C virus-related hepatocellular carcinoma, although its exact function in this process is unknown.[245]

Functional validation of these findings revealed that, at 24 hours after infection, cells infected with *dl*331 have a cell cycle profile very similar to mock-infected cells, while those infected with *dl*309 show an increase in S-phase at the expense of G2/M phase. This difference was transient, having disappeared by 28 hour after infection, but repeatable. Possibly, the relative upregulation of cell cycle-advancing genes in the *dl*331-infected cells results in a faster transition through the S-phase analogue induced by the viral infection. A shorter time spent in S-phase before the accumulation of the cyclins required to push the cell into attempting to enter G2/M phase – and possibly a subsequent mitotic catastrophe – could allow less time for *dl*331 to replicate than *dl*309, resulting in a lower yield of viral progeny from the infection.

This interaction of VA-RNAI with the host genes observed to be expressed is complex and, while the predominance of cell cycle regulatory genes was striking, the mechanism for their regulation is not clear. They do not fit the expected profile of gene regulation in response to the UPR, autophagic or apoptotic pathways most typically associated with VA-RNAI's most well established function of inhibiting eIF2α phosphorylation. Rather, they represent an emerging new pathway in VA-RNAI's modulation of the host's response against the virus.

9 Appendix: Gene Lists

Comparison of mRNA levels in cells infected with *dl*331 and *dl*309. These data represent accumulation over time, normalised against mock-infected cells. Positive values indicate that mRNA levels are higher in cells infected with *dl*331 compared to *dl*309 (i.e. higher in absence of VAI)

Table 24 - Earliest responses [-1.5 ≥ 20h ≥ 1.5 AND -1≥ 24h ≥ 1]

NAME	6 HOURS	12 HOURS	20 HOURS	24 HOURS	28 HOURS
PX domain containing serine/threonine kinase	0	0	5	1.128438959	0
SEC31 homolog A (S. cerevisiae)	0	0	1.654742824	-1.39939952	0
family with sequence similarity 111, member B	1.554230796	0	2.138064859	1.272571317	2.88895585
B-cell CLL/lymphoma 2	0	0	1.58057891	1.3787149	1.665709233
neurofilament, medium polypeptide 150kDa	0	0	2.67523975	2.893371654	1.546744543
histone cluster 1, H3h	-1.58589909	0.215381605	1.540490925	1.690959165	1.441054275
zinc finger protein 239	0	0	1.599879515	1.6155161	0
histone cluster 2, H4a	0	-1.01288904	2.299484032	2.158513445	0.856063565
histone cluster 1, H3a	0	0	2.074250521	1.940475043	2.102196952
histone cluster 1, H2aj	0	0	1.660517409	1.15259055	1.850082617
heat shock 70kDa protein 2	0	0	1.602951934	1.702076425	0.688318496
histone cluster 1, H2ai	0	0	1.749087654	1.196256988	1.039128338
histone cluster 1, H2al	0	0	2.605586226	2.719489933	3.344029184
hect domain and RLD 5	0	0	1.657661661	1.855130933	1.274931362
X (inactive)-specific transcript	0	0	1.582002943	1.932871181	1.583120294
doublesex and mab-3 related transcription factor 2	0	0	2.14378336	2.472678677	0.771401096
hypothetical LOC387763	0	0	1.706268677	2.652177101	3.05398332
hypothetical protein LOC645580	0	0	1.634234993	1.487782683	1.882322384
zinc finger protein 711	0	0	1.653020668	1.863060301	1.63605671
glyoxalase domain containing 1	0	0	1.749842316	1.754052685	1.265095701
transmembrane protein 46	-1.04829724	0	1.947623881	2.033617389	3.025536179
arylsulfatase G	0	0	1.552736688	1.458363375	1.257766821
thioredoxin reductase 1	0	0	1.692239853	1.602468847	1.12289458
G kinase anchoring protein 1	0	0	1.568873289	1.174174886	1.279305936

nuclear localized factor 1	0	0	1.552028834	1.648835807	1.4649685
chondroitin sulfate proteoglycan 5 (neuroglycan C)	0	0	1.592906503	1.003631037	0.814777719

Table 25 - Later responses: [-1 ≤ 20h ≤ 1 AND -1.5 ≥ 24h ≥ 1.5]

NAME	6 HOURS	12 HOURS	20 HOURS	24 HOURS	28 HOURS
chromosome 8 open reading frame 47	0	0	0	1.519089761	-1.02112867
solute carrier family 19 (folate transporter), member 1	0	0	0	1.778661683	0.504498641
schlafen family member 13	-0.441604475	0	0	1.693226446	1.045700173
hypothetical protein LOC646762	1.053412927	0	0.066862587	1.577998069	0.356491591
heat shock 70kDa protein 1B	0.217334572	1.127373304	0.884545179	1.921417662	1.169529652
chromosome 1 open reading frame 107	0	0	0	1.583200678	1.269324737
cyclin E2	-0.348058312	0	0	1.62375762	0.90733804
solute carrier family 27 (fatty acid transporter), member 2	0	0	0.611507888	2.396500656	1.110016055
solute carrier family 27 (fatty acid transporter), member 2	0	0	0.254171412	1.603487951	0.730194791
zinc finger protein 165	-0.362292984	0	0	1.770450854	0
distal-less homeobox 2	0	0	0	1.517969072	1.926493625
peripheral myelin protein 22	0	0	0.092402791	1.947706367	0.947545689
histone cluster 1, H2bg	-0.273912355	0	0.975907613	1.608922088	1.28689101
transmembrane protein 97	0	0	0	1.869629123	0.689908813
v-myb myeloblastosis viral oncogene homolog (avian)-like 1	-0.385082564	-1.04939238	0	1.531051858	1.59333635
glypican 1	0	0	-0.07084755	-1.73423356	-0.63384358
histone cluster 2, H2aa3	0	0	0.520812827	1.543640644	0.661240312
v-maf musculoaponeurotic fibrosarcoma oncogene homolog B (avian)	0.090477317	1.209815218	0.81836236	1.65706072	1.265776358
chromosome 1 open reading frame 109	0	0	0	1.554710552	1.015821039
E2F transcription factor 8	-0.14562247	-1.02597981	0	1.541775644	1.235571679
cell division cycle associated 7	0	0	0	1.531911019	0.620309498
coiled-coil domain containing 77	-1.082506512	0	0	1.540611613	0
cell division cycle associated 7-like	-1.089280622	0	0	1.659266279	0.59147214
ubiquitin-like, containing PHD and RING finger domains, 1	-0.080102248	0	0	1.775322046	0.708837821
aspartate beta-hydroxylase domain containing 2	0	0	0	1.55837563	1.010022505
similar to CG12314 gene product	-0.242694707	0	0.596807318	1.871446942	1.487323886
MAP7 domain containing 2	0	0	0	1.578698145	1.632968118
ankyrin repeat domain 34	0	0	0.038454518	1.53354609	0.390863745

hypothetical protein LOC201725	-0.008840566	-1.44254652	0	1.512685488	0
transmembrane protein 56	0	0	0	1.628561337	1.578547976
isoleucyl-tRNA synthetase	0	0	0	1.527206131	0
KISS1 receptor	0	0	0	1.65457862	1.113503044
hypothetical protein FLJ13305	-1.197169813	0	0	1.592710426	1.268057831

10 Bibliography

1 Ma, Y. & Mathews, M. B. Structure, function, and evolution of adenovirus-associated RNA: a phylogenetic approach. *J Virol* **70**, 5083-5099 (1996).

2 Goncalves, M. A. & de Vries, A. A. Adenovirus: from foe to friend. *Rev Med Virol* **16**, 167-186 (2006).

3 Leen, A. M. & Rooney, C. M. Adenovirus as an emerging pathogen in immunocompromised patients. *Br J Haematol* **128**, 135-144 (2005).

4 Vellinga, J., Van der Heijdt, S. & Hoeben, R. C. The adenovirus capsid: major progress in minor proteins. *J Gen Virol* **86**, 1581-1588 (2005).

5 Green, M. & Pina, M. Biochemical studies on adenovirus multiplication. IV. Isolation, purification, and chemical analysis of adenovirus. *Virology* **20**, 199-207 (1963).

6 Santis, G. *et al.* Molecular determinants of adenovirus serotype 5 fibre binding to its cellular receptor CAR. *J Gen Virol* **80 (Pt 6)**, 1519-1527 (1999).

7 Wiethoff, C. M., Wodrich, H., Gerace, L. & Nemerow, G. R. Adenovirus protein VI mediates membrane disruption following capsid disassembly. *J Virol* **79**, 1992-2000 (2005).

8 Colby, W. W. & Shenk, T. Adenovirus type 5 virions can be assembled in vivo in the absence of detectable polypeptide IX. *J Virol* **39**, 977-980 (1981).

9 Zhang, W. & Arcos, R. Interaction of the adenovirus major core protein precursor, pVII, with the viral DNA packaging machinery. *Virology* **334**, 194-202 (2005).

10 Davison, A. J., Benko, M. & Harrach, B. Genetic content and evolution of adenoviruses. *J Gen Virol* **84**, 2895-2908 (2003).

11 Zhang, Y. & Bergelson, J. M. Adenovirus receptors. *J Virol* **79**, 12125-12131 (2005).

12 Yanagi, Y., Takeda, M., Ohno, S. & Seki, F. Measles virus receptors and tropism. *Jpn J Infect Dis* **59**, 1-5 (2006).

13 Honda, T. *et al.* The coxsackievirus-adenovirus receptor protein as a cell adhesion molecule in the developing mouse brain. *Brain Res Mol Brain Res* **77**, 19-28 (2000).

14 Cohen, C. J. *et al.* The coxsackievirus and adenovirus receptor is a transmembrane component of the tight junction. *Proc Natl Acad Sci U S A* **98**, 15191-15196 (2001).

15 Dechecchi, M. C., Tamanini, A., Bonizzato, A. & Cabrini, G. Heparan sulfate glycosaminoglycans are involved in adenovirus type 5 and 2-host cell interactions. *Virology* **268**, 382-390 (2000).

16 Meier, O. & Greber, U. F. Adenovirus endocytosis. *J Gene Med* **6 Suppl 1**, S152-163 (2004).

[17] Bai, M., Harfe, B. & Freimuth, P. Mutations that alter an Arg-Gly-Asp (RGD) sequence in the adenovirus type 2 penton base protein abolish its cell-rounding activity and delay virus reproduction in flat cells. *J Virol* **67**, 5198-5205 (1993).

[18] Chardonnet, Y. & Dales, S. Early events in the interaction of adenoviruses with HeLa cells. I. Penetration of type 5 and intracellular release of the DNA genome. *Virology* **40**, 462-477 (1970).

[19] Greber, U. F. Virus assembly and disassembly: the adenovirus cysteine protease as a trigger factor. *Rev Med Virol* **8**, 213-222 (1998).

[20] Greber, U. F., Willetts, M., Webster, P. & Helenius, A. Stepwise dismantling of adenovirus 2 during entry into cells. *Cell* **75**, 477-486 (1993).

[21] Seth, P., Willingham, M. C. & Pastan, I. Binding of adenovirus and its external proteins to Triton X-114. Dependence on pH. *J Biol Chem* **260**, 14431-14434 (1985).

[22] Wang, K., Guan, T., Cheresh, D. A. & Nemerow, G. R. Regulation of adenovirus membrane penetration by the cytoplasmic tail of integrin beta5. *J Virol* **74**, 2731-2739 (2000).

[23] Reese, E. L. & Haimo, L. T. Dynein, dynactin, and kinesin II's interaction with microtubules is regulated during bidirectional organelle transport. *J Cell Biol* **151**, 155-166 (2000).

[24] Medina-Kauwe, L. K. Endocytosis of adenovirus and adenovirus capsid proteins. *Adv Drug Deliv Rev* **55**, 1485-1496 (2003).

[25] Cobrinik, D. Pocket proteins and cell cycle control. *Oncogene* **24**, 2796-2809 (2005).

[26] Bandara, L. R. & La Thangue, N. B. Adenovirus E1a prevents the retinoblastoma gene product from complexing with a cellular transcription factor. *Nature* **351**, 494-497 (1991).

[27] Berk, A. J. Recent lessons in gene expression, cell cycle control, and cell biology from adenovirus. *Oncogene* **24**, 7673-7685 (2005).

[28] Turnell, A. S. & Mymryk, J. S. Roles for the coactivators CBP and p300 and the APC/C E3 ubiquitin ligase in E1A-dependent cell transformation. *Br J Cancer* **95**, 555-560 (2006).

[29] Woo, J. L. & Berk, A. J. Adenovirus ubiquitin-protein ligase stimulates viral late mRNA nuclear export. *J Virol* **81**, 575-587 (2007).

[30] Tauber, B. & Dobner, T. Molecular regulation and biological function of adenovirus early genes: the E4 ORFs. *Gene* **278**, 1-23 (2001).

[31] Thomas, D. L., Schaack, J., Vogel, H. & Javier, R. Several E4 region functions influence mammary tumorigenesis by human adenovirus type 9. *J Virol* **75**, 557-568 (2001).

[32] Dix, I. & Leppard, K. N. Open reading frames 1 and 2 of adenovirus region E4 are conserved between human serotypes 2 and 5. *J Gen Virol* **73 (Pt 11)**, 2975-2976 (1992).

[33] Kleinberger, T. Induction of apoptosis by adenovirus E4orf4 protein. *Apoptosis* **5**, 211-215 (2000).
[34] Robert, A. *et al.* Adenovirus E4orf4 hijacks rho GTPase-dependent actin dynamics to kill cells: a role for endosome-associated actin assembly. *Mol Biol Cell* **17**, 3329-3344 (2006).
[35] Querido, E. *et al.* Identification of three functions of the adenovirus e4orf6 protein that mediate p53 degradation by the E4orf6-E1B55K complex. *J Virol* **75**, 699-709 (2001).
[36] Wodrich, H. *et al.* Switch from capsid protein import to adenovirus assembly by cleavage of nuclear transport signals. *Embo J* **22**, 6245-6255 (2003).
[37] D'Halluin, J. C. Virus assembly. *Curr Top Microbiol Immunol* **199 (Pt 1)**, 47-66 (1995).
[38] Zhang, W. & Imperiale, M. J. Requirement of the adenovirus IVa2 protein for virus assembly. *J Virol* **77**, 3586-3594 (2003).
[39] Tollefson, A. E., Scaria, A., Ying, B. & Wold, W. S. Mutations within the ADP (E3-11.6K) protein alter processing and localization of ADP and the kinetics of cell lysis of adenovirus-infected cells. *J Virol* **77**, 7764-7778 (2003).
[40] Tollefson, A. E. *et al.* The adenovirus death protein (E3-11.6K) is required at very late stages of infection for efficient cell lysis and release of adenovirus from infected cells. *J Virol* **70**, 2296-2306 (1996).
[41] Walters, R. W. *et al.* Adenovirus fiber disrupts CAR-mediated intercellular adhesion allowing virus escape. *Cell* **110**, 789-799 (2002).
[42] Jooss, K. & Chirmule, N. Immunity to adenovirus and adeno-associated viral vectors: implications for gene therapy. *Gene Ther* **10**, 955-963, doi:10.1038/sj.gt.3302037
3302037 [pii] (2003).
[43] Appledorn, D. M. *et al.* Adenovirus vector-induced innate inflammatory mediators, MAPK signaling, as well as adaptive immune responses are dependent upon both TLR2 and TLR9 in vivo. *J Immunol* **181**, 2134-2144, doi:181/3/2134 [pii] (2008).
[44] Yamaguchi, T. *et al.* Role of MyD88 and TLR9 in the innate immune response elicited by serotype 5 adenoviral vectors. *Hum Gene Ther* **18**, 753-762, doi:10.1089/hum.2007.016 (2007).
[45] Cerullo, V. *et al.* Toll-like receptor 9 triggers an innate immune response to helper-dependent adenoviral vectors. *Mol Ther* **15**, 378-385, doi:6300031 [pii]
10.1038/sj.mt.6300031 (2007).
[46] Abbas, A. L., AH. *Cellular and Molecular Immunology*. 5 edn, Vol. 1 (Saunders, 2000).
[47] Hartman, Z. C., Appledorn, D. M. & Amalfitano, A. Adenovirus vector induced innate immune responses: impact upon efficacy and toxicity in gene therapy and vaccine applications. *Virus Res* **132**, 1-14, doi:S0168-1702(07)00366-8 [pii]
10.1016/j.virusres.2007.10.005 (2008).

[48] Muruve, D. A. The innate immune response to adenovirus vectors. *Hum Gene Ther* **15**, 1157-1166, doi:10.1089/hum.2004.15.1157 (2004).
[49] Nanduri, S., Carpick, B. W., Yang, Y., Williams, B. R. & Qin, J. Structure of the double-stranded RNA-binding domain of the protein kinase PKR reveals the molecular basis of its dsRNA-mediated activation. *Embo J* **17**, 5458-5465 (1998).
[50] Williams, B. R. Signal integration via PKR. *Sci STKE* **2001**, RE2 (2001).
[51] Lodish, H. *et al.* in *Molecular Cell Biology* (ed Tenney. S) Ch. Chapter 4: Nucleic Acids, the Genetic Code and the Synthesis of Macromolecules, 130 (W.H. Freeman and Company, 1999).
[52] Rebouillat, D. & Hovanessian, A. G. The human 2',5'-oligoadenylate synthetase family: interferon-induced proteins with unique enzymatic properties. *J Interferon Cytokine Res* **19**, 295-308 (1999).
[53] Bisbal, C. & Silverman, R. H. Diverse functions of RNase L and implications in pathology. *Biochimie* (2007).
[54] Castelli, J., Wood, K. A. & Youle, R. J. The 2-5A system in viral infection and apoptosis. *Biomed Pharmacother* **52**, 386-390 (1998).
[55] Ghosh, A., Sarkar, S. N. & Sen, G. C. Cell growth regulatory and antiviral effects of the P69 isozyme of 2-5 (A) synthetase. *Virology* **266**, 319-328 (2000).
[56] Patterson, J. B., Thomis, D. C., Hans, S. L. & Samuel, C. E. Mechanism of interferon action: double-stranded RNA-specific adenosine deaminase from human cells is inducible by alpha and gamma interferons. *Virology* **210**, 508-511 (1995).
[57] Lei, M., Liu, Y. & Samuel, C. E. Adenovirus VAI RNA antagonizes the RNA-editing activity of the ADAR adenosine deaminase. *Virology* **245**, 188-196 (1998).
[58] Burns, C. M. *et al.* Regulation of serotonin-2C receptor G-protein coupling by RNA editing. *Nature* **387**, 303-308 (1997).
[59] Scadden, A. D. & Smith, C. W. Specific cleavage of hyper-edited dsRNAs. *Embo J* **20**, 4243-4252 (2001).
[60] Imaizumi, T. *et al.* Retinoic acid-inducible gene-I is induced in endothelial cells by LPS and regulates expression of COX-2. *Biochem Biophys Res Commun* **292**, 274-279 (2002).
[61] Yoneyama, M. *et al.* The RNA helicase RIG-I has an essential function in double-stranded RNA-induced innate antiviral responses. *Nat Immunol* **5**, 730-737 (2004).
[62] Yoneyama, M. *et al.* Shared and unique functions of the DExD/H-box helicases RIG-I, MDA5, and LGP2 in antiviral innate immunity. *J Immunol* **175**, 2851-2858 (2005).
[63] Nanbo, A., Yoshiyama, H. & Takada, K. Epstein-Barr virus-encoded poly(A)- RNA confers resistance to apoptosis mediated through Fas by blocking the PKR pathway in human epithelial intestine 407 cells. *J Virol* **79**, 12280-12285 (2005).
[64] Ruf, I. K., Lackey, K. A., Warudkar, S. & Sample, J. T. Protection from interferon-induced apoptosis by Epstein-Barr virus small

RNAs is not mediated by inhibition of PKR. *J Virol* **79**, 14562-14569 (2005).
65 Samanta, M., Iwakiri, D., Kanda, T., Imaizumi, T. & Takada, K. EB virus-encoded RNAs are recognized by RIG-I and activate signaling to induce type I IFN. *Embo J* **25**, 4207-4214 (2006).
66 Seth, R. S., L; Chen, ZJ. Antiviral Innate Immunity Pathways. *Cell Research* **16**, 141-147 (2006).
67 Maher, S. G., Romero-Weaver, A. L., Scarzello, A. J. & Gamero, A. M. Interferon: cellular executioner or white knight? *Curr Med Chem* **14**, 1279-1289 (2007).
68 Sen, G. C. Viruses and interferons. *Annu Rev Microbiol* **55**, 255-281 (2001).
69 Goodbourn, S., Didcock, L. & Randall, R. E. Interferons: cell signalling, immune modulation, antiviral response and virus countermeasures. *J Gen Virol* **81**, 2341-2364 (2000).
70 Samuel, C. E. Antiviral actions of interferons. *Clin Microbiol Rev* **14**, 778-809, table of contents (2001).
71 Haller, O., Staeheli, P. & Kochs, G. Interferon-induced Mx proteins in antiviral host defense. *Biochimie* (2007).
72 Espert, L. *et al.* ISG20, a new interferon-induced RNase specific for single-stranded RNA, defines an alternative antiviral pathway against RNA genomic viruses. *J Biol Chem* **278**, 16151-16158 (2003).
73 Chawla-Sarkar, M. *et al.* Apoptosis and interferons: role of interferon-stimulated genes as mediators of apoptosis. *Apoptosis* **8**, 237-249 (2003).
74 Talloczy, Z., Virgin, H. W. t. & Levine, B. PKR-dependent autophagic degradation of herpes simplex virus type 1. *Autophagy* **2**, 24-29 (2006).
75 Talloczy, Z. *et al.* Regulation of starvation- and virus-induced autophagy by the eIF2alpha kinase signaling pathway. *Proc Natl Acad Sci U S A* **99**, 190-195 (2002).
76 Lee, H. K. & Iwasaki, A. Autophagy and antiviral immunity. *Curr Opin Immunol* **20**, 23-29, doi:S0952-7915(08)00005-8 [pii]
10.1016/j.coi.2008.01.001 (2008).
77 Berkova, Z. *et al.* Rotavirus NSP4 induces a novel vesicular compartment regulated by calcium and associated with viroplasms. *J Virol* **80**, 6061-6071, doi:80/12/6061 [pii]
10.1128/JVI.02167-05 (2006).
78 Lee, H. K., Lund, J. M., Ramanathan, B., Mizushima, N. & Iwasaki, A. Autophagy-dependent viral recognition by plasmacytoid dendritic cells. *Science* **315**, 1398-1401, doi:1136880 [pii]
10.1126/science.1136880 (2007).
79 Kunz, J. B., Schwarz, H. & Mayer, A. Determination of four sequential stages during microautophagy in vitro. *J Biol Chem* **279**, 9987-9996, doi:10.1074/jbc.M307905200
M307905200 [pii] (2004).

[80] Strawbridge, A. B. & Blum, J. S. Autophagy in MHC class II antigen processing. *Curr Opin Immunol* **19**, 87-92, doi:S0952-7915(06)00241-X [pii]
10.1016/j.coi.2006.11.009 (2007).
[81] Ossendorp, F., Mengede, E., Camps, M., Filius, R. & Melief, C. J. Specific T helper cell requirement for optimal induction of cytotoxic T lymphocytes against major histocompatibility complex class II negative tumors. *J Exp Med* **187**, 693-702 (1998).
[82] Paludan, C. *et al.* Endogenous MHC class II processing of a viral nuclear antigen after autophagy. *Science* **307**, 593-596, doi:1104904 [pii]
10.1126/science.1104904 (2005).
[83] Crotzer, V. L. & Blum, J. S. Cytosol to lysosome transport of intracellular antigens during immune surveillance. *Traffic* **9**, 10-16, doi:TRA664 [pii]
10.1111/j.1600-0854.2007.00664.x (2008).
[84] Schmid, D., Pypaert, M. & Munz, C. Antigen-loading compartments for major histocompatibility complex class II molecules continuously receive input from autophagosomes. *Immunity* **26**, 79-92, doi:S1074-7613(06)00525-5 [pii]
10.1016/j.immuni.2006.10.018 (2007).
[85] Yawalkar, N. *et al.* A comparative study of the expression of cytotoxic proteins in allergic contact dermatitis and psoriasis: spongiotic skin lesions in allergic contact dermatitis are highly infiltrated by T cells expressing perforin and granzyme B. *Am J Pathol* **158**, 803-808 (2001).
[86] Paludan, C. *et al.* Epstein-Barr nuclear antigen 1-specific CD4(+) Th1 cells kill Burkitt's lymphoma cells. *J Immunol* **169**, 1593-1603 (2002).
[87] Sparks-Thissen, R. L., Braaten, D. C., Kreher, S., Speck, S. H. & Virgin, H. W. t. An optimized CD4 T-cell response can control productive and latent gammaherpesvirus infection. *J Virol* **78**, 6827-6835, doi:10.1128/JVI.78.13.6827-6835.2004
78/13/6827 [pii] (2004).
[88] Gutierrez, M. G. *et al.* Autophagy is a defense mechanism inhibiting BCG and Mycobacterium tuberculosis survival in infected macrophages. *Cell* **119**, 753-766, doi:S0092867404011067 [pii]
10.1016/j.cell.2004.11.038 (2004).
[89] Ling, Y. M. *et al.* Vacuolar and plasma membrane stripping and autophagic elimination of Toxoplasma gondii in primed effector macrophages. *J Exp Med* **203**, 2063-2071, doi:jem.20061318 [pii]
10.1084/jem.20061318 (2006).
[90] Harris, J. *et al.* T helper 2 cytokines inhibit autophagic control of intracellular Mycobacterium tuberculosis. *Immunity* **27**, 505-517, doi:S1074-7613(07)00417-7 [pii]
10.1016/j.immuni.2007.07.022 (2007).

[91] Wang, M. L. *et al.* Immune-mediated signaling in intestinal goblet cells via PI3-kinase- and AKT-dependent pathways. *Am J Physiol Gastrointest Liver Physiol* **295**, G1122-1130, doi:90430.2008 [pii] 10.1152/ajpgi.90430.2008 (2008).

[92] Codogno, P. & Meijer, A. J. Autophagy and signaling: their role in cell survival and cell death. *Cell Death Differ* **12 Suppl 2**, 1509-1518, doi:4401751 [pii] 10.1038/sj.cdd.4401751 (2005).

[93] Harris, J. *et al.* Th1-Th2 polarisation and autophagy in the control of intracellular mycobacteria by macrophages. *Vet Immunol Immunopathol* **128**, 37-43, doi:S0165-2427(08)00385-1 [pii] 10.1016/j.vetimm.2008.10.293 (2009).

[94] Horwitz, M. S. Adenovirus immunoregulatory genes and their cellular targets. *Virology* **279**, 1-8 (2001).

[95] Burgert, H. G. & Blusch, J. H. Immunomodulatory functions encoded by the E3 transcription unit of adenoviruses. *Virus Genes* **21**, 13-25 (2000).

[96] Horwitz, M. S. Function of adenovirus E3 proteins and their interactions with immunoregulatory cell proteins. *J Gene Med* **6 Suppl 1**, S172-183 (2004).

[97] Snouwaert, J., Bunick, D., Hutchison, C. & Fowlkes, D. M. Large numbers of random point and cluster mutations within the adenovirus VA I gene allow characterization of sequences required for efficient transcription. *Nucleic Acids Res* **15**, 8293-8303 (1987).

[98] Sano, M., Kato, Y. & Taira, K. Sequence-specific interference by small RNAs derived from adenovirus VAI RNA. *FEBS Lett* **580**, 1553-1564 (2006).

[99] Maran, A. & Mathews, M. B. Characterization of the double-stranded RNA implicated in the inhibition of protein synthesis in cells infected with a mutant adenovirus defective for VA RNA. *Virology* **164**, 106-113 (1988).

[100] Katze, M. G., DeCorato, D., Safer, B., Galabru, J. & Hovanessian, A. G. Adenovirus VAI RNA complexes with the 68 000 Mr protein kinase to regulate its autophosphorylation and activity. *Embo J* **6**, 689-697 (1987).

[101] Galabru, J., Katze, M. G., Robert, N. & Hovanessian, A. G. The binding of double-stranded RNA and adenovirus VAI RNA to the interferon-induced protein kinase. *Eur J Biochem* **178**, 581-589 (1989).

[102] Ghadge, G. D., Swaminathan, S., Katze, M. G. & Thimmapaya, B. Binding of the adenovirus VAI RNA to the interferon-induced 68-kDa protein kinase correlates with function. *Proc Natl Acad Sci U S A* **88**, 7140-7144 (1991).

[103] Furtado, M. R. *et al.* Functional dissection of adenovirus VAI RNA. *J Virol* **63**, 3423-3434 (1989).

[104] Wang, Y. *et al.* Virus-associated RNA I-deleted adenovirus, a potential oncolytic agent targeting EBV-associated tumors. *Cancer Res* **65**, 1523-1531 (2005).

[105] Schneider, R. J., Safer, B., Munemitsu, S. M., Samuel, C. E. & Shenk, T. Adenovirus VAI RNA prevents phosphorylation of the eukaryotic initiation factor 2 alpha subunit subsequent to infection. *Proc Natl Acad Sci U S A* **82**, 4321-4325 (1985).

[106] Schumann, M. & Dobbelstein, M. Activating Ras mutations fail to ensure efficient replication of adenovirus mutants lacking VA-RNA. *Cell Cycle* **5**, 315-321 (2006).

[107] Desai, S. Y. *et al.* Activation of interferon-inducible 2'-5' oligoadenylate synthetase by adenoviral VAI RNA. *J Biol Chem* **270**, 3454-3461 (1995).

[108] Taylor, D. R., Puig, M., Darnell, M. E., Mihalik, K. & Feinstone, S. M. New antiviral pathway that mediates hepatitis C virus replicon interferon sensitivity through ADAR1. *J Virol* **79**, 6291-6298 (2005).

[109] Mori, K. *et al.* Anti-interferon activity of adenovirus-2-encoded VAI and VAII RNAs in translation in cultured human cells. *Virus Res* **42**, 53-63 (1996).

[110] Weber, F., Wagner, V., Kessler, N. & Haller, O. Induction of interferon synthesis by the PKR-inhibitory VA RNAs of adenoviruses. *J Interferon Cytokine Res* **26**, 1-7 (2006).

[111] Andersson, M. G. *et al.* Suppression of RNA interference by adenovirus virus-associated RNA. *J Virol* **79**, 9556-9565 (2005).

[112] Cascallo, M. *et al.* Deletion of VAI and VAII RNA genes in the design of oncolytic adenoviruses. *Hum Gene Ther* **17**, 929-940 (2006).

[113] Alemany, R. Cancer selective adenoviruses. *Mol Aspects Med* **28**, 42-58 (2007).

[114] Fujiwara, T., Urata, Y. & Tanaka, N. Telomerase-specific oncolytic virotherapy for human cancer with the hTERT promoter. *Curr Cancer Drug Targets* **7**, 191-201 (2007).

[115] Everts, B. & van der Poel, H. G. Replication-selective oncolytic viruses in the treatment of cancer. *Cancer Gene Ther* **12**, 141-161 (2005).

[116] Post, D. E., Khuri, F. R., Simons, J. W. & Van Meir, E. G. Replicative oncolytic adenoviruses in multimodal cancer regimens. *Hum Gene Ther* **14**, 933-946 (2003).

[117] Galanis, E. *et al.* Use of viral fusogenic membrane glycoproteins as novel therapeutic transgenes in gliomas. *Hum Gene Ther* **12**, 811-821 (2001).

[118] Sauthoff, H., Heitner, S., Rom, W. N. & Hay, J. G. Deletion of the adenoviral E1b-19kD gene enhances tumor cell killing of a replicating adenoviral vector. *Hum Gene Ther* **11**, 379-388 (2000).

[119] Kitajewski, J., Schneider, R. J., Safer, B. & Shenk, T. An adenovirus mutant unable to express VAI RNA displays different growth responses and sensitivity to interferon in various host cell lines. *Mol Cell Biol* **6**, 4493-4498 (1986).

[120] Schneider, R. J., Weinberger, C. & Shenk, T. Adenovirus VAI RNA facilitates the initiation of translation in virus-infected cells. *Cell* **37**, 291-298 (1984).
[121] Svensson, C. & Akusjarvi, G. Defective RNA splicing in the absence of adenovirus-associated RNAI. *Proc Natl Acad Sci U S A* **83**, 4690-4694 (1986).
[122] Kreivi, J. P. & Akusjarvi, G. Regulation of adenovirus alternative RNA splicing at the level of commitment complex formation. *Nucleic Acids Res* **22**, 332-337 (1994).
[123] Thimmappaya, B., Weinberger, C., Schneider, R. J. & Shenk, T. Adenovirus VAI RNA is required for efficient translation of viral mRNAs at late times after infection. *Cell* **31**, 543-551 (1982).
[124] Cascallo, M., Capella, G., Mazo, A. & Alemany, R. Ras-dependent oncolysis with an adenovirus VAI mutant. *Cancer Res* **63**, 5544-5550 (2003).
[125] Princiotta, M. F. *et al.* Quantitating protein synthesis, degradation, and endogenous antigen processing. *Immunity* **18**, 343-354, doi:S1074761303000517 [pii] (2003).
[126] Dubouloz, F., Deloche, O., Wanke, V., Cameroni, E. & De Virgilio, C. The TOR and EGO protein complexes orchestrate microautophagy in yeast. *Mol Cell* **19**, 15-26, doi:S1097-2765(05)01347-X [pii]
10.1016/j.molcel.2005.05.020 (2005).
[127] Farre, J. C. & Subramani, S. Peroxisome turnover by micropexophagy: an autophagy-related process. *Trends Cell Biol* **14**, 515-523, doi:10.1016/j.tcb.2004.07.014
S0962-8924(04)00193-X [pii] (2004).
[128] Twig, G. *et al.* Fission and selective fusion govern mitochondrial segregation and elimination by autophagy. *Embo J* **27**, 433-446, doi:7601963 [pii]
10.1038/sj.emboj.7601963 (2008).
[129] Tolkovsky, A. M. Mitophagy. *Biochim Biophys Acta*, doi:S0167-4889(09)00060-3 [pii]
10.1016/j.bbamcr.2009.03.002 (2009).
[130] Kanki, T. & Klionsky, D. J. Mitophagy in yeast occurs through a selective mechanism. *J Biol Chem* **283**, 32386-32393, doi:M802403200 [pii]
10.1074/jbc.M802403200 (2008).
[131] Dice, J. F. Chaperone-mediated autophagy. *Autophagy* **3**, 295-299, doi:4144 [pii] (2007).
[132] Majeski, A. E. & Dice, J. F. Mechanisms of chaperone-mediated autophagy. *Int J Biochem Cell Biol* **36**, 2435-2444, doi:10.1016/j.biocel.2004.02.013
S1357272504000883 [pii] (2004).
[133] Gracy, R. W., Talent, J. M. & Zvaigzne, A. I. Molecular wear and tear leads to terminal marking and the unstable isoforms of aging. *J Exp Zool* **282**, 18-27, doi:10.1002/(SICI)1097-010X(199809/10)282:1/2<18::AID-JEZ5>3.0.CO;2-Q [pii] (1998).

[134] Agarraberes, F. A., Terlecky, S. R. & Dice, J. F. An intralysosomal hsp70 is required for a selective pathway of lysosomal protein degradation. *J Cell Biol* **137**, 825-834 (1997).
[135] Berg, T. O., Fengsrud, M., Stromhaug, P. E., Berg, T. & Seglen, P. O. Isolation and characterization of rat liver amphisomes. Evidence for fusion of autophagosomes with both early and late endosomes. *J Biol Chem* **273**, 21883-21892 (1998).
[136] Xie, Z. & Klionsky, D. J. Autophagosome formation: core machinery and adaptations. *Nat Cell Biol* **9**, 1102-1109, doi:ncb1007-1102 [pii]
10.1038/ncb1007-1102 (2007).
[137] Menendez-Benito, V. & Neefjes, J. Autophagy in MHC class II presentation: sampling from within. *Immunity* **26**, 1-3, doi:S1074-7613(07)00105-7 [pii]
10.1016/j.immuni.2007.01.005 (2007).
[138] Lindmo, K. & Stenmark, H. Regulation of membrane traffic by phosphoinositide 3-kinases. *J Cell Sci* **119**, 605-614, doi:119/4/605 [pii]
10.1242/jcs.02855 (2006).
[139] Axe, E. L. *et al.* Autophagosome formation from membrane compartments enriched in phosphatidylinositol 3-phosphate and dynamically connected to the endoplasmic reticulum. *J Cell Biol* **182**, 685-701, doi:jcb.200803137 [pii]
10.1083/jcb.200803137 (2008).
[140] Derubeis, A. R., Young, M. F., Jia, L., Robey, P. G. & Fisher, L. W. Double FYVE-containing protein 1 (DFCP1): isolation, cloning and characterization of a novel FYVE finger protein from a human bone marrow cDNA library. *Gene* **255**, 195-203, doi:S0378-1119(00)00303-6 [pii] (2000).
[141] He, C., Baba, M., Cao, Y. & Klionsky, D. J. Self-interaction is critical for Atg9 transport and function at the phagophore assembly site during autophagy. *Mol Biol Cell* **19**, 5506-5516, doi:E08-05-0544 [pii]
10.1091/mbc.E08-05-0544 (2008).
[142] Xie, Z., Nair, U. & Klionsky, D. J. Atg8 controls phagophore expansion during autophagosome formation. *Mol Biol Cell* **19**, 3290-3298 (2008).
[143] Xie, Z., Nair, U. & Klionsky, D. J. Dissecting autophagosome formation: the missing pieces. *Autophagy* **4**, 920-922, doi:6692 [pii] (2008).
[144] Kabeya, Y. *et al.* LC3, a mammalian homologue of yeast Apg8p, is localized in autophagosome membranes after processing. *Embo J* **19**, 5720-5728 (2000).
[145] Kabeya, Y. *et al.* LC3, GABARAP and GATE16 localize to autophagosomal membrane depending on form-II formation. *J Cell Sci* **117**, 2805-2812 (2004).

[146] Noda, N. N. *et al.* Structural basis of target recognition by Atg8/LC3 during selective autophagy. *Genes Cells* **13**, 1211-1218, doi:GTC1238 [pii]
10.1111/j.1365-2443.2008.01238.x (2008).
[147] Chang, Y. Y. & Neufeld, T. P. An Atg1/Atg13 complex with multiple roles in TOR-mediated autophagy regulation. *Mol Biol Cell* **20**, 2004-2014, doi:E08-12-1250 [pii]
10.1091/mbc.E08-12-1250 (2009).
[148] Rubinsztein, D. C., Gestwicki, J. E., Murphy, L. O. & Klionsky, D. J. Potential therapeutic applications of autophagy. *Nat Rev Drug Discov* **6**, 304-312, doi:nrd2272 [pii]
10.1038/nrd2272 (2007).
[149] Seglen, P. O., Gordon, P. B. & Holen, I. Non-selective autophagy. *Semin Cell Biol* **1**, 441-448 (1990).
[150] Kopitz, J., Kisen, G. O., Gordon, P. B., Bohley, P. & Seglen, P. O. Nonselective autophagy of cytosolic enzymes by isolated rat hepatocytes. *J Cell Biol* **111**, 941-953 (1990).
[151] Kraft, C., Reggiori, F. & Peter, M. Selective types of autophagy in yeast. *Biochim Biophys Acta*, doi:S0167-4889(09)00055-X [pii]
10.1016/j.bbamcr.2009.02.006 (2009).
[152] Seibenhener, M. L. *et al.* Sequestosome 1/p62 is a polyubiquitin chain binding protein involved in ubiquitin proteasome degradation. *Mol Cell Biol* **24**, 8055-8068 (2004).
[153] Komatsu, M. *et al.* Homeostatic levels of p62 control cytoplasmic inclusion body formation in autophagy-deficient mice. *Cell* **131**, 1149-1163 (2007).
[154] Seibenhener, M. L., Geetha, T. & Wooten, M. W. Sequestosome 1/p62--more than just a scaffold. *FEBS Lett* **581**, 175-179 (2007).
[155] Ravikumar, B. *et al.* Inhibition of mTOR induces autophagy and reduces toxicity of polyglutamine expansions in fly and mouse models of Huntington disease. *Nat Genet* **36**, 585-595, doi:10.1038/ng1362
ng1362 [pii] (2004).
[156] Kraft, C., Deplazes, A., Sohrmann, M. & Peter, M. Mature ribosomes are selectively degraded upon starvation by an autophagy pathway requiring the Ubp3p/Bre5p ubiquitin protease. *Nat Cell Biol* **10**, 602-610, doi:ncb1723 [pii]
10.1038/ncb1723 (2008).
[157] Beau, I., Esclatine, A. & Codogno, P. Lost to translation: when autophagy targets mature ribosomes. *Trends Cell Biol* **18**, 311-314, doi:S0962-8924(08)00134-7 [pii]
10.1016/j.tcb.2008.05.001 (2008).
[158] Lum, J. J., DeBerardinis, R. J. & Thompson, C. B. Autophagy in metazoans: cell survival in the land of plenty. *Nat Rev Mol Cell Biol* **6**, 439-448, doi:nrm1660 [pii]
10.1038/nrm1660 (2005).

[159] Melendez, A. *et al.* Autophagy genes are essential for dauer development and life-span extension in C. elegans. *Science* **301**, 1387-1391, doi:10.1126/science.1087782
301/5638/1387 [pii] (2003).
[160] Kuma, A. *et al.* The role of autophagy during the early neonatal starvation period. *Nature* **432**, 1032-1036, doi:nature03029 [pii]
10.1038/nature03029 (2004).
[161] Heintz, N. Developmental biology: survival by self-digestion. *Nature* **432**, 963, doi:432963a [pii]
10.1038/432963a (2004).
[162] Lum, J. J. *et al.* Growth factor regulation of autophagy and cell survival in the absence of apoptosis. *Cell* **120**, 237-248, doi:S009286740401150X [pii]
10.1016/j.cell.2004.11.046 (2005).
[163] Cutler, N. S., Heitman, J. & Cardenas, M. E. TOR kinase homologs function in a signal transduction pathway that is conserved from yeast to mammals. *Mol Cell Endocrinol* **155**, 135-142, doi:S0303-7207(99)00121-5 [pii] (1999).
[164] Heitman, J., Movva, N. R. & Hall, M. N. Targets for cell cycle arrest by the immunosuppressant rapamycin in yeast. *Science* **253**, 905-909 (1991).
[165] Strimpakos, A. S., Karapanagiotou, E. M., Saif, M. W. & Syrigos, K. N. The role of mTOR in the management of solid tumors: an overview. *Cancer Treat Rev* **35**, 148-159, doi:S0305-7372(08)00288-0 [pii]
10.1016/j.ctrv.2008.09.006 (2009).
[166] Schmelzle, T. & Hall, M. N. TOR, a central controller of cell growth. *Cell* **103**, 253-262, doi:S0092-8674(00)00117-3 [pii] (2000).
[167] Kamada, Y. *et al.* Tor-mediated induction of autophagy via an Apg1 protein kinase complex. *J Cell Biol* **150**, 1507-1513 (2000).
[168] Pattingre, S., Espert, L., Biard-Piechaczyk, M. & Codogno, P. Regulation of macroautophagy by mTOR and Beclin 1 complexes. *Biochimie* **90**, 313-323, doi:S0300-9084(07)00228-3 [pii]
10.1016/j.biochi.2007.08.014 (2008).
[169] Chang, Y. Y. *et al.* Nutrient-dependent regulation of autophagy through the target of rapamycin pathway. *Biochem Soc Trans* **37**, 232-236, doi:BST0370232 [pii]
10.1042/BST0370232 (2009).
[170] Qu, X. *et al.* Promotion of tumorigenesis by heterozygous disruption of the beclin 1 autophagy gene. *J Clin Invest* **112**, 1809-1820, doi:10.1172/JCI20039
JCI200320039 [pii] (2003).
[171] Tsuchihara, K., Fujii, S. & Esumi, H. Autophagy and cancer: dynamism of the metabolism of tumor cells and tissues. *Cancer Lett* **278**, 130-138, doi:S0304-3835(08)00796-9 [pii]
10.1016/j.canlet.2008.09.040 (2009).
[172] Pattingre, S. & Levine, B. Bcl-2 inhibition of autophagy: a new route to cancer? *Cancer Res* **66**, 2885-2888, doi:66/6/2885 [pii]

10.1158/0008-5472.CAN-05-4412 (2006).
173 Mathew, R. *et al.* Autophagy suppresses tumor progression by limiting chromosomal instability. *Genes Dev* **21**, 1367-1381, doi:gad.1545107 [pii]
10.1101/gad.1545107 (2007).
174 Weinberg, R. A. in *The Biology of Cancer* Vol. 1 eds S Masson & A Grose) Ch. 13.6 - Endothelial cells enable neovascularisation, 556-563 (Garland Science, Taylor & Francis Group, LLC, 2007).
175 Amaravadi, R. K. *et al.* Autophagy inhibition enhances therapy-induced apoptosis in a Myc-induced model of lymphoma. *J Clin Invest* **117**, 326-336, doi:10.1172/JCI28833 (2007).
176 Kondo, Y. & Kondo, S. Autophagy and cancer therapy. *Autophagy* **2**, 85-90, doi:2463 [pii] (2006).
177 Seglen, P. O. & Gordon, P. B. Amino acid control of autophagic sequestration and protein degradation in isolated rat hepatocytes. *J Cell Biol* **99**, 435-444 (1984).
178 Seglen, P. O., Gordon, P. B. & Poli, A. Amino acid inhibition of the autophagic/lysosomal pathway of protein degradation in isolated rat hepatocytes. *Biochim Biophys Acta* **630**, 103-118 (1980).
179 Punnonen, E. L. & Reunanen, H. Effects of vinblastine, leucine, and histidine, and 3-methyladenine on autophagy in Ehrlich ascites cells. *Exp Mol Pathol* **52**, 87-97, doi:0014-4800(90)90061-H [pii] (1990).
180 Klionsky, D. J., Cuervo, A. M. & Seglen, P. O. Methods for monitoring autophagy from yeast to human. *Autophagy* **3**, 181-206 (2007).
181 Chaumorcel, M., Souquere, S., Pierron, G., Codogno, P. & Esclatine, A. Human cytomegalovirus controls a new autophagy-dependent cellular antiviral defense mechanism. *Autophagy* **4**, 46-53 (2008).
182 Yokoyama, T. *et al.* Autophagy-inducing agents augment the antitumor effect of telerase-selve oncolytic adenovirus OBP-405 on glioblastoma cells. *Gene Ther* **15**, 1233-1239 (2008).
183 Paglin, S. *et al.* A novel response of cancer cells to radiation involves autophagy and formation of acidic vesicles. *Cancer Res* **61**, 439-444 (2001).
184 Kirisako, T. *et al.* The reversible modification regulates the membrane-binding state of Apg8/Aut7 essential for autophagy and the cytoplasm to vacuole targeting pathway. *J Cell Biol* **151**, 263-276 (2000).
185 Mizushima, N. & Yoshimori, T. How to interpret LC3 immunoblotting. *Autophagy* **3**, 542-545 (2007).
186 Tanida, I., Minematsu-Ikeguchi, N., Ueno, T. & Kominami, E. Lysosomal turnover, but not a cellular level, of endogenous LC3 is a marker for autophagy. *Autophagy* **1**, 84-91 (2005).
187 Kuma, A., Matsui, M. & Mizushima, N. LC3, an autophagosome marker, can be incorporated into protein aggregates independent of autophagy: caution in the interpretation of LC3 localization. *Autophagy* **3**, 323-328 (2007).

188 Strnad, P., Zatloukal, K., Stumptner, C., Kulaksiz, H. & Denk, H. Mallory-Denk-bodies: lessons from keratin-containing hepatic inclusion bodies. *Biochim Biophys Acta* **1782**, 764-774 (2008).
189 Ciechomska, I. A. & Tolkovsky, A. M. Non-autophagic GFP-LC3 puncta induced by saponin and other detergents. *Autophagy* **3**, 586-590 (2007).
190 Korkhov, V. M. GFP-LC3 labels organised smooth endoplasmic reticulum membranes independently of autophagy. *J Cell Biochem* (2009).
191 Stumptner, C., Fuchsbichler, A., Heid, H., Zatloukal, K. & Denk, H. Mallory body--a disease-associated type of sequestosome. *Hepatology* **35**, 1053-1062 (2002).
192 Bjorkoy, G. *et al.* Monitoring autophagic degradation of p62/SQSTM1. *Methods Enzymol* **452**, 181-197 (2009).
193 Kirkin, V. *et al.* A role for NBR1 in autophagosomal degradation of ubiquitinated substrates. *Mol Cell* **33**, 505-516 (2009).
194 Milano, V., Piao, Y., LaFortune, T. & de Groot, J. Dasatinib-induced autophagy is enhanced in combination with temozolomide in glioma. *Mol Cancer Ther* **8**, 394-406 (2009).
195 Biederbick, A., Kern, H. F. & Elsasser, H. P. Monodansylcadaverine (MDC) is a specific in vivo marker for autophagic vacuoles. *Eur J Cell Biol* **66**, 3-14 (1995).
196 Munafo, D. B. & Colombo, M. I. A novel assay to study autophagy: regulation of autophagosome vacuole size by amino acid deprivation. *J Cell Sci* **114**, 3619-3629 (2001).
197 Iwai-Kanai, E. *et al.* A method to measure cardiac autophagic flux in vivo. *Autophagy* **4**, 322-329 (2008).
198 Contento, A. L., Xiong, Y. & Bassham, D. C. Visualization of autophagy in Arabidopsis using the fluorescent dye monodansylcadaverine and a GFP-AtATG8e fusion protein. *Plant J* **42**, 598-608 (2005).
199 Niemann, A., Takatsuki, A. & Elsasser, H. P. The lysosomotropic agent monodansylcadaverine also acts as a solvent polarity probe. *J Histochem Cytochem* **48**, 251-258 (2000).
200 Bampton, E. T., Goemans, C. G., Niranjan, D., Mizushima, N. & Tolkovsky, A. M. The dynamics of autophagy visualized in live cells: from autophagosome formation to fusion with endo/lysosomes. *Autophagy* **1**, 23-36 (2005).
201 Niemann, A., Baltes, J. & Elsasser, H. P. Fluorescence properties and staining behavior of monodansylpentane, a structural homologue of the lysosomotropic agent monodansylcadaverine. *J Histochem Cytochem* **49**, 177-185 (2001).
202 Mizushima, N. Methods for monitoring autophagy. *Int J Biochem Cell Biol* **36**, 2491-2502 (2004).
203 Bett, A. J., Krougliak, V. & Graham, F. L. DNA sequence of the deletion/insertion in early region 3 of Ad5 dl309. *Virus Res* **39**, 75-82 (1995).

[204] O'Reilly DR, M. L., Luckow VA. in *In Baculovirus Expression Vectors: A Laboratory Manual* 132-134 (Oxford University Press, 1994).

[205] Gentleman, R. C. *et al.* Bioconductor: open software development for computational biology and bioinformatics. *Genome Biol* **5**, R80 (2004).

[206] Smyth, G. K., Michaud, J. & Scott, H. S. Use of within-array replicate spots for assessing differential expression in microarray experiments. *Bioinformatics* **21**, 2067-2075 (2005).

[207] Kooperberg, C., Aragaki, A., Strand, A. D. & Olson, J. M. Significance testing for small microarray experiments. *Stat Med* **24**, 2281-2298 (2005).

[208] Gale, M., Jr. & Katze, M. G. Molecular mechanisms of interferon resistance mediated by viral-directed inhibition of PKR, the interferon-induced protein kinase. *Pharmacol Ther* **78**, 29-46 (1998).

[209] Kouroku, Y. *et al.* ER stress (PERK/eIF2alpha phosphorylation) mediates the polyglutamine-induced LC3 conversion, an essential step for autophagy formation. *Cell Death Differ* **14**, 230-239 (2007).

[210] Li, J. *et al.* Inhibition of autophagy by 3-MA enhances the effect of 5-FU-induced apoptosis in colon cancer cells. *Ann Surg Oncol* **16**, 761-771, doi:10.1245/s10434-008-0260-0 (2009).

[211] von Bultzingslowen, I., Jontell, M., Hurst, P., Nannmark, U. & Kardos, T. 5-Fluorouracil induces autophagic degeneration in rat oral keratinocytes. *Oral Oncol* **37**, 537-544, doi:S1368837501000094 [pii] (2001).

[212] Kirn, D., Martuza, R. L. & Zwiebel, J. Replication-selective virotherapy for cancer: Biological principles, risk management and future directions. *Nat Med* **7**, 781-787 (2001).

[213] Strong, J. E., Coffey, M. C., Tang, D., Sabinin, P. & Lee, P. W. The molecular basis of viral oncolysis: usurpation of the Ras signaling pathway by reovirus. *Embo J* **17**, 3351-3362, doi:10.1093/emboj/17.12.3351 (1998).

[214] Bergmann, M. *et al.* A genetically engineered influenza A virus with ras-dependent oncolytic properties. *Cancer Res* **61**, 8188-8193 (2001).

[215] Farassati, F., Yang, A. D. & Lee, P. W. Oncogenes in Ras signalling pathway dictate host-cell permissiveness to herpes simplex virus 1. *Nat Cell Biol* **3**, 745-750, doi:10.1038/35087061 35087061 [pii] (2001).

[216] Mundschau, L. J. & Faller, D. V. Endogenous inhibitors of the dsRNA-dependent eIF-2 alpha protein kinase PKR in normal and ras-transformed cells. *Biochimie* **76**, 792-800, doi:0300-9084(94)90083-3 [pii] (1994).

[217] Braidwood, L., Dunn, P. D., Hardy, S., Evans, T. R. & Brown, S. M. Antitumor Activity of a Selectively Replication Competent Herpes Simplex Virus (HSV) with Enzyme Prodrug Therapy. *Anticancer Res* **29**, 2159-2166, doi:29/6/2159 [pii] (2009).

[218] Matthews, K. *et al.* Identifying the safety profile of Ad5.SSTR/TK.RGD, a novel infectivity-enhanced bicistronic adenovirus, in anticipation of a phase I clinical trial in patients with recurrent ovarian cancer. *Clin Cancer Res* **15**, 4131-4137, doi:1078-0432.CCR-08-3354 [pii]
10.1158/1078-0432.CCR-08-3354 (2009).
[219] Yang, G., Thompson, J. A., Fang, B. & Liu, J. Silencing of H-ras gene expression by retrovirus-mediated siRNA decreases transformation efficiency and tumorgrowth in a model of human ovarian cancer. *Oncogene* **22**, 5694-5701, doi:10.1038/sj.onc.1206858
1206858 [pii] (2003).
[220] Zheng, J. N. *et al.* Inhibition of renal cancer cell growth by oncolytic adenovirus armed short hairpin RNA targeting hTERT gene. *Cancer Biol Ther* **8**, 84-91, doi:7204 [pii] (2009).
[221] Zheng, J. N. *et al.* Inhibition of renal cancer cell growth in vitro and in vivo with oncolytic adenovirus armed short hairpin RNA targeting Ki-67 encoding mRNA. *Cancer Gene Ther* **16**, 20-32, doi:cgt200861 [pii]
10.1038/cgt.2008.61 (2009).
[222] Shen, W., Wang, C. Y., Wang, X. H. & Fu, Z. X. Oncolytic adenovirus mediated Survivin knockdown by RNA interference suppresses human colorectal carcinoma growth in vitro and in vivo. *J Exp Clin Cancer Res* **28**, 81, doi:1756-9966-28-81 [pii]
10.1186/1756-9966-28-81 (2009).
[223] Xu, N., Segerman, B., Zhou, X. & Akusjarvi, G. Adenovirus virus-associated RNAII-derived small RNAs are efficiently incorporated into the rna-induced silencing complex and associate with polyribosomes. *J Virol* **81**, 10540-10549, doi:JVI.00885-07 [pii]
10.1128/JVI.00885-07 (2007).
[224] Lu, S. & Cullen, B. R. Adenovirus VA1 noncoding RNA can inhibit small interfering RNA and MicroRNA biogenesis. *J Virol* **78**, 12868-12876, doi:78/23/12868 [pii]
10.1128/JVI.78.23.12868-12876.2004 (2004).
[225] Zhang, P. & Samuel, C. E. Protein kinase PKR plays a stimulus- and virus-dependent role in apoptotic death and virus multiplication in human cells. *J Virol* **81**, 8192-8200, doi:JVI.00426-07 [pii]
10.1128/JVI.00426-07 (2007).
[226] Xi, Q., Cuesta, R. & Schneider, R. J. Tethering of eIF4G to adenoviral mRNAs by viral 100k protein drives ribosome shunting. *Genes Dev* **18**, 1997-2009, doi:10.1101/gad.1212504
18/16/1997 [pii] (2004).
[227] Bessis, N., GarciaCozar, F. J. & Boissier, M. C. Immune responses to gene therapy vectors: influence on vector function and effector mechanisms. *Gene Ther* **11 Suppl 1**, S10-17, doi:10.1038/sj.gt.3302364
3302364 [pii] (2004).

[228] Sakurai, H., Kawabata, K., Sakurai, F., Nakagawa, S. & Mizuguchi, H. Innate immune response induced by gene delivery vectors. *Int J Pharm* **354**, 9-15, doi:S0378-5173(07)00506-6 [pii]
10.1016/j.ijpharm.2007.06.012 (2008).
[229] Blais, J. D. *et al.* Activating transcription factor 4 is translationally regulated by hypoxic stress. *Mol Cell Biol* **24**, 7469-7482, doi:10.1128/MCB.24.17.7469-7482.2004
24/17/7469 [pii] (2004).
[230] Moretti, L., Cha, Y. I., Niermann, K. J. & Lu, B. Switch between apoptosis and autophagy: radiation-induced endoplasmic reticulum stress? *Cell Cycle* **6**, 793-798, doi:4036 [pii] (2007).
[231] Bernales, S., McDonald, K. L. & Walter, P. Autophagy counterbalances endoplasmic reticulum expansion during the unfolded protein response. *PLoS Biol* **4**, e423, doi:06-PLBI-RA-0898R3 [pii]
10.1371/journal.pbio.0040423 (2006).
[232] Kondratyev, M., Avezov, E., Shenkman, M., Groisman, B. & Lederkremer, G. Z. PERK-dependent compartmentalization of ERAD and unfolded protein response machineries during ER stress. *Exp Cell Res* **313**, 3395-3407, doi:S0014-4827(07)00329-1 [pii]
10.1016/j.yexcr.2007.07.006 (2007).
[233] Buchkovich, N. J., Yu, Y., Zampieri, C. A. & Alwine, J. C. The TORrid affairs of viruses: effects of mammalian DNA viruses on the PI3K-Akt-mTOR signalling pathway. *Nat Rev Microbiol* **6**, 266-275, doi:nrmicro1855 [pii]
10.1038/nrmicro1855 (2008).
[234] Lee, C., Kim, J. S. & Waldman, T. PTEN gene targeting reveals a radiation-induced size checkpoint in human cancer cells. *Cancer Res* **64**, 6906-6914, doi:64/19/6906 [pii]
10.1158/0008-5472.CAN-04-1767 (2004).
[235] Sasaki, S. *et al.* hRFI overexpressed in HCT116 cells modulates Bcl-2 family proteins when treated with 5-fluorouracil. *Oncol Rep* **15**, 1293-1298 (2006).
[236] Fessler, S. P. & Young, C. S. Control of adenovirus early gene expression during the late phase of infection. *J Virol* **72**, 4049-4056 (1998).
[237] Moritz, C. & Dobbelstein, M. E1A genes of adenovirus type 2 and type 5 are expressed at different levels. *Arch Virol* **151**, 1085-1092, doi:10.1007/s00705-005-0702-y (2006).
[238] Alexander, D. E., Ward, S. L., Mizushima, N., Levine, B. & Leib, D. A. Analysis of the role of autophagy in replication of herpes simplex virus in cell culture. *J Virol* **81**, 12128-12134, doi:JVI.01356-07 [pii]
10.1128/JVI.01356-07 (2007).
[239] Alexander, D. E. & Leib, D. A. Xenophagy in herpes simplex virus replication and pathogenesis. *Autophagy* **4**, 101-103, doi:5222 [pii] (2008).
[240] Abedin, M. J., Wang, D., McDonnell, M. A., Lehmann, U. & Kelekar, A. Autophagy delays apoptotic death in breast cancer cells

following DNA damage. *Cell Death Differ* **14**, 500-510, doi:4402039 [pii]
10.1038/sj.cdd.4402039 (2007).
241 Karantza-Wadsworth, V. *et al.* Autophagy mitigates metabolic stress and genome damage in mammary tumorigenesis. *Genes Dev* **21**, 1621-1635, doi:21/13/1621 [pii]
10.1101/gad.1565707 (2007).
242 Munoz-Gamez, J. A. *et al.* PARP-1 is involved in autophagy induced by DNA damage. *Autophagy* **5**, 61-74, doi:7272 [pii] (2009).
243 Lee, S. B., Rodriguez, D., Rodriguez, J. R. & Esteban, M. The apoptosis pathway triggered by the interferon-induced protein kinase PKR requires the third basic domain, initiates upstream of Bcl-2, and involves ICE-like proteases. *Virology* **231**, 81-88, doi:S0042682297984944 [pii] (1997).
244 Zhao, P., Lu, Y., Liu, L. & Zhong, M. Aberrant expression of ID2 protein and its correlation with EBV-LMP1 and P16(INK4A) in classical Hodgkin lymphoma in China. *BMC Cancer* **8**, 379, doi:1471-2407-8-379 [pii]
10.1186/1471-2407-8-379 (2008).
245 Tsunedomi, R. *et al.* Identification of ID2 associated with invasion of hepatitis C virus-related hepatocellular carcinoma by gene expression profile. *Int J Oncol* **29**, 1445-1451 (2006).